

Characterization of the Vacuolar Sugar Transporter
Early Responsive to Dehydration-Like4 (ERDL4) from
Arabidopsis and its Role in Cold and in Dark Induced
Senescence

vom Fachbereich Biologie der Rheinland-Pfälzischen Technischen Universität
Kaiserslautern-Landau zur Verleihung des akademischen Grades

„Doktor der Naturwissenschaften“

genehmigte Dissertation

von

Azkiya Khan, MSc.

Wissenschaftliche Aussprache: 14. Juli 2022

Berichterstattende:

Prof. Dr. H. Ekkehard Neuhaus (Betreuer)

Prof. Dr. Matthias Hahn

Table of Contents

| | |
|---|----|
| 1. Introduction | 1 |
| 1.1. Sugars in plants: A complex regulatory network | 1 |
| 1.2. Photosynthesis and partitioning of photosynthates..... | 2 |
| 1.3. Plant vacuole and sugar transporters across tonoplast..... | 5 |
| 1.4. Early Responsive to Dehydration6-Likes (ERDLs) subfamily of MST..... | 7 |
| 1.5. Fructose synthesis and metabolism..... | 8 |
| 1.6. Sugars in abiotic stress tolerance..... | 9 |
| 1.7. Crosstalk between sugar transporters | 10 |
| 1.8. Objective of this work | 11 |
| 2. Material and Methods | 12 |
| 2.1. Chemicals and kits..... | 12 |
| 2.2. Computerized analysis | 12 |
| 2.3. Bioinformatics analysis | 12 |
| 2.4. Plant specific methods..... | 13 |
| 2.4.1. Plant material..... | 13 |
| 2.4.2. Growth on soil under standard conditions..... | 13 |
| 2.4.3. Growth under stress conditions | 14 |
| 2.4.4. Surface sterilization of seeds | 14 |
| 2.4.5. Growth in sterile liquid medium and agar plates | 14 |
| 2.5. Microbiological and molecular biological methods..... | 15 |
| 2.5.1. Bacterial and yeast strains | 15 |
| 2.5.2. Cultivation of bacteria..... | 16 |
| 2.5.3. Vectors and plasmids | 17 |
| 2.5.4. Oligonucleotides | 17 |

| | |
|--|----|
| 2.5.5. Isolation of gDNA from <i>A.thaliana</i> | 19 |
| 2.5.6. DNA amplification by PCR..... | 20 |
| 2.5.7. Agarose gel electrophoresis and DNA gel extraction | 21 |
| 2.5.8. Determination of nucleic acid concentration | 22 |
| 2.5.9. DNA sequencing analysis | 22 |
| 2.5.10. Production of competent <i>E.coli</i> cells and their transformation..... | 22 |
| 2.5.11. Production of competent <i>Agrobacterium tumefaciens</i> cells and their transformation..... | 23 |
| 2.5.12. Yeast growth and transformation..... | 24 |
| 2.5.13. Cloning and expression of <i>ERDL4</i> and uptake of radiolabelled solutes in <i>X.laevis</i> oocytes..... | 25 |
| 2.5.14. Plasmid isolation from <i>E. coli</i> | 26 |
| 2.5.15. Generation of <i>ERDL4</i> overexpression construct in <i>tst1/2</i> double knockout background | 27 |
| 2.5.16. Transformation of <i>A.thaliana</i> (Floral-dip method)..... | 27 |
| 2.5.17. RNA isolation from <i>A.thaliana</i> and cDNA synthesis | 28 |
| 2.5.18. Quantitative real time polymerase chain reaction (qRT-PCR)..... | 28 |
| 2.5.19. Histochemical analysis by GUS staining..... | 29 |
| 2.5.20. GFP fluorescence analysis..... | 29 |
| 2.5.21. Root tissue embedding and cross-sections | 30 |
| 2.6. Biochemical analysis | 30 |
| 2.6.1. Ethanolic sugar extraction | 30 |
| 2.6.2. Starch extraction..... | 30 |
| 2.6.3. Sugar quantification..... | 31 |
| 2.6.4. Anthocyanin and chlorophyll quantification | 32 |
| 2.7. Physiological analysis | 33 |

| | |
|--|----|
| 2.7.1 Root and silique length | 33 |
| 2.7.2. Inflorescence length and inflorescence weight | 33 |
| 2.7.3. Seeds analysis | 33 |
| 2.7.4. Phloem exudate isolation and quantification of soluble sugars | 34 |
| 2.7.5. Electrical conductivity and LT50% | 34 |
| 2.8. Transcriptomic analysis (RNA-Seq) | 35 |
| 3. Results | 36 |
| 3.1. Sequence and homology analysis | 36 |
| 3.1.1. Promoter analysis of <i>ERDL4</i> | 38 |
| 3.1.2. Subcellular localization of <i>ERDL4</i> | 38 |
| 3.1.3. Genotyping and biochemical characterization of <i>ERDL4</i> mutants | 39 |
| 3.1.4. Subcellular compartmentation of sugars in <i>ERDL4</i> mutants | 41 |
| 3.1.5. Phenotypic characterization of <i>ERDL4</i> mutants | 42 |
| 3.1.6. Root growth analysis from 35S- <i>ERDL4</i> lines | 44 |
| 3.1.7. Analysis of phloem sugar export | 44 |
| 3.1.8. Inflorescence analysis of 35S- <i>ERDL4</i> lines | 45 |
| 3.1.9. Silique analysis of <i>ERDL4</i> mutants | 47 |
| 3.1.10. Seed yield analysis from <i>ERDL4</i> mutants | 48 |
| 3.1.11. Seed quality and physiological analysis from <i>ERDL4</i> mutants | 49 |
| 3.1.12. Differential expression analysis in 35S- <i>ERDL4</i> lines corresponds to fructose effect | 50 |
| 3.1.13. Sugar transporters are diurnally regulated | 53 |
| 3.1.14. Expression analysis of vacuolar sugar transporters in <i>ERDL4</i> mutants | 55 |
| 3.1.15. Sugar quantification from <i>tst-ERDL4</i> lines | 57 |
| 3.2. Fructose: A key signalling factor for vacuolar sugar homeostasis | 59 |
| 3.3. Role of <i>ERDL4</i> in abiotic stresses | 62 |

| | |
|---|-----|
| 3.3.1. <i>ERDL4</i> expression in response to cold | 62 |
| 3.3.2. <i>ERDL4</i> influences cold acclimation and freezing tolerance | 64 |
| 3.3.3. <i>ERDL4</i> response to long-term cold | 65 |
| 3.3.4. Role of <i>ERDL4</i> in dark induced senescence | 68 |
| 4. Discussion..... | 71 |
| 4.1. Outcomes of regulated vacuolar sugar export | 71 |
| 4.1.1. <i>ERDL4</i> is homologous to <i>ERDL6</i> but essentially quite different | 71 |
| 4.1.2. <i>ERDL4</i> is a vacuolar protein and resides in the tonoplast | 73 |
| 4.1.3. <i>ERDL4</i> mediates vacuolar fructose export influencing plant organ development | 73 |
| 4.1.4. <i>ERDL4</i> overexpression correlates with cytosolic fructose Induction | 75 |
| 4.1.5. <i>ERDL4</i> and cold response..... | 78 |
| 4.1.6. <i>ERDL4</i> and dark induced senescence..... | 80 |
| 4.2. Conclusion..... | 82 |
| 4.3. Outlook | 83 |
| 5. Summary | 85 |
| 6. Bibliography | 87 |
| 7.1. Supplementary figures..... | 103 |
| 7.2. Abbreviations..... | 120 |
| 7.3. List of Figures | 121 |
| 7.4. List of Tables | 131 |

1. Introduction

1.1. Sugars in plants: A complex regulatory network

Plants rely on sugars for their diel energy and growth. These sugars are synthesized via photosynthesis during daytime in the cytosol of mesophyll cells, a process fueled by triose-phosphates exported from the chloroplast (Ruan, 2014). However, sucrose biosynthesis continues even at night, the degradation of transitory starch provides maltose to the cytosol and the subsequent conversion of this disaccharide further drives sucrose biosynthesis (Smith & Zeeman, 2020). These sugars serve as an important regulator for many anabolic reactions, allow cellulose biosynthesis, serve as glycosyl donors for lipid and protein modification in membranes and provide the substrates for oxidative phosphorylation (Crowe et al., 1988; Sheen et al., 1999; Ruan, 2014).

The most abundant sugars present in vascular plants are the disaccharide sucrose and the two monosaccharides, glucose and fructose. Although sucrose is considered as a signalling molecule as well but there is no direct evidence, as it is rapidly hydrolysed to monosaccharides. Sucrose import and its hydrolysis is maintained via an intricate network of cell wall invertases (CW-INV), cytosolic invertases (C-INV) and vacuolar invertases (V-INV). The hydrolysed products, glucose and fructose, are taken up by hexose transporters which are either present on plasma membrane or vacuolar membrane, the tonoplast (Roitsch & González, 2004).

These sugars are found in several cell compartments like cytosol including mitochondria, vacuole and plastids (Krueger et al., 2011; Fürtauer et al., 2019; Patzke et al., 2019) but mainly sugars are stored in the vacuoles, representing the largest cell organelle (Martinoia et al., 2012). Interestingly, vacuolar sugar levels fluctuate during the diurnal phase, but also in response to developmental demands or onset of various environmental stimuli (Smith & Stitt, 2007; Jänkänpää et al., 2012; Nägele & Heyer, 2013; Fürtauer et al., 2019).

Arabidopsis hexokinase1 (*AtHKK1*) has been identified as a core glucose sensor which perceives glucose signals and mediates different processes (Jang et al., 1997; Yanagisawa et

al., 2003; Moore et al., 2003; Cho et al., 2006). *HXK1* overexpression results in inhibition of photosynthesis related genes, pointing its role in monitoring glucose levels. High glucose levels transport a small amount of HXK1 to the nucleus where it forms complex with proteasome subunit and directly inhibits *chlorophyll A/B-binding protein 2 (CAB2)* (Jang et al., 1997; Cho et al., 2006).

Sucrose is the major form of organic carbon exported from source leaves to sink organs after photosynthesis. Although no direct sensor for sucrose has been identified in *Arabidopsis* yet, the existence of such sensors based on the already demonstrated sucrose-specific signalling pathways have been postulated (Wind et al., 2010; Horacio & Martinez-Noel, 2013). Studies indicate that proteins interacting with sucrose could simultaneously perceive sucrose presence. In *Arabidopsis* Sucrose Phosphate Synthase (*SPS*) is a main regulator of sucrose synthesis in the cytosol. *SPS* enzymes are encoded by four *SPS* genes in *Arabidopsis*. *SPS1F*, *SPS3F* and *SPS4F* are expressed in leaves, stems and flowers whereas, *SPS2F* is solely expressed in roots (Lutfiyya et al., 2007; Volkert et al., 2014). *SPS* mediates sucrose synthesis by formation of sucrose-6-phosphate via UDP-glucose and fructose-6-phosphate which is dephosphorylated to sucrose (**Figure 1.1**) (Huber & Huber, 1996).

Sugars also influence the vegetative and reproductive development of the plant. There have been multiple studies where *Arabidopsis* sugar mutants showed growth and developmental abnormalities (Cheng et al., 2002; Moore et al., 2003; Chen & Jones, 2004). Sugars also induce flowering and control the transition from vegetative to reproductive phase in many species (Cho et al., 2018). Exposure of *Arabidopsis* plants to long day (16 hrs light/8 hrs dark) induces flowering and leads to elevated levels of starch and sucrose (Corbesier et al., 1998).

1.2. Photosynthesis and partitioning of photosynthates

In oilseed *Arabidopsis thaliana*, seed reserves are utilized to initiate heterotrophic germination via gluconeogenesis. 95% of the carbon fuel for gluconeogenesis comes from fatty acids generated after lipid hydrolysis. Autotrophic seedlings can then synthesize their own sugars using carbon dioxide, water and solar energy, the process is known as photosynthesis (A. Baker et al., 2006). Triose-phosphate molecules produced can be stored as starch. These triose-phosphate molecules can also be exported to the cytosol to take part in

glycolysis and synthesize the transport sugar sucrose and its hydrolysed products glucose and fructose (**Figure 1.1**).

Different environmental stimuli like day/night cycles, biotic and abiotic stresses result in the fluctuations of soluble sugars as well as the amount of starch stored, by decreasing or increasing the efficiency of photosynthesis.

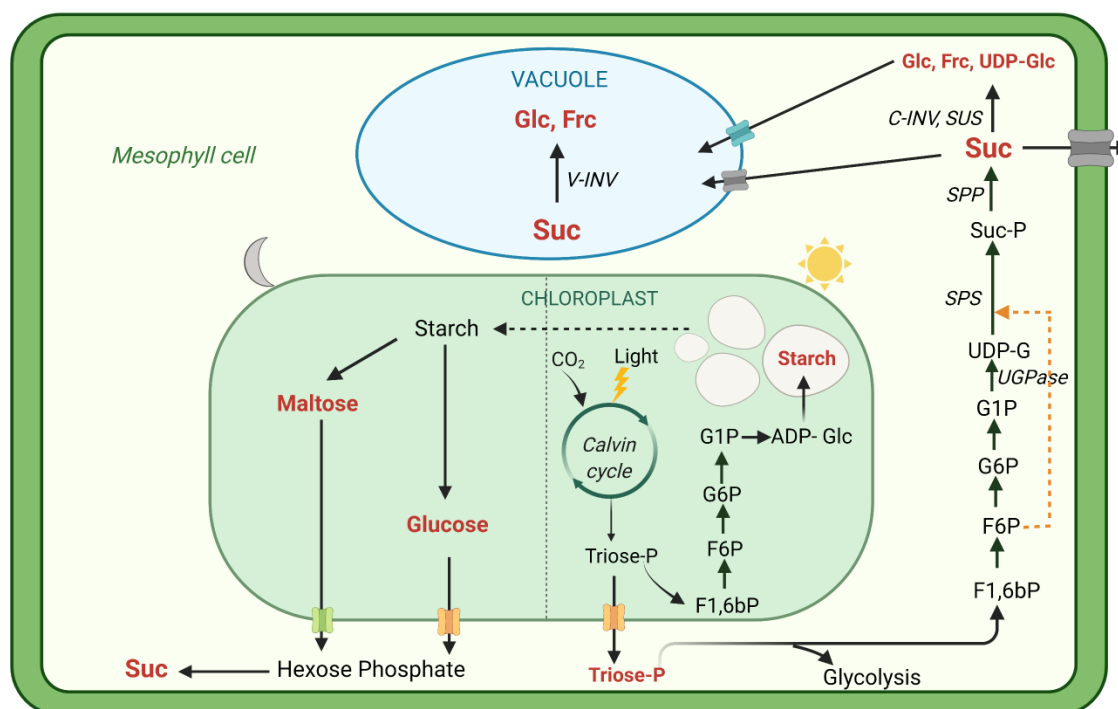


Figure 1.1. Generation of starch and transport sugar sucrose. During the course of photosynthesis, triose phosphate is formed, which after export into the cytosol is converted into UDP-glucose in several reactions and with the participation of various enzymes. Then UDP-glucose and fructose-6-bisphosphate react to sucrose phosphate through sucrose phosphate synthase. Finally, sucrose phosphate phosphatase catalyzes the dephosphorylation of sucrose phosphate, which produces sucrose. As per the demand of the cell sucrose is then hydrolyzed into monosaccharides glucose, fructose or UDP-glucose via cytosolic invertases (cINV) or sucrose synthase (SUS) respectively. Different sugar transporters are present on the tonoplast to transport this sugar in and out of the vacuole. At night the stored starch is degraded, and the degradation products are transported to the cytosol via specialized transporters. *This figure was created with BioRender.com.*

Photosynthate formed in the chloroplast is mainly transported from cytosol to the sink organs in the form of sucrose. The amount of sucrose in the cytosol is determined by two factors:

1. **Carbon import**, involves the import of sugar from chloroplasts to the cytosol
2. **Carbon export**, transport of sucrose from cytosol to other heterotrophic tissues to fulfill their energy demands

Sucrose is loaded into the phloem for distant transport and is then unloaded into the sink tissues (Taiz et al., 2015). For intercellular transport and phloem loading/unloading of sugars different membrane proteins have been identified acting as sugar transporters across membranes. These transporters belong majorly to three transporter families, Monosaccharide Transporters (MSTs), Sucrose Transporters (SUTs) (Schneider et al., 2012; Schulz et al., 2011) and Sugars Will Eventually Be Exported Transporters (SWEETs) (Chen et al., 2010; Eom et al., 2015). Since MSTs and SUTs possess 12 transmembrane domains they belong to Major Facilitator Superfamily (MFS) of transporters while having only seven transmembrane domains SWEETs form a distinct family of transporters.

Sucrose after synthesis is transported from the mesophyll cell to parenchyma cell and then to phloem parenchyma transfer cell (PPTCs). This symplastic movement is aided by plasmodesmata pores present in the plasma membrane. PPTCs are specialized cells harbouring cell wall ingrowths which aid in increasing plasma membrane surface area (Offler et al., 2003; Nguyen & McCurdy, 2015). SWEET11/12 transporters present in PPTCs then transport the sucrose to the apoplast via apoplastic transport. Transporters of the SUT1/SUC2 type take up sucrose and load it into sieve element/companion cell complex of the phloem (Riesmeier et al., 1992; Stadler & Sauer, 1996; Baker et al., 2012) (**Figure 1.2**). Phloem loading rates depend on sugar availability and sink demand (Jiao & Grodzinski, 1996; Grodzinski et al., 1998) as well as on phloem loading capacity, which changes with different environmental stimuli modulating the expression of the corresponding transporter genes (Kühn et al., 1996).

As seen under drought stress, the phloem loading increases by upregulation of SWEET11/12 transporters mediated by increased activity of SnRK2.2, 2.3 and 2.6 resulting in more sucrose export promoting root growth (Chen et al., 2021). In another study, high-light exposure and drought resulted in enhanced sucrose export due to upregulation of SUC2 aided by WAKL8 kinase activation (Q. Xu et al., 2020). On the contrary, phloem sucrose export is reduced when plants are exposed to cold stress. Since cold mediated sugar accumulation in the vacuole and chloroplast resulted in reduced cytosolic sugar fraction (Rodrigues et al., 2020; Wormit et al., 2006).

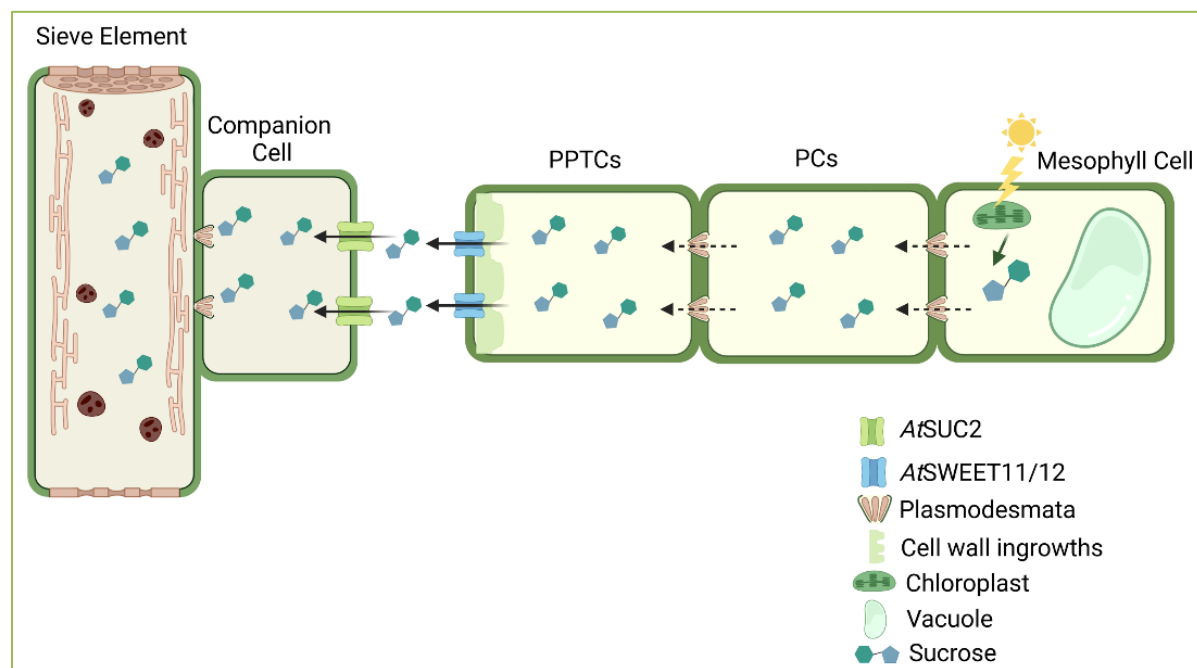


Figure 1.2. Sugar transport and phloem loading. Sucrose synthesized via photosynthesis in the mesophyll cell is transported symplastically into parenchyma cells (PCs) and then to phloem parenchyma transfer cells (PPTCs) through plasmodesmata pores. Depending on endogenous sucrose concentration, part of this sucrose is deposited as cell wall ingrowths in PPTCs and the rest is transported via SWEET11/12 transporters to the apoplast. SUC2 transporters uptake this sugar from the apoplast into companion cells and subsequently to the sieve element for the long-distance transport via phloem. *This figure was created with BioRender.com.*

Sucrose upon reaching the sink tissues via phloem can either be metabolized, cleaved by cytosolic invertases/sucrose synthases or transported to the vacuole where it can be stored/hydrolyzed via vacuolar invertases to glucose and fructose (Ruan, 2014; Vu et al., 2020). From the vacuole these sugars can be transported to the cytosol via different transporters present on the tonoplast.

1.3. Plant vacuole and sugar transporters across tonoplast

With the advancements in cell fractionation and biochemical techniques, specialized vacuolar compartments in cells from various organs were identified (Paris et al., 1996; Fleurat-Lessard et al., 1997; Berthiaume et al., 1995; Webb et al., 1999). The central vacuole occupies a large portion, about 90% of the total cell volume, and is essential for most of the cellular functions (H. Winter et al., 1994). Among many functions like, protoplasmic homeostasis, metabolic product storage, xenobiotic sequestration, and cytoplasmic constituent digestion, its main role is in turgor maintenance which is also justified by its large volume (Martinoia et al., 2007). Most of the sugars are also stored in the vacuoles and are mobilized by the presence of specific

transport proteins present on the vacuolar membrane, the tonoplast. These transport processes are mostly energized and requires movement of solutes against the concentration gradient in a counter exchange of a proton. This is accomplished mostly via vacuolar-type H⁺-ATPase (V-ATPase) and H⁺-translocating inorganic pyrophosphatase (V-PPase) (Sze et al., 1999; Maeshima, 2000; Maeshima, 2001; Drozdowicz & Rea, 2001).

There have been studies which showed the substantial effects on plant growth if vacuolar homeostasis is altered. Overexpression of V-PPase in Arabidopsis is known to increase drought and salt stress tolerance (Gamboa et al., 2013). Reduced expression of V-ATPase A subunit in tomato fruits leads to reduced fruit size and seed number but an increased sucrose composition in tomato fruits (Amemiya et al., 2006).

So far, various proteomic investigations have aided in identification of significant number of distinct tonoplast sugar transporters (Carter et al., 2004; Schmidt et al., 2007; Whiteman et al., 2008a; Whiteman et al., 2008b; Schulze et al., 2012). However, for vacuolar sugar import of glucose, fructose and sucrose, Tonoplast Sugar Transporters (TSTs) and Vacuolar Glucose Transporter1 (VGT1), have been identified (Wormit et al., 2006; Wingenter et al., 2010; Jung et al., 2015; Aluri & Büttner, 2007) both belonging to MST family (Büttner, 2007). TSTs are known to mediate cold specific vacuolar glucose and fructose accumulation and loss of *TST1* and *TST2* abolishes this sugar build up (**Figure 1.3**) (Wormit et al., 2006). Isolated TST1 overexpressing vacuoles demonstrate vacuolar sucrose transport as well (Schulz et al., 2011) however, cold acclimated *tst1-2* double knockout plants show no change in sucrose accumulation as compared to WT.

Considering the fact that maintenance of sugar homeostasis is a coordinated action of vacuolar sugar importers and exporters, vacuole being a temporary storage of sugars also possesses several sugar exporters catalysing sugar export to the cytosol thus maintaining the overall balance. Export of glucose is mediated by Early Responsive to Dehydration6-Like6 (ERDL6) and a glucose facilitator Early Responsive to Dehydration6-Like1 (ESL1) (Poschet et al., 2011; Klemens et al., 2014; Yamada et al., 2010). The two also belong to Early Responsive to Dehydration6-Likes (ERDLs) subfamily of MST family. Sucrose export is mediated by Sucrose Transporter4 (SUT4) (Schneider et al., 2012). Some of the SWEET transporters, SWEET16 and

SWEET17 also reside on tonoplast and mediate glucose, fructose and sucrose flux (**Figure 1.3**) (Klemens et al., 2013; Guo et al., 2014; Chen et al., 2015).

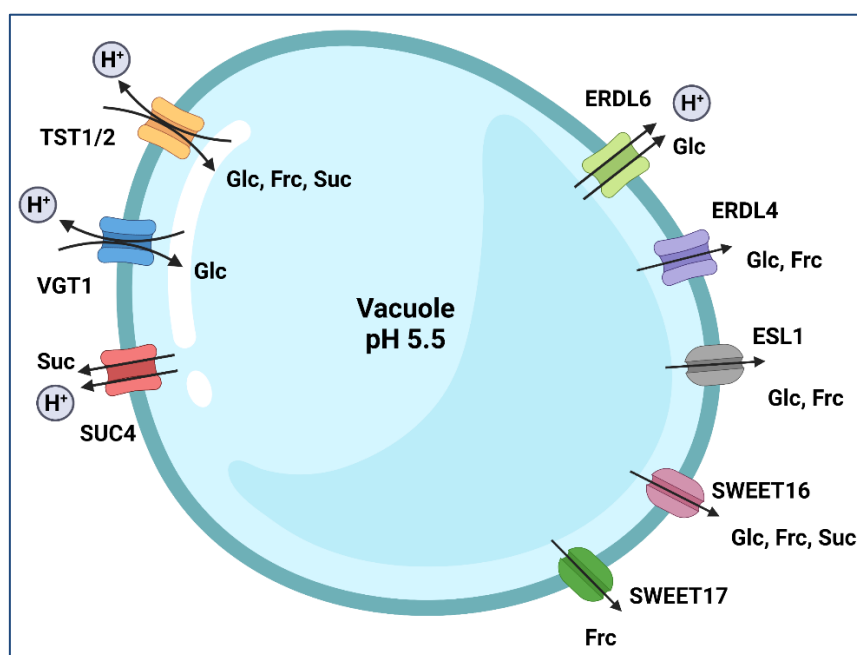


Figure 1.3. Sugar transporters present on the vacuolar membrane. The import of monosaccharides glucose and fructose is mediated via VGT or TST proteins in counter-exchange of a proton H⁺. They both represent subclasses of MST family proteins. TSTs can also mediate sucrose. Export of monosaccharides can be mediated by ERDL6, ESL1 and by the sugar facilitator proteins SWEET16 or SWEET17 belonging to SWEET family, or via sucrose/H⁺ symporter SUC4-type proteins. *This figure was created with BioRender.com.*

1.4. Early Responsive to Dehydration6-Likes (ERDLs) subfamily of MST

Although Early Responsive To Dehydration6-Likes (ERDLs) represent the largest subfamily of Monosaccharide Sugar Transporter family in Arabidopsis having 19 members which share 48-95% similarity with each other but only few members have been functionally characterized. Homologues of Arabidopsis ERDL genes also exist in sugar beet like *BvIMPs*, and they also show high homology with mammalian Glucose Transporters (GLUT) which are facilitators (Chiou & Bush, 1996; Endler et al., 2006; Büttner, 2007). *AtERD6*, the first ERD gene to be identified, has been demonstrated to have similarity to sugar transporters of bacteria, yeasts, plants and mammals. It also possesses 12 transmembrane domains making it a putative sugar transporter and is triggered by dehydration and cold stress. (Kiyosue et al., 1998). ERD6-like 1 (*AtESL1*, At1g08920), is characterized as a low affinity tonoplast localized facilitator having specificity for multiple substrates like glucose, fructose, xylose, mannose and galactose with expression levels fluctuating under abiotic stresses such as salinity and drought (Yamada et

al., 2010). ERD6-like7 (*AtERDL7*, *At2g48020*) is a vacuolar membrane protein and mediated zinc efflux when expressed in yeast cells (Remy et al., 2014). ERD6-Like 6, (*AtERDL6*, *At1g75220*) is a proton coupled vacuolar glucose exporter showing high expression during dark, heat and wounding stress whereas, its downregulation occurs in cold and exogenous sugar supply (Poschet et al., 2011; Klemens et al., 2014). Having such diverse expression patterns, substrate specificity and mode of transport makes this family of transporters a big riddle to solve.

1.5. Fructose synthesis and metabolism

Other than glucose and sucrose, fructose is also a prominent soluble sugar primarily stored in the vacuole. Although it is not as abundant as the other two, but plant vacuole also possesses fructose specific transporters mediating fructose influx and efflux (**Figure 1.3**). Vacuolar fructose serves multiple functions in plants. It is involved in the maintenance of turgor pressure and act as scavengers of oxidative stress (Pontis, 1989; Bogdanović et al., 2008). As it is not present in ample quantities in plants its role might also be to serve as a plant regulatory signalling molecule. This is observed by its interaction with hormones like abscisic acid (ABA) and ethylene where it serves as a signalling molecule in early seedling development (Cho & Yoo, 2011; Li et al., 2011).

Fructose in plants is first produced as a secondary product of photosynthesis. Triose-P transported to the cytosol, where two triose-P molecules are joined to form one fructose 1,6-biphosphate molecule (F1,6BP). Dephosphorylation of F1,6BP yields F6P, which is isomerized to glucose 6-phosphate (G6P). G6P can be used to make sugar nucleotides like UDP-glucose (UDP-G). In a procedure catalysed by sucrose phosphate synthase, UDP-G and F6P are joined to generate sucrose-6-phosphate (sucrose-6P), which is then dephosphorylated to yield sucrose, a non-reducing glucose–fructose disaccharide (Dennis & Blakeley, 2000) (**Figure 1.1**). For efficient utilization of sucrose, it must be cleaved and both sucrose cleaving enzymes, invertases and sucrose synthases, generate free fructose which needs to be phosphorylated. Fructose can be phosphorylated by hexokinases (HXK) or fructokinases (FRK). However, HXKs have lower affinity for fructose than FRKs (Granot et al., 2013). Phosphorylated fructose is processed back into sucrose synthesis aiding in sugar metabolism.

1.6. Sugars in abiotic stress tolerance

These vacuolar sugars also play a significant role during abiotic stresses as well. Due to constantly changing environmental conditions plants have evolved intricate mechanisms to sense and respond to these environmental cues. During different stresses, plants need to reprogram their cell signalling networks to elicit adaptive changes in response to stress (Ahuja et al., 2010; Skirycz & Inzé, 2010; Thao & Tran, 2012). In general, osmotic stresses like drought salinity and low temperature can increase soluble sugars concentration in the vacuole (Strand et al., 1999; Dubey & Singh, 1999). This sugar accumulation helps in reducing the membrane permeability like in case of frost tolerance, by interacting with phospholipids (Klotke et al., 2004; Strauss & Hauser, 1986; Anchooguy et al., 1987). Whereas heavy metal stress and nutrient shortage can decrease sugar concentration. Like in case of *Sassafras* (*Sassafras tzumu*) seedlings, where increasing Cd concentrations decrease soluble sugar content (Gill et al., 2001; Zhao et al., 2021).

Stress signals are perceived and communicated to other compartments by specialized signalling pathways. During stresses solute accumulation in the vacuole is one of the primary responses which can be mediated by change in number or activity of the transporter. Phosphorylation is known to change the proteins functional state hence regulating its activity (Li et al., 2014; Straub et al., 2017). Many tonoplast related proteomic studies highlighted presence of phosphorylated proteins pointing towards phosphorylation dependent regulation of tonoplast intrinsic proteins (Whiteman et al., 2008a; Endler et al., 2009). TST1 which is the major vacuolar sugar importer in Arabidopsis was found to be phosphorylated by a mitogen-activated triple kinase-like protein kinase VIK (Wingenter et al., 2011). During cold stress, loss of VIK in mutant plants, failed to accumulate sugars and showed similar sugar levels like *tst1-2* double knockout (Wingenter et al., 2011). Recently in cotton, CBL-CIPK6 complex was identified to phosphorylate TST2 at Ser⁴⁴⁸ thus regulating sugar homeostasis. Moreover, Ser⁴⁴⁸ is also conserved in Arabidopsis and many other plant species, overexpression of *GhCIPK6* in Arabidopsis plants led to higher sugar accumulation and better dark survival suggesting conservation of this sugar homeostasis pathway across species (Deng et al., 2020).

Furthermore, SNF1-related protein kinase (SnRKs) family of kinases are critical in connecting stress and metabolic responses (Polge & Thomas, 2007; Halford & Hey, 2009; Hey et al., 2009; Coello et al., 2012). SnRK3 or CBL-interacting protein kinases (CIPKs) interact with Calcineurin-

B-like (CBL) calcium-binding proteins and activate a downstream signalling pathway in response to stress by transiently spiking Ca^+ levels which are sensed by CBL-CIPKs complex (Gong et al., 2004; Chae et al., 2009; Weini & Kudla, 2009). CIPKs are known to be involved in mediating responses to drought, cold, sugar and salt stress (Hrabak et al., 2003; Gong et al., 2004; Chae et al., 2009). *MdCIPK13* was recently identified to increase salt tolerance in apple plants by phosphorylating *MdSUT2.2* at Ser²⁵⁴ to enhance its stability and transport resulting in higher sucrose accumulation. Mutation of *MdSUT2.2* at Ser²⁵⁴ with Alanine resulted in less sucrose accumulation in the mutant plants than the plants expressing native *MdSUT2.2* making them less salt tolerant. In another study during drought stress *MdCIPK22* phosphorylates Ser³⁸¹ of *MdSUT2.2* making them more drought tolerant. Overexpression of *MdCIPK22* accumulated more sucrose indicated by esculin uptake in mutant plants and had overall more total sugars which helped in drought stress (Ma et al., 2019a; Ma et al., 2019b).

1.7. Crosstalk between sugar transporters

Plants have evolved several complex regulatory mechanisms to adjust their environment dependent fluctuating needs maintaining normal growth and development. Hence it is reasonable to assume that engineering cellular sugar levels by modifying activities of different sugar transporters would lead to activation of sugar transporters web which eventually act to optimize the sugar levels in the cytosol. However, only few studies have reported the coordinated action of sugar transporters so far.

In cucumber, *CsSUT1* downregulation led to downregulation of Sugar Transport Protein10 (STP10) and Sugar Will Eventually Be Exported Transporter5a (SWEET5a) causing male sterility (Sun et al., 2019). Since alterations in sugar levels have been linked to male sterility (Goetz et al., 2001; Wang & Ruan, 2016) and Arabidopsis STP10 is involved in pollen tube growth (Rottmann et al., 2016), downregulation of these transporters in *CsSUT1*-RNAi lines resulted in under supply of glucose, fructose, sucrose and starch leading to male sterility. Recently, upregulation of *MdERDL6* in apple and tomato mediating glucose export into the cytosol, induced TSTs expression promoting sugar accumulation in leaves and fruits consequently increasing plant height and fruit size (L. Zhu et al., 2021). This is in accordance with the observation that exogenous sugar supply induces TSTs levels (Wormit et al., 2006). Such

synchronized regulation from sugar transporters suggests that sugar homeostasis in plants is maintained by complex interconnected network of sugar transporters.

1.8. Objective of this work

Given the pivotal role sugars play in plant development and in stress survival, our understanding of sugar transport proteins is still limited. Therefore, the current research aims to characterize a member of the ERDLs subfamily, *AtERDL4* (ERD6-like4, At1g19450). The physiological and molecular data has been raised on its localization and expression patterns. To gain deeper insights into function of *ERDL4* in sugar metabolism following questions are dealt with:

- To clarify the question, what should be the role of *ERDL4* in sugar metabolism, we studied the physiological impact of both overexpression and knockout lines of *ERDL4* in Arabidopsis.
- What effects could alter *ERDL4* levels have on the source to sink transport?
- How can sink development be affected by changing cytosolic sugar concentrations?
- How different transporters work in tandem to adjust metabolic imbalances?
- How posttranslational modifications modify transporters activity?
- Furthermore, for the purpose of a deeper understanding the role of *AtERDL4* is examined under various abiotic stress factors e.g., cold and dark.

2. Material and Methods

2.1. Chemicals and kits

The chemicals and enzymes used in the course of this work were obtained from Applichem – ITW Reagents (Darmstadt), Merck (Darmstadt), Sigma-Aldrich (Munich), Roche (Mannheim) and Carl Roth (Karlsruhe).

2.2. Computerized analysis

The gene sequences used in this work were taken from the Aramemnon database (<https://aramemnon.uni-koeln.de/>) and NCBI (<https://www.ncbi.nlm.nih.gov/>). The analysis of DNA sequences was carried out using the BioEdit 7.0.5.3 program (<https://bioedit.software.informer.com/>). In order to quantify the gene expression by means of qRT-PCR, the software Bio-Rad CFX-Manager 3.1 (<https://bio-rad-cfx-manager.software.informer.com/3.1/>) was used for evaluation. The program ImageJ 1.52a (<https://imagej.nih.gov/ij/>) was used for root and silique length calculation.

2.3. Bioinformatics analysis

For multiple sequence alignment Clustal Omega (<https://www.ebi.ac.uk/Tools/msa/clustalo/>) was used. Determination of phosphorylation sites was carried out with NetPhos 3.1 Server (<http://www.cbs.dtu.dk/services/NetPhos/>) and PhosPhAt 4.0 (<http://phosphat.uni-hohenheim.de/phosphat.html>). TMHMM Server V. 2.0 (<http://www.cbs.dtu.dk/services/TMHMM/>) was used for confirmation of transmembrane helices. In order to visualise the secondary structures Protter 1.0 (<https://wlab.ethz.ch/protter/start/>) was used. Cis-acting regulatory elements were determined via Agris-AtcisDB (<https://agris-knowledgebase.org/AtcisDB/>) and PlantCare servers (<http://bioinformatics.psb.ugent.be/webtools/plantcare/html/>).

2.4. Plant specific methods

2.4.1. Plant material

In this work all experiments were carried out on *Arabidopsis thaliana* (*At*) WT plants and transgenic plants in the background of the Columbia (Col-0) and *tst1/2* double knockout, **Table 2.1**).

Table 2.1. Arabidopsis plants used in this study.

| Plants (genotypes) | Resistance | Features | Reference |
|---------------------------------|---------------------------|--|--------------------------|
| Columbia | - | <i>A. thaliana</i> WT | |
| 35S-ERDL4 #1,2 | Kanamycin | Overexpression of <i>ERDL4</i> in WT background CaMV35S-Promotor | Klemens (unpublished) |
| erdl4-1,2 | Kanamycin Sulfadiazine | T-DNA insertion knockout lines of <i>ERDL4</i> <i>erdl4-1</i> (SALK_116041c), <i>erdl4-2</i> (GABI-KAT 600B02) | |
| tst1-2 | BASTA | T-DNA-Insertion double mutant from <i>TST1</i> (At1g20840, SAIL_296_E01) and <i>TST2</i> (At4g35300, SAIL_124_H03) | (Wormit et al., 2006) |
| tst-ERDL4 #5,6 | Kanamycin | Overexpression of <i>ERDL4</i> in <i>tst1/2</i> double knockout background CaMV35S-Promotor | This work |
| 35S:GFP:ERDL4 | Kanamycin | GFP coupled <i>ERDL4</i> overexpression lines in background of WT | Klemens (unpublished) |
| ERDL4_{prom}:GUS | BASTA | <i>ERDL4</i> promoter GUS plants in background of WT | Klemens (unpublished) |

2.4.2. Growth on soil under standard conditions

After the seeds had been stratified for 24 hours at 4°C, the plants were cultivated in climate chamber (Weiss-Gallenkamp, Heidelberg) on standard soil of ED73 type (Patzer, www.einheitserde.de) at a constant temperature of 22°C and a light intensity of 120 $\mu\text{mol photons m}^{-2} \text{s}^{-1}$ (μE) in a 10 h day/14 h night regime (short day).

To obtain seeds and inflorescence stem analysis, plants were grown under standard conditions for four weeks in soil and then transferred to long-day conditions (16 h day/8 h night) at a constant temperature of 22°C and a light intensity of 200 $\mu\text{mol photons m}^{-2} \text{s}^{-1}$ (μE).

2.4.3. Growth under stress conditions

2.4.3.1. Cold acclimation/adaptation

For cold acclimation plants were grown in standard short-day conditions for four weeks and then transferred to 4°C Fitotron climatic chambers (Weiss Technik, Reiskirchen) for three days at a light intensity of 120 $\mu\text{mol photons m}^{-2} \text{s}^{-1}$ (μE) in the 10 h day/14 h night regime. For cold adaptation plants were kept in 4°C for 4 weeks after 4 weeks of growth in standard short days. For cold acclimation kinetics 4 weeks old plants were transferred to 4°C for 3 days and then transferred to standard conditions for 5 days. Samples were collected at the respective time points.

2.4.3.2 Dark recovery

For dark recovery experiments, the plants were grown for five weeks under standard conditions in soil and then exposed to continuous dark for five days at 22°C. After the dark incubation, the plants were allowed to recover for a further seven days in standard conditions.

2.4.4. Surface sterilization of seeds

The seeds were surface sterilized in 1.5 ml Eppendorf tubes with addition of 500 μl of 70% ethanol for 10 min. Followed by centrifugation at 11,000 g for 30 s. Seeds were then sterilised with 5% sodium hypochlorite for 10 min and subsequently washed three times with sterilised water. The supernatant was discarded under sterile conditions and in the last step another 500 μl sterile ddH₂O was added. Seeds were stratified for 2 days in dark at 4°C before the transfer to sterile ½ MS agar plates or liquid medium.

2.4.5. Growth in sterile liquid medium and agar plates

The cultivation of plants in sterile conditions, both on agar plates and in liquid medium was carried out in ½ MS medium (**Table 2.2**). For cultivation on agar plates, surface sterilized seeds were plated out in sterile conditions. For cultivation in sterile liquid culture, each well of a 6-well plate was filled with 6 ml of medium and 25 surface-sterilized and cold stratified seeds were added in each well. The plates were sealed with parafilm and incubated under standard conditions at a constant temperature of 22°C and a light intensity of 120 $\mu\text{mol photons m}^{-2} \text{s}^{-1}$

(μE) in a 10 h day/14 h night rhythm. Growth in liquid medium took place on a shaker at 70 rpm.

For selection of homozygous transgenic plants, appropriate antibiotic was also added to the medium.

Table 2.2. Composition of $\frac{1}{2}$ MS medium

| Reagent | Amount |
|---|-------------|
| Murashige-Skoog Medium (Basal salt mixture) | 2.203 g/l |
| MES | 0.05% (w/v) |
| Sucrose | 0.5% (w/v) |
| pH 5.7 with (KOH) | |
| Plant agar | 0.8% (w/v) |

2.5. Microbiological and molecular biological methods

2.5.1. Bacterial and yeast strains

The bacterial and yeast strains used in the course of this work and their respective information is given in **Table 2.3**.

Table 2.3. Bacterial and yeast strains used

| Bacterial Strain | Resistance | Use | Source |
|---|--|---|--------------------------|
| <i>E. coli</i> XL1 Blue | Tetracyclin | Cloning | (Bullock, 1987) |
| <i>E. coli</i> DH5 α | - | Cloning | (Grant et al., 1990) |
| <i>Agrobacterium tumefaciens</i> (GV3101) | Rifampicin, Gentamycin | Transformation of <i>Arabidopsis thaliana</i> | (Koncz & Schell, 1986) |
| Yeast Strain | Genotype | Use | Source |
| W303 | MAT α trp1-1 ade2-1 leu2-3,112 his3-11,15 ura3 | Heterologous expression | (Ralser et al., 2012) |
| EBY.VW-4000 | trp1-289 leu2-3,112 ura3-52 his3- Δ 200, MAL2-8c, SUC2, Δ gal2, Δ agt1, Δ stl1, Δ mph2, Δ mph3, Δ hxt1-17 | Heterologous expression | (Wieczorke et al., 1999) |

2.5.2. Cultivation of bacteria

Culturing of *E. coli* was carried out overnight, under aerobic and sterile conditions at 37°C either on LB agar plates or in LB liquid medium with appropriate antibiotics for selection at 170 rpm (**Table 2.4**).

Table 2.4. Composition of LB medium

| Reagent | Amount |
|------------------|------------|
| Yeast Extract | 0.5% (w/v) |
| Pepton | 1% (w/v) |
| NaCl | 0.5% (w/v) |
| pH 7.0 with NaOH | |
| Agar | 1.5% (w/v) |

For cultivation of *Agrobacterium tumefaciens*, the bacteria were allowed to grow under sterile conditions on YEB agar plates, for at least three days, or liquid YEB medium overnight at 30°C (**Table 2.5**).

Table 2.5. Composition of YEB medium

| Reagent | Amount |
|-------------------|------------|
| Beef Extract | 0.5% (w/v) |
| Yeast Extract | 0.1% (w/v) |
| Pepton | 0.5% (w/v) |
| Sucrose | 0.5% (w/v) |
| MgSO ₄ | 2 mM |
| Agar | 1.5% (w/v) |

In addition, appropriate antibiotics were also added to the YEB medium depending on the plasmid-mediated resistance. An overview of the concentration of the antibiotics used for selection is given in (**Table 2.6**). For later use recombinant bacterial cells were stored from overnight cultures in 15 % (v/v) glycerol at -80°C.

Table 2.6. Antibiotics and their respective concentration

| Antibiotic | Stock Solution | Final Concentration in Medium |
|---------------|---------------------------------|-------------------------------|
| Ampicillin | 100 mg/ml in 50% EtOH | 200 µg/ml |
| Tetracyclin | 5 mg/ml in 50% EtOH | 10 µg/ml |
| Spectinomycin | 50 mg/ml in ddH ₂ O | 50 µg/ml |
| Gentamycin | 25 mg/ml in ddH ₂ O | 25 µg/ml |
| Streptomycin | 150 mg/ml in ddH ₂ O | 12.5 µg/ml |
| Rifampicin | 25 mg/ml in 100% MeOH | 100 µg/ml |
| Kanamycin | 100 mg/ml in ddH ₂ O | 25 µg/ml |
| Zeocin | 100 mg/ml in ddH ₂ O | 50 µg/ml |

2.5.3. Vectors and plasmids

Plasmids used in this study are listed in **(Table 2.7)**.

Table 2.7. Plasmids used in this study

| Plasmid | Resistance | Use | Reference |
|--------------|---|--|--------------------------|
| pBSK | Ampicillin | Cloning | (Bullock, 1987) |
| pHannibal | Ampicillin | Cloning | (Wesley et al., 2001) |
| pART27 | Spectinomycin (Bacterial), Kanamycin (Plant) | Overexpression Lines (tst1/2), CaMV35S-Promotor | (Gleave, 1992) |
| pDONR™/Zeo | Zeocin | Gateway cloning | Thermo Fisher Scientific |
| pK7FWG2 | Spectinomycin (Bacterial), Kanamycin (Plant) | CaMV35S-GFP Fusion, Gateway™ | (Karimi et al., 2002) |
| pK2GW7 | Spectinomycin (Bacterial), Kanamycin (Plant) | Overexpression Lines (WT), 35S-Promotor, Gateway™ | (Karimi et al., 2002) |
| pGPTV-Bar | Basta | Promotor GUS Analysis | (Becker et al., 1992) |
| pGWFD196 | Ampicillin | C-Terminal GFP fusion, Gateway™ Shuttle vector, URA3 | (Li et al., 2008) |
| pDRf1-GW | Ampicillin | 2-NBDG assay, Gateway™ Shuttle vector,URA3 | (Loqué et al., 2007) |
| pGem-HE-Juel | Ampicillin | Expression in <i>Xenopus laevis</i> oocytes | (Liman et al., 1992) |

2.5.4. Oligonucleotides

The oligonucleotides used for genotyping, cloning, qRT-PCR expression analysis and sequencing are mentioned in **(Table 2.8, 2.9, 2.10, 2.11)** respectively.

Table 2.8. Primers used for genotyping of knock out mutants

| Primer | Sequence (5'→3') |
|--|---------------------------|
| Genotyping of knock out mutants | |
| <i>Salk_LP</i> | ATATGTGAGCGAACATGGGAC |
| <i>SALK_LBb1.3</i> | ATTTTGCCGATTCGGAAC |
| <i>SALK_RP</i> | TTGCAAATGATATCGAAAGCC |
| <i>GK_Fwd</i> | ATGAGTTTTAGGGATGATAATACGG |
| <i>GK_LBP</i> | CCCATTGGACGTGAATGTAGACAC |
| <i>GK_Rev</i> | TCATCTGAACAAACCTTGGATC |
| <i>ERDL4_F</i> | ATGAGTTTTAGGGATGATAATAC |
| <i>ERDL4_R</i> | TCATCTGAACAAAGCTTGGATCTC |
| <i>Ef1-Alpha_F</i> | GAGACCACCAAGTACTACTGCAC |
| <i>EF1-Alpha_R</i> | GTTGGTCCCTTGACCAGTCAAG |

Table 2.9. Primers used for cloning

| | Primer | Sequence (5'→3') |
|--|-----------------------|--|
| Cloning | | |
| <i>GFP</i> | <i>ERDL4_gw_F</i> | ggggacaagttgtacaaaaaagcaggcttaATGAGTTTTAGGGATGATAATACG |
| | <i>ERDL4_gw_R</i> | ggggaccactttgtacaagaaagctgggtaTCTGAACAAAGCTTGGATC |
| <i>GUS</i> | <i>ERDL4_gus_for</i> | TCTAGAT TCAATATCAACGAGGTAGCG |
| | <i>ERDL4_gus_rev</i> | TCCCTCTT CCCGGG TATCATCC |
| <i>Overexpression in WT background</i> | <i>ERDL4_Fwd</i> | ggggacaagttgtacaaaaaagcaggcttaATGAGTTTTAGGGATGATAATACG |
| | <i>ERDL4_Rev</i> | ggggaccactttgtacaagaaagctgggtaTCATCTGAACAAAGCTTGGATCTC |
| <i>Overexpression in tst1/2 background</i> | <i>ERDL4_Xho_s</i> | ctcgag aacaATGAGTTTTAGGGATGATAATACG |
| | <i>ERDL4_Bam_as</i> | ggatcc TCATCTGAACAAAGCTTGGATCTC |
| <i>Heterologous expression in yeast</i> | <i>ERDL4_gw_F</i> | ggggaccactttgtacaagaaagctgggtaTCTGAACAAAGCTTGGATC |
| | <i>ERDL4_gw_R</i> | ggggaccactttgtacaagaaagctgggtaTCTGAACAAAGCTTGGATC |
| <i>Expression in Xenopus oocytes</i> | <i>ERDL4BamH1_Fwd</i> | GGATCC ATGAGTTTTAGGGATGATAATACG |
| | <i>ERDL4Xba1_Rev</i> | TCTAGAT TCATCTGAACAAAGCTTGGATCTC |

Table 2.10. Primers used for qRT-PCR expression analysis

| Primer | Forward (5'→3') | Reverse (5'→3') | |
|------------------------------------|----------------------------|---------------------------|-----------|
| qRT-PCR Expression Analysis | | | |
| <i>AtActin2</i> | AATCACAGCACTTGACCAAGC | CCTTGGAGATCCACATCTGCTG | At3G18780 |
| <i>AtSAND</i> | AACTCTATGCAGCATTGATCCACT | TGATTGCATATCTTTATCGCCATC | At2G28390 |
| <i>AtPP2A-A3</i> | TAACGTGGCCAAAATGATGC | GTTCTCCACAACCGCTTGGT | At1G13320 |
| <i>AtERDL4</i> | TGGAGTTGGCGTTGTTTCAGGTAG | GGATAAAGCAGGTCGTGCGGCTT | At1G19450 |
| <i>AtERDL6</i> | GGTCGTCGGCTTCTGCTTACTATC | GCCTTGAATTGTTGCAGCTGCT | At1G75220 |
| <i>AtTST1</i> | TTGCCGGCGAATTCTACTAAAAGAG | CAAGGATGGGACAATGCCACCA | At1G20840 |
| <i>AtTST2</i> | CATGGATCTTTCTGGTGAAGGAC | GATAAGACCGCGTGCACAATGC | At4G35300 |
| <i>AtVGT1</i> | TCGAGGCAAATGCTTGAAAGCTC | CCAACAGATAACTGGGCAACCAA | At3G03090 |
| <i>AtVGT2</i> | ATGCACCATCAATACTGCAGACC | CAGGTGATGCAACAAGGGTCTCA | At5G17010 |
| <i>AtSweet16</i> | GAGATGCAAACCTCGCGTTCTAGT | GCACACTTCTCGTCGCACA | At3G16690 |
| <i>AtSweet17</i> | AGTGACAACAAAAGAGCGTGAAATAC | ACTTAAACCGTTGCTTAAACCAACC | At4G15920 |
| <i>AtCAB1</i> | TACTTGCGCCACACTCTCACC | TTCCGGTCAAAGCAGGAGAGG | At1G29930 |
| <i>AtNR1</i> | CTGAGCTGGCAAATTCCGAAGC | TGCGTGACCAGGTGTTGTAATC | At1G77760 |
| <i>AtSUC2</i> | TAGCCATTGTCGTCCTCAGATG | ACCACCGAATAGTTCGTCGAATGG | At1G22710 |
| <i>AtABI4</i> | GGTCCGTACGGTATCCCTTT | GGTGTGGAATTGTCCCATC | At2G40220 |
| <i>AtVIK</i> | ATGGCTCTGAAGTATTCAAGC | TCTTGAGAATGTCCAGAAACGACG | At1G14000 |
| <i>AtCIPK6</i> | CGTCGTTTGTGTCGTGGAAGTG | TGCTTCGTGACGCAACATATCGG | At4G30960 |
| <i>AtSAG13</i> | AGGGAGCATCGTCTCATATCC | CCAGCTGATTCATGGCTCCTTTG | At2G29350 |
| <i>AtDIN2</i> | ACCACCATGTGGAATGGAAACTG | TTTCGTAAGCCTCCGGGTGTG | At3G60140 |

Table 2.11. Primers used for sequencing

| Primer | Forward (5'→3') |
|-------------------|-----------------------|
| Sequencing | |
| <i>T3</i> | AATTAACCCTCACTAAAGGG |
| <i>T7</i> | TAATACGACTCACTATAGGG |
| <i>M13_F</i> | GTA AACGACGGCCAG |
| <i>M13_R</i> | CAGGAAACAGCTATGAC |
| <i>attB1</i> | CAAGTTTGTACAAAAAAGCAG |
| <i>attB2</i> | CCACTTTGTACAAGAAAGC |

2.5.5. Isolation of gDNA from *A. thaliana*

To isolate genomic DNA, fresh leaf material was homogenised with 500 µl of shorty extraction buffer (**Table 2.12**) in a 1.5 ml eppendorf tube and inverted several times. Samples were centrifuged at 20,000 g and 4°C for 5 min. 350 µl of the supernatant was transferred to a new 1.5 ml eppendorf tube with 350 µl of isopropanol and mixed gently by inverting 4-5 times. The samples were then centrifuged for 10 min at 20,000 g and 4°C and the supernatant was discarded. The pellet was washed with 500 µl of 70% ethanol. Samples were then centrifuged

again for 10 min at 20,000 g and 4°C and the supernatant was discarded. The pellet was air dried at room temperature with an open lid and subsequently the genomic DNA was re-suspended in 50 µl of ddH₂O.

Table 2.12. Composition of shorty extraction buffer

| Reagent | Concentration |
|-----------------|---------------|
| Tris | 200 mM |
| LiCl | 400 mM |
| EDTA | 25 mM |
| SDS | 1% (w/v) |
| pH 9.0 with HCl | |

2.5.6. DNA amplification by PCR

To amplify DNA sequences, either Pfu polymerase synthesized within the working group or S7 Fusion polymeraseTM from Mobidiag (www.mobidiag.com) was used according to the manufacturer's instructions. The DNA was amplified in a thermal cycler (Biometra). The composition of the 10x Pfu reaction buffer is listed in **(Table 2.13)** and the details of the Pfu PCR approach can be found in **(Table 2.14)**. The PCR program used for DNA amplification with Pfu polymerase is given in **(Table 2.15)**.

Table 2.13. Composition of Pfu reaction buffer

| Reagent | Concentration |
|---|---------------|
| Tris | 200 mM |
| KCl | 100 mM |
| (NH ₄) ₂ SO ₄ | 100 mM |
| MgSO ₄ | 20 mM |
| Triton®X-100 | 1% (v/v) |
| BSA | 1 mg/ml |
| pH 8.8 with HCl | |

Table 2.14. Pfu PCR reaction setup

| Reagent | Volume [μ l] |
|-------------------------|---------------------|
| DNA | 0.5 – 1 |
| Pfu-buffer (10X) | 6 |
| dNTPs (10 μ M) | 6 |
| Forward Primer (100 mM) | 0.5 |
| Reverse Primer (100 mM) | 0.5 |
| Pfu-Polymerase | 0.9 |
| ddH ₂ O | Add upto 60 μ l |

Table 2.15. PCR program used for Pfu polymerase

| Step | Temperature [$^{\circ}$ C] | Time [s] | Cycles |
|----------------------|-----------------------------|----------|--------|
| Initial denaturation | 95 | 150 | } 35X |
| Denaturation | 95 | 30 | |
| Annealing | 52 - 60 | 30 | |
| Elongation | 72 | 120/Kb | |

2.5.7. Agarose gel electrophoresis and DNA gel extraction

To separate the different DNA fragments amplified by PCR according to their sizes, agarose gel electrophoresis was used. Appropriate amount of 6x loading dye (Thermo Fischer Scientific) was added to the PCR sample first. The samples were then loaded onto 1% agarose gel (w/v) in 1 x Tris-acetate EDTA (TAE) - Buffer (**Table 2.16**) with addition of 0.005% ethidium bromide (v/v). GeneRuler™ DNA Ladder Mix (Thermo Fischer Scientific) was used as a marker and 1 x TAE buffer as the running buffer. The gel was then run at a constant voltage of 120V for about 30 minutes and analyzed with UV trans-illuminator (BioDocAnalyze, Biometra).

Desired DNA fragment from the agarose gel was cut with the gel cutter and extracted with the NucleoSpin® Gel and PCR Clean-up kit (Macherey-Nagel) according to manufacturer's protocol.

Table 2.16. Composition of 1X TAE buffer

| Reagent | Concentration |
|-------------|---------------|
| Tris | 40 mM |
| Acetic acid | 20 mM |
| EDTA | 1 mM |

2.5.8. Determination of nucleic acid concentration

To determine the nucleic acid concentration 1 μ l sample was analyzed with NanoPhotometer® N50 (Implen).

2.5.9. DNA sequencing analysis

For the sequencing of the plasmids, the samples were prepared according to the Sanger protocol from SEQ-IT (Kaiserslautern).

2.5.10. Production of competent *E.coli* cells and their transformation

Chemically competent *E. coli* cells were prepared using the Rubidium chloride method (Hanahan, 1983). For this purpose, 20 ml LB medium (**Table 2.4**) was inoculated with bacterial cells and was allowed to grow for at least 12 h at 170 rpm and 37°C (starter-culture). For the main culture, 250 ml of ψ B medium (**Table 2.17**) was inoculated with 2.5 ml of the starter-culture and incubated at 170 rpm and 37°C to an OD₆₀₀ = 0.5. The bacteria were then placed on ice for 15 min and centrifuged at 3000 g and 4°C for 5 min. After discarding the supernatant, the pellet was re-suspended in 80 ml TFBI (**Table 2.18**) and placed on ice for 15 min. It was then again centrifuged, and the supernatant was discarded. The pellet was re-suspended in 8 ml TFBII (**Table 2.19**). The cells were incubated on ice for 15 min and finally 50 μ l aliquots were prepared from the suspension at 4°C (cold room), which were then frozen in liquid nitrogen and stored at -80°C.

Table 2.17. Composition of ψ B medium

| Reagent | Concentration |
|--------------------------------------|---------------|
| Yeast extract | 0.5% (w/v) |
| Pepton | 2% (w/v) |
| MgSO ₄ ·7H ₂ O | 0.4% (w/v) |
| KCl | 0.075% (w/v) |
| pH 7.6 with KOH | |

Table 2.18. Composition of TFBI medium

| Reagent | Concentration |
|--|---------------|
| KCH ₃ CO ₂ | 30 mM |
| RbCl | 100 mM |
| CaCl ₂ | 10 mM |
| MnCl ₂ | 50 mM |
| Glycerine | 15% (v/v) |
| pH 5.8 with Acetic acid (Filter Sterilize) | |

Table 2.19. Composition of TFBII medium

| Reagent | Concentration |
|-------------------------------------|---------------|
| MOPS | 10 mM |
| RuCl | 10 mM |
| CaCl ₂ | 75 mM |
| Glycerin | 15% (v/v) |
| pH 6.5 with NaOH (Filter Sterilize) | |

The transformation of the plasmids in chemically competent *E. coli* cells was carried out according to the heat-shock mediated transformation. After thawing the aliquots of competent cells for 20 min on ice, 1 µg of plasmid DNA or 1 µl of BP or LR reaction was added to the bacterial cells and incubated on ice for 30 min. The heat shock was then carried out at 42°C for 45 s and the bacteria were then cooled on ice for 2 min. 225 µl of ψB medium (**Table 2.17**) was added to the cells and the cells were allowed to grow for 1 hour at 37°C at 170 rpm. After 1 hour 20, 100 and 200 µl of cells were plated in LB agar plates with suitable antibiotics.

2.5.11. Production of competent *Agrobacterium tumefaciens* cells and their transformation

In order to produce chemically competent *A. tumefaciens* cells, a starter culture was first set up with 20 ml YEB medium (**Table 2.5**) with the appropriate antibiotics and inoculated with bacterial cells. The cell culture was allowed to grow for at least 12 h at 170rpm and at 30°C. For the main culture, 2 ml of the starter culture was added to 200 ml of YEB medium with appropriate antibiotics and grown at 30°C and 170rpm to an OD₆₀₀ = 0.5. The cells were then centrifuged at 3000 g and 4°C for 10 min. The pellet was re-suspended in 50 ml TE buffer (**Table 2.20**) and was again centrifuged. The supernatant was discarded, and the pellet was re-suspended in 20 ml of YEB medium with appropriate antibiotics. 500 µl aliquots of the cells

were prepared from the suspension and frozen in liquid nitrogen, which were then stored at -80°C.

Table 2.20. Composition of TE buffer

| Reagent | Concentration |
|-----------------|---------------|
| Tris | 10 mM |
| EDTA | 1 mM |
| pH 7.5 with HCl | |

The transformation in *A. tumefaciens* was performed using the freeze/thaw method. After the aliquots had been thawed on ice for 2 hours, 1 µg of plasmid DNA was added to the cells. The cells were then placed on ice for 5 min and then freeze in liquid nitrogen for 5 min. Followed by incubation at 30°C (5 min), 1 ml of YEB medium (**Table 2.5**) was added and the cells were allowed to grow for 4-6 h at 30°C and 190 rpm. Finally, 300µl of the cells were plated out on YEB agar plates with the appropriate antibiotics and the plates were incubated for 2-3 days at 30°C.

2.5.12. Yeast growth and transformation

Yeast cells were cultivated either in yeast extract-peptone-dextrose (YPD) medium (**Table 2.21**) or synthetic complete (SC) medium (**Table 2.22**).

Table 2.21. Composition of YPD medium

| Reagent | Concentration |
|---------------|---------------|
| Yeast Extract | 1% |
| Pepton | 2% |
| Glucose | 2% |

Table 2.22. Composition of SC medium

| Reagent | Concentration |
|--|---------------|
| YNB with NH ₄ SO ₄ | 0.67% |
| Glucose | 2% |
| Amino acids | 100 mg/L |

Saccharomyces cerevisiae strain W303 was transformed according to the Lithium acetate/single-stranded carrier DNA/Polyethylene glycol (LiAc/ssDNA/PEG) method (Gietz & Schiestl, 2007). To achieve this, a yeast pre-culture (2-5 ml) was grown overnight in permissive or selective conditions at 30°C. The overnight culture was diluted to a final concentration of 5×10^8 cells/ml in SC medium. Cells were pelleted down at 13,000 *g* for 30 s. The pellet was washed with 1 ml of ddH₂O and following centrifugation the supernatant was discarded. The following reagents were then added to the pellet in the same order as indicated (**Table 2.23**). The homogenate was vortexed to ensure complete suspension and incubated for 90 minutes at 42°C in waterbath. The cells subsequently harvested by centrifugation, were re-suspended in ddH₂O and spread on plates with selective media.

Table 2.23. Setting up of yeast transformation reaction

| Reagent | Amount [μl] |
|---|--------------------------------|
| 50 % PEG | 240 |
| 1 M LiAc | 36 |
| ssDNA (denatured prior to use, 2 mg/ml) | 50 |
| plasmid DNA | X (up to 1 μg) |
| ddH ₂ O | X (up to 360 μl, final volume) |

2.5.13. Cloning and expression of *ERDL4* and uptake of radiolabelled solutes in *X.laevis* oocytes

The preparation and injection of *X. laevis* oocytes were performed as described by (Aguero et al., 2018) with little modifications. For this purpose, the oocytes were ordered from Ecocyte Bioscience (Oespeler Kirchweg, Dortmund, <https://ecocyte.net>). *ERDL4* cDNA was amplified with the primers harboring *BamH1* and *Xba1* restriction enzyme sites (**Table 2.9**) and then cloned into corresponding sites of vector pGem-HE. Capped RNA (cRNA) required for the safe delivery and integration of RNA, was synthesized via mMACHINE™ T7 Transcription Kit (Invitrogen, Thermo Fisher Scientific) according to manufacturer's protocol. cRNA was injected using nano-injector (Nano Liter 2010, World Precision Instruments, www.wpiins.com) at 25 ng / 27.6 ml of *ERDL4* or RNase-free water (as a control) per oocyte. For uptake studies, eight to 10 injected oocytes were incubated for 1 h in 200 ml of oocyte Ringer buffer medium (**Table 2.24**) supplemented with 1 mM of cold sugars including 2.5 μCi/ml ¹⁴C-labeled sugar. After 1 h, uptake was stopped, oocytes were washed four times with 4 ml of ice cold Ringer buffer and single oocytes were transferred in scintillation vials. Each oocyte was

lysed with 100 ml of 10% (w/v) SDS for 1 h, scintillation cocktail was added and subsequently radioactivity was quantified in a scintillation counter.

Table 2.24. Composition of oocyte Ringer buffer medium

| Reagent | Concentration |
|--------------------------------------|---------------|
| Stock Solution A | |
| HEPES | 5 mM |
| NaCl | 82.5 mM |
| KCl | 2.5 mM |
| CaCl ₂ ·2H ₂ O | 1 mM |
| MgCl ₂ ·6H ₂ O | 1 mM |
| NaOH | 3.8 mM |
| Stock Solution B | |
| Na ₂ HPO ₄ | 1 mM |
| pH 7.8 with NaOH | |

2.5.14. Plasmid isolation from *E. coli*

For sequencing and Gateway™ cloning plasmid isolation was carried out using Nucleospin Plasmid® Kit (Macherey-Nagel, Düren) according to manufacturer's protocol.

For other purposes plasmid isolation was carried out according to the principle of alkaline lysis. For this purpose, 4 ml of overnight culture was pellet down after centrifugation at 5000 rpm for 2 min at 20°C. The supernatant was discarded, and pellet was completely re-suspended in 200 µl P1 buffer (Qiagen, Hilden) containing 1 mg/ml DNase-free RNase. 200 µl of SDS-containing P2 buffer (NaOH) (Qiagen, Hilden) was then added, which supports the alkaline lysis of the cells. The samples were incubated for 5 min at 20°C. Followed by incubation, 200 µl of P3 buffer (Acetic acid) (Qiagen, Hilden), was added to the samples. After careful inverting, the lysate was incubated for 10 min on ice and centrifuged for 20 min at 14000 rpm and 4°C. 550 µl of the supernatant was then transferred to a new centrifuge tube having 385 µl isopropanol. The mixture was centrifuged again for 15 min at 14000 rpm and 4°C. Supernatant was discarded and the resulting pellet was washed with 500 µl of 70% ethanol. Samples were again centrifuged for 5 min at 14000 rpm and 4°C. The supernatant was discarded, and the pellet was dried. Finally, the dry pellet was dissolved in ddH₂O depending on the copy number of the plasmid. For pBSK (high copy number) pellet was dissolved in 40 µl of ddH₂O.

2.5.15. Generation of *ERDL4* overexpression construct in *tst1/2* double knockout background

ERDL4 cDNA was amplified with the primers harbouring *Xho1* and *BamH1* restriction enzyme sites in the sense and antisense primers respectively (**Table 2.9**) and Pfu polymerase to generate the blunt ends. pBSK plasmid was digested with *EcoRV* restriction enzyme to generate blunt ends which then aids in ligation of the PCR product. The ligated product was then transformed in XL1 blue competent cells via heat shock transformation. Positive colonies were selected from Amp/Tet LB plates through blue/white screening of IPTG/X-Gal and confirmed through sequencing.

Next to attach CaMV35S promoter to our cDNA, the cDNA fragment was excised from pBSK plasmid of positive colony via *Xho1* and *BamH1* digestion and inserted to pHannibal vector already digested with the respective enzymes to create the ligation sites. The ligated product was again transformed into XL1 blue competent cells and positive colonies were selected from Amp/Tet plates via blue/white screening.

After confirming the positive colonies with sequencing, the positive pHannibal plasmid was digested with *Not1* and *Pvu1* restriction enzymes to excise our desired fragment and ligated to pART27, the final vector for transformation to *Agrobacterium tumefaciens*, already digested with *Not1* to create the ligation sites. The ligated product was subsequently transformed into XL1 blue competent cells and positive colonies were selected on Spec/Tet with blue/white screening. Colonies were then confirmed via sequencing.

Plasmid from a positive colony was used to transform into *A.tumefaciens* followed by transformation to *Arabidopsis* plants.

2.5.16. Transformation of *A.thaliana* (Floral-dip method)

In order to generate stable transgenic *Arabidopsis* lines by *Agrobacterium*-mediated transformation, the method described by (X. Zhang et al., 2006) was used. The plants were returned to their normal growth conditions after transformation and the seeds were harvested after they reached full maturity and were completely dried.

2.5.17. RNA isolation from *A.thaliana* and cDNA synthesis

The RNA isolation was carried out using the NucleoSpin® RNA Plant Kit (Macherey-Nagel) according to the manufacturer's instructions. 50 mg of fresh plant material was used for this purpose. The RNA was eluted from the column with 40 µl of RNase-free ddH₂O and the concentration was determined with NanoPhotometer® N50 (Implen).

Preparation of cDNA was accomplished by means of qScript™ cDNA Synthesis Kit (Quantabio) according to manufacturer's instructions. 1 µg RNA was used for each sample. The resulting cDNA was then used, after dilution to a factor of (1:10), for expression analysis via qRT-PCR.

2.5.18. Quantitative real time polymerase chain reaction (qRT-PCR)

To perform gene expression analysis CFX96™ Real Time Cycler (Bio-Rad) was used. The gene specific primers for transcript analysis were designed using the QuantPrime website (<https://www.quantprime.de>) and genes *Actin2* (At3G18780), *SAND* (At2g28390) and *PP2A* (At1g13320) served as a reference. A list of the primers used can be found in (Table 2.10). The reaction setup for qRT-PCR is shown in (Table 2.25) and the program used is listed in the (Table 2.26). The gene expression was quantified with the Bio-Rad CFX Manager 3.1 software (<https://bio-rad-cfx-manager.software.informer.com/3.1/>).

Table 2.25. Reaction setup for qRT-PCR

| Reagent | Amount [µl] |
|-------------------------------|-------------|
| ddH ₂ O | 2 |
| PerfeCTa SYBR® Green (Quanta) | 5 |
| Forward Primer [5 mM] | 1 |
| Reverse Primer [5 mM] | 1 |
| cDNA (1:10) | 1 |

Table 2.26. Program used for qRT-PCR

| Step | Temperature [°C] | Time [s] | Cycle |
|----------------------|------------------|----------|-------|
| Initial Denaturation | 95 | 180 | |
| Denaturation | 95 | 10 | 35 x |
| Elongation | 60 | 40 | |

2.5.19. Histochemical analysis by GUS staining

The staining was carried out following the protocol by (Sessions et al., 1999) The plants were incubated for 20 min in ice-cooled 90% acetone. After removal of the acetone, the plants were washed twice with staining buffer (**Table 2.27**) on ice. Thereafter, the staining solution (**Table 2.27**) was added to the plants and the solution was vacuum infiltrated into the plants for 30 min. This was followed by incubation of the plants in staining solution overnight at 37°C in dark. The next day, the plants were de-stained with increasing concentrations of ethanol (20%, 35%, 50%, 70%; 30 min each) and then examined for blue staining via Leica MZ10F modular stereo microscope. Pictures were taken using a Leica DFC420C digital microscope camera (<https://www.leica-microsystems.com/>). The stained plant tissue was stored in the dark in 70% ethanol.

Table 2.27. Composition of GUS staining buffer and solution

| | Reagent | Concentration | |
|---|----------------------------------|---------------|---|
| For staining buffer pH 7.0 with NaOH | NaH ₂ PO ₄ | 100 mM | For staining solution pH 7.0 with NaOH |
| | Calciumhexacyanoferrate (II) | 5 mM | |
| | Calciumhexacyanoferrate (III) | 5 mM | |
| | EDTA | 10 mM | |
| | Triton X-100 | 0.1% (v/v) | |
| | X-Gluc | 2 mM | |

2.5.20. GFP fluorescence analysis

Tobacco and *Arabidopsis* transformed protoplasts were observed for detection of GFP fluorescence via Leica TCS SP52 confocal microscope. The objective used was HCX PL APO 63.0/1.20 oil mot CORR CS objective with a Vis Argon Laser (488nm), the emission wavelength for GFP was set at 495-540nm and chloroplasts auto fluorescence at 651nm-704nm.

2.5.21. Root tissue embedding and cross-sections

For making root cross-sections, GUS stained roots were fixed following the method described by Gallagher & Chang, 1992, in 2% glutaraldehyde prior to embedding. 2% glutaraldehyde was prepared in 50 mM PIPES (pH 7.2). The fixation helps to minimize endogenous GUS activity. After fixation samples were washed 3 times with 50 mM PIPES buffer at room temperature (20 min each). Samples were then dehydrated through a graded series of Ethanol-H₂O 30, 40, 50, 60, 70, 80 and 95% (15 min each) and finally 100% EtOH (3 times, 15 min).

Technovit[®] 7100 (Kulzer GmbH, Wehrheim) hydrophilic resin was used to embed the samples according to the guidelines provided by the manufacturer. Cross-sections were prepared using the microtome (Reichert-Jung 2030) and the pictures were taken using a Leica DFC420C digital microscope camera (<https://www.leica-microsystems.com/>).

2.6. Biochemical analysis

2.6.1. Ethanolic sugar extraction

For sugar extraction, 50 mg of plant material ground into a fine powder in liquid nitrogen was mixed with 500 µl of 80% ethanol (v/v) and then vortexed for 20 s. The samples were incubated in the thermoblock for 30 min at 500 rpm and 80°C. Followed by vortexing, the samples were allowed to cool on ice and centrifuged for 10 min at 16000 *g* and 4°C. 400 µl of the supernatant was transferred to a new 1.5 ml reaction tube out of which 200 µl of the supernatant was evaporated in a vacuum concentrator. Resulting pellet was mixed in 200 µl of ddH₂O. The sugar quantification was carried out using the NADP-coupled enzymatic test (section 2.6.3).

2.6.2. Starch extraction

For the extraction of starch, the remaining pellet from sugar extraction in section 2.6.1 was washed two times with 1 ml of 80% ethanol (v/v) and then centrifuged for 10 min at 16000 *g* 4°C. The supernatant was discarded, and the pellet was dissolved in 1 ml of ddH₂O. The samples were centrifuged again for 10 min at 16,000 *g* and 4°C. The supernatant was discarded and 150 µl of ddH₂O was added to the samples. After autoclaving at 121°C for 20

min the samples were cooled down at room temperature and 150 μ l of enzyme master mix, consisting of α -amylase (Sigma) and Amyloglucosidase (Roche) (**Table 2.28**), was added to the samples. The samples were incubated overnight, or at least 4 hours, at 37°C and 170 rpm. The starch in the extract was broken down into its glucose units. Finally, the samples were heated at 95°C for 10 min to stop the reaction and then centrifuged for 10 min at 16,000 g . The supernatant was transferred to a new reaction tube. The starch quantification was carried out by means of NADP-coupled enzymatic assay (**Section 2.6.3**).

Table 2.28. Composition of enzyme master mix for starch digestion

| Reagent | Concentration |
|---|---------------|
| α -Amylase (<i>Bacillus subtilis</i> , Sigma) | 50 U/ml |
| Amyloglucosidase (<i>Aspergillus niger</i> , Roche) | 6.3 U/ml |
| Sodium Acetate (pH 4.8) | 200 mM |

2.6.3. Sugar quantification

Soluble sugars glucose, fructose and sucrose were quantified following their extraction from plant tissue (section 2.6.1). For that purpose, 190 μ l of premix (**Table 2.29**) was added to the 96 well transparent bottom plate, to which 4-20 μ l of extracted and water solubilized sample was added. The measurement was carried out photometrically at a wavelength of 340 nm in a Microplate Reader Infinite[®] M Nano (Tecan) with the aid of an NADPH-coupled enzymatic assay (**Table 2.30**). The sugar content was determined using the following formula (**Formula 1**).

Table 2.29. Composition of premix for sugar quantification

| Reagent | Concentration |
|---|---------------|
| HEPES (pH 7.5) | 105.1 mM |
| MgCl ₂ | 12.6 mM |
| ATP | 2.5 mM |
| NADP | 1 mM |
| Glucose-6-Phosphate-Dehydrogenase (<i>Leuconostoc</i> , Class II, Roche) | 0.5 U |

Table 2.30. Enzymes used for NADP-coupled enzymatic test

| Enzyme | Amount [μl] |
|---------------------------------------|-------------|
| Hexokinase (Yeast, Roche) * | 1.2 |
| Phosphoglucosomerase (Yeast, Roche) * | 1.2 |
| Invertase (Yeast, Sigma) * | 2 |

*Enzymes were made as a 1:10 dilution in 333 mM HEPES (pH 7.5)

Formula 1. Soluble sugar calculation

$$C_{Glucose} \left[\frac{\mu\text{mol}}{g} \right] = \frac{\Delta E_{Hexokinase-Blank} * V_{Total} * F * V_{Extraction}}{\epsilon_{NADPH} * d * V_{Sample} * m}$$

$$C_{Fructose} \left[\frac{\mu\text{mol}}{g} \right] = \frac{\Delta E_{Phosphoglucosomerase-Hexokinase} * V_{Total} * F * V_{Extraction}}{\epsilon_{NADPH} * d * V_{Sample} * m}$$

$$C_{Sucrose} \left[\frac{\mu\text{mol}}{g} \right] = \frac{\Delta E_{Invertase-Phosphoglucosomerase} * V_{Total} * F * V_{Extraction}}{\epsilon_{NADPH} * d * V_{Sample} * m * 2}$$

$E = Extinction$

$V_{Total} = Total\ volume\ in\ one\ well\ [ml]$

$F = Dilution\ factor\ during\ sample\ preparation$

$V_{Extraction} = Extraction\ volume\ [ml]$

$\epsilon_{NADPH} = Extinction\ coefficient\ of\ NADPH = 6.22 \frac{ml}{\mu\text{mol} * cm}$

$d = 0.51\ cm$

$V_{sample} = Sample\ volume\ [ml]$

$m = Fresh\ weight\ [g]$

2.6.4. Anthocyanin and chlorophyll quantification

Fresh plant material was ground with liquid nitrogen to a fine powder, and extracted with 80% methanol containing 5% HCl overnight at 4°C. After centrifugation at 14,000 g for 20 min, the extracts were transferred to new tubes and the amounts of anthocyanins were quantified photometrically at wavelengths of 530 nm and 657 nm via Microplate Reader Infinite® M Nano

(Tecan) following the equation described by (Mancinelli et al., 1975). The formula for anthocyanin extraction is given below (**Formula 2**).

Formula 2. Anthocyanin calculation

$$A530nm_{corr} = \frac{A530nm - 0.25 * A657nm}{FW [g]}$$

$$FW = \text{Fresh weight of the sample [g]}$$

2.7. Physiological analysis

2.7.1 Root and silique length

To determine the root length, the plants that had previously been cultivated on vertical ½ MS agar plates were scanned and the root length was quantified using the ImageJ software (<https://imagej.nih.gov/ij/>). For determining silique length, mature green siliques from the middle position of the inflorescence stem were harvested for each genotype and photographed. The picture was then analyzed by ImageJ software to calculate the length of the siliques.

2.7.2. Inflorescence length and inflorescence weight

To determine the differences in bolting among different mutants, inflorescence stem lengths were recorded. For this purpose, the plants were cultivated for four weeks under standard short day conditions and then transferred to the long day for flowering induction. As soon as the first plant started to bolt, the length was measured daily until they showed no change in length for 3 consecutive days. Once flowering was complete, the weight of the entire shoot was determined, and the number of lateral stems were counted.

2.7.3. Seeds analysis

2.7.3.1. 1000 Seeds weight

To determine the weight of 1,000 air-dried seeds, harvested at the same time point for all the genotypes, were counted and weighed.

2.7.3.2. Lipid content

To extract total lipids from the seeds, the protocol of Reiser et al., 2004, was used with slight modifications. 0.1 g of air-dried seeds were homogenized in liquid nitrogen in a mortar. 1.5 ml of isopropanol was then added, and the mixture was further homogenized. The suspension was transferred to a 1.5 ml reaction tube and incubated at 4°C and 100 rpm for 12 h. After centrifugation at 13000 *g* for 10 minutes, the supernatant was transferred to a pre-weighed 1.5 ml reaction tube and incubated at 60°C for 12 h in order to completely evaporate isopropanol. The remaining pellet was weighed gravimetrically to determine the total lipids.

2.7.4. Phloem exudate isolation and quantification of soluble sugars

In order to analyze the sugar content in the phloem exudate, the method described by Xu et al., (2019) was used with slight modifications. For this purpose, six-week-old source leaves were cut off from the base of the petiole with a sharp razor blade after exposure to light for 4 hours and the petiole was immediately submerged in K₂-EDTA buffer (20 mM, pH 7.0). 3 leaves per plant were stacked and another 1 mm of the petiole was cut while being submerged under the solution and the leaves were transferred directly to a 0.2 ml reaction tube with 500 µl of the of ddH₂O. Exudates were collected for 6 hours in dark and humid environment. The water was evaporated via vacuum concentrator and then diluted again in 100 µl of ddH₂O. The sugar concentration was then quantified using NADP-coupled enzymatic test (Section 2.6.3).

2.7.5. Electrical conductivity and LT50%

In order to analyze the frost tolerance of plants, the electrical conductivity was determined, which was caused by frost induced ion loss from leaves. For this purpose, the method described by Klemens et al., (2013) was applied with slight modifications. After cultivation on soil for 4 weeks under standard conditions, the plants were acclimated for four days at 4 ° C. A medium-sized leaf was cut off and transferred to a test tube filled with 2 ml of ddH₂O so that the leaf was completely submerged in water. The test tube was cooled down to -1°C in the cryostat for 1 h and then the ice crystals were induced. The ice crystals were formed by dipping a frozen (in liquid nitrogen) wire loop in the water for 5 seconds without touching the leaf material. After a further incubation of 30 min at -1°C the temperature was reduced by 1°C after every 30 min until a temperature of -10°C was reached. The samples were taken at each

increment and thawed on ice at 4°C overnight. The next morning the completely thawed samples were incubated for 24 h at 150 rpm and 4°C 3 ml of ddH₂O was added and the mixture was incubated at 150 rpm and 4°C for a further 30 min. After the samples had reached room temperature, the first measurement of the electrical conductivity was carried out with the conductivity measuring device LF 521 (Wissenschaftliche Werkstätten, Weilheim). It was ensured that the leaf tissue was not destroyed during the measurement. The samples were then boiled for 2 h at 100°C and then cooled down for at least 1 h at 150 rpm and 4°C. The samples were incubated for 30 min at room temperature and the second measurement of the electrical conductivity was taken. To calculate the electrical conductivity, the electrolyte loss from the first measurement was divided by the total electrolyte loss from the second measurement.

2.8. Transcriptomic analysis (RNA-Seq)

RNA sequencing was done with Novogene (UK). The samples were harvested at midday and stored in liquid nitrogen prior to freezing at -80°C. Preparation of RNA was done according to **(Section 2.5.17)**.

3. Results

Different environmental conditions and abiotic stresses lead to altered sugar concentration. These changes are mediated by the controlled regulation of the activities of sugar importers and exporters residing in the vacuolar membrane (Hedrich et al., 2015). In the Arabidopsis Monosaccharide Transporter-Like (MST) family, the least studied subclade is of Early Responsive to Dehydration6-Likes (ERDLs). One of its members, *AtERDL6* (At1g75220) has already been identified as a tonoplast localized Glc exporter (Poschet et al., 2011) and there might be other putative sugar transporters present within the subclade.

The present study describes the molecular and functional characterization of a new member of ERDL subfamily, *AtERDL4* (At1g19450), which is the closest homolog to *AtERDL6*. It is localized on tonoplast and catalyses Glc and Frc export by concomitantly inducing TST2 expression, coding for the major vacuolar sugar loader. Here data is presented on phenotypic characterization, molecular expression and involvement in different abiotic stresses via plants with subsequently elevated and reduced levels of *AtERDL4*.

3.1. Sequence and homology analysis

AtERDL4 is localized on chromosome 1 of Arabidopsis thaliana genome. Data from various databases (e.g., Aramemnon and TAIR) and a comparison with other AtMST members suggests a nucleotide coding sequence of 1,467 bps for ERDL4, having 17 putative exons. Moreover, it encodes a 481-amino acid (a.a) protein and shares 92% of sequence identity with *AtERDL6* (**Figure 3.1 A**). Whereas ERDL6 possesses 480 a.a protein. Evolutionary analysis of all the 19 members of ERDL subfamily revealed that ERDL4 and ERDL6 are homologous and are closest neighbours (**Figure 3.1 B**). Both proteins possess 12 putative transmembrane domains (TMD). Some highly conserved motifs, PESPRWL (TMD 6-7), DKAGRR (TMD 8-9) and PETKG (TMD 12), indicating sugar transport properties, were also found common between the two proteins (Henderson, 1991) (**Figure 3.1 C**).

RESULTS

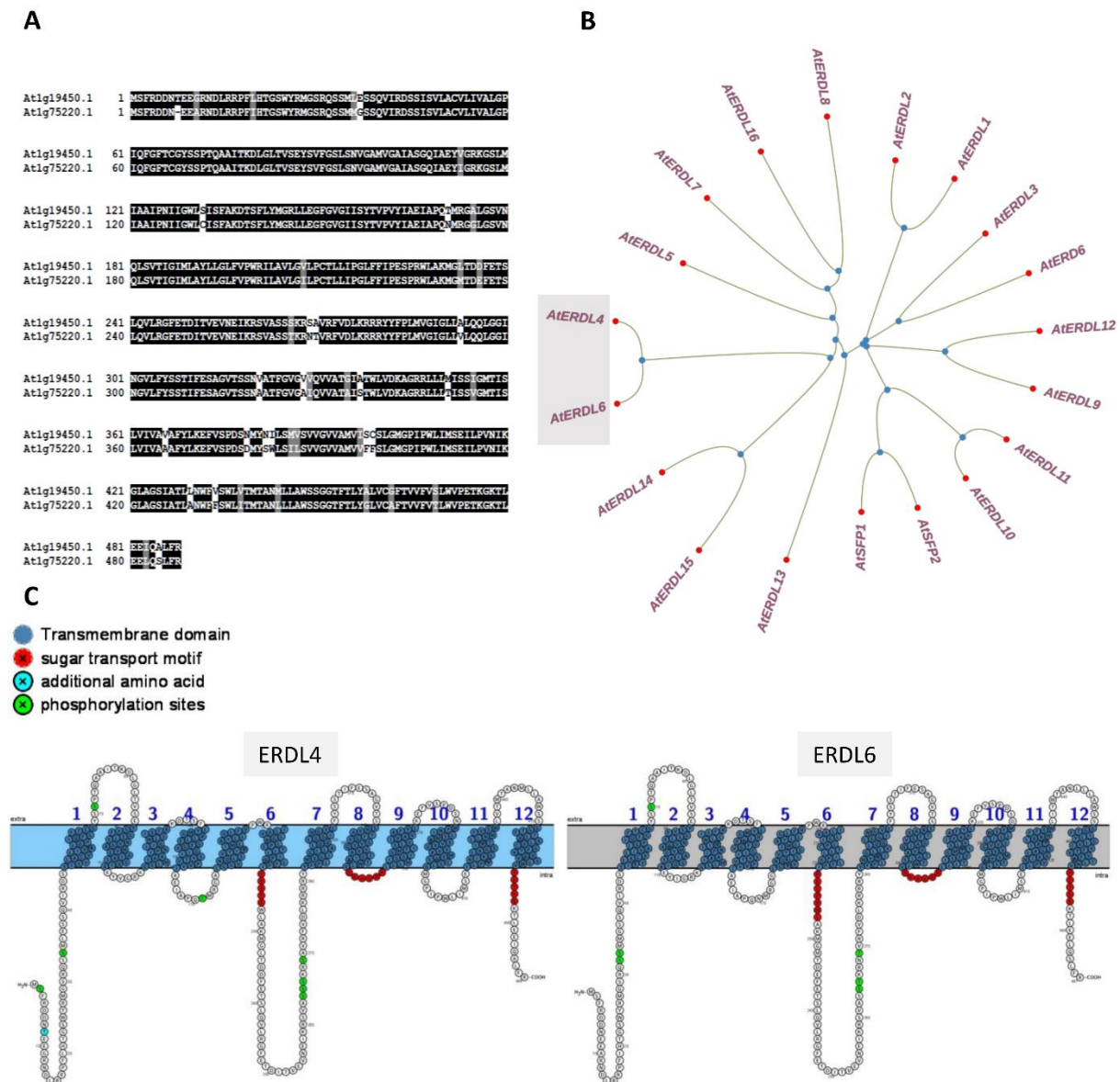


Figure 3.1. A. Multiple sequence alignment of *AtERDL4* and *AtERDL6* protein sequence. *AtERDL4* protein consist of 488 a.a whereas, *AtERDL6* protein is 487 amino acid long. Both exhibiting 92% protein sequence identity (Clustal Omega; <https://www.ebi.ac.uk/Tools/msa/clustalo/>). Shaded alignment is generated using BoxShade software (https://embnet.vital-it.ch/software/BOX_form.html). Black colour shows conserved regions, gray colour indicates a.a substituted with similar characteristics/properties and white colour shows the mutant regions. **B.** Phylogenetic tree is generated using protein sequences of all the 19 members of ERDLs subfamily via neighbor joining method with CLUSTAL alignment and viewed with online tool, interactive tree of life, available at (<https://itol.embl.de/>) (Lutenic and Bork, 2021). **C.** Schematic depiction of the *AtERDL4* (left) and *AtERDL6* (right) protein's secondary structure visualized via the webtool Protter (<http://wlab.ethz.ch/protter/start/>). Transmembrane domains, colored in dark blue, were identified using the tool TMHMM (<http://www.cbs.dtu.dk/services/TMHMM/>). Highly conserved motifs indicating a sugar transport activity of the respective protein are highlighted in red. Putative phosphorylation sites assigned with a score higher than 0.7 detected via the web tool NetPhos 3.1 Server (<http://www.cbs.dtu.dk/services/NetPhos/>) were colored in green and additional a.a in *AtERDL4* is in cyan.

3.1.1. Promoter analysis of *ERDL4*

Promoter region of *ERDL4*, 1000 bp upstream to the start codon, was selected for cis-acting elements analysis. There are consensus sequences within this range that serve as transcription factor recognition sequences. These sequences are referred to as cis-acting elements. Transcription is a dynamic process that responds to the needs of the organism. TATA, CAAT, and GC boxes are the most essential cis-acting elements for RNA polymerase II transcription. The promoter region of *ERDL4* include all three cis-acting elements. Apart from these constitutive cis-acting elements, there are other elements responsible for stress, environmental factors, hormonal-induced, organ, and metabolite specific transcription, present in each promoter at varying frequencies (**Figure 3.2**). In this study, WT and *ERDL4* mutants are being studied under various stresses such as cold and dark for which specific cis-acting elements can be found in the promoter which confirms role of *ERDL4* in these stresses.

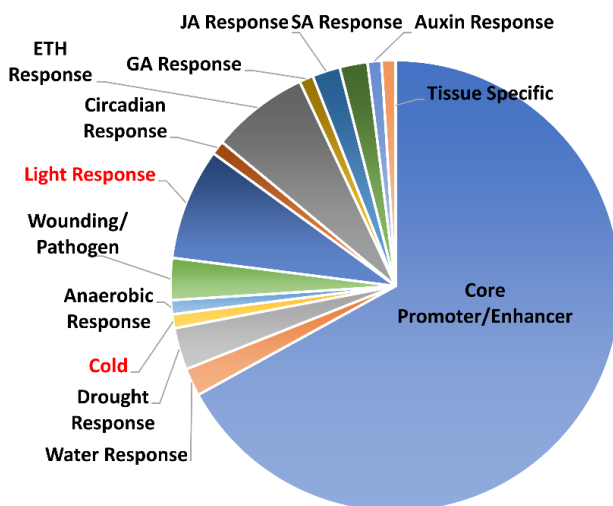


Figure 3.2. Pie distribution of cis-acting elements. Upstream promoter region (1500 bp) of *AtERDL4* was analysed with PlantCare database (<http://bioinformatics.psb.ugent.be/webtools/plantcare>) for identification of cis-acting elements. Pie chart represents the percentage of elements present within the promoter. In red are the elements related to stresses examined in this study.

3.1.2. Subcellular localization of *ERDL4*

Subcellular localization of *ERDL4* was confirmed via transient expression of *ERDL4*-GFP fusion protein in *Arabidopsis* mesophyll protoplasts resulting in a GFP signal (green) that resides on the vacuolar membrane, tonoplast, attached are the chloroplasts (violet autofluorescence) (**Figure 3.3 B-D**). It was further confirmed by the lysis of the protoplasts via mild osmotic shock which

mediated vacuole release and the GFP fluorescence can be seen as a green ring depicting the vacuolar membrane (**Figure 3.3 E-F**).

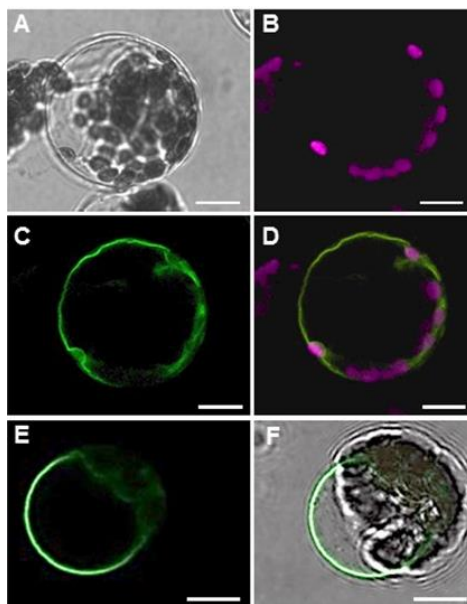


Figure 3.3. Subcellular localization of *AtERDL4-GFP* in *Arabidopsis*. *Arabidopsis* protoplasts (**A to F**) were transiently transformed with an *AtERDL4-GFP* fusion protein construct. After 20 hours of incubation, protoplasts were lysed by mild osmotic shock and analysed by confocal laser scanning microscopy. **A.** Bright-field image of a protoplast after lysis, leaving the intact vacuole with attached chloroplasts. **B to F.** Fluorescence image of a lysed protoplast showing *AtERDL4-GFP* localization to the tonoplast (green) and chlorophyll autofluorescence (magenta) of attached chloroplasts. Bars = 10 μm .

3.1.3. Genotyping and biochemical characterization of *ERDL4* mutants

To investigate the putatively altered vacuolar sugar homeostasis due to altered expression of *ERDL4* in *Arabidopsis*, T-DNA insertion lines of *ERDL4* (*erdl4-1*, SALK_116041C) and (*erdl4-2*, GABI-KAT 600B02) were used for further experimentation (**Figure 3.4 A**). The mutants were first checked for the presence of WT band for *ERDL4* (**Figure 3.4 B**). For this purpose, genomic DNA was extracted from WT and *erdl4* mutant plants and used for PCR analysis using *ERDL4* full-length gene primers. WT band of *ERDL4*, ~3000 bp, was present only in the WT plants whereas, it was disturbed in the mutant plants due to possible T-DNA insertion. *erdl4-1* mutant plants were also checked for the presence of T-DNA insertion via the T-DNA and gene specific primers (**Figure 3.4 C**). T-DNA insertion was confirmed by the presence of T-DNA band in both mutants. To check whether this insertion influenced the transcript expression, *ERDL4* gene was amplified using cDNA which gives the band in WT at ~1500 bp. The full-length transcript

expression failed in *erd14* mutants (**Figure 3.4 D**) confirming the T-DNA insertion in the coding region.

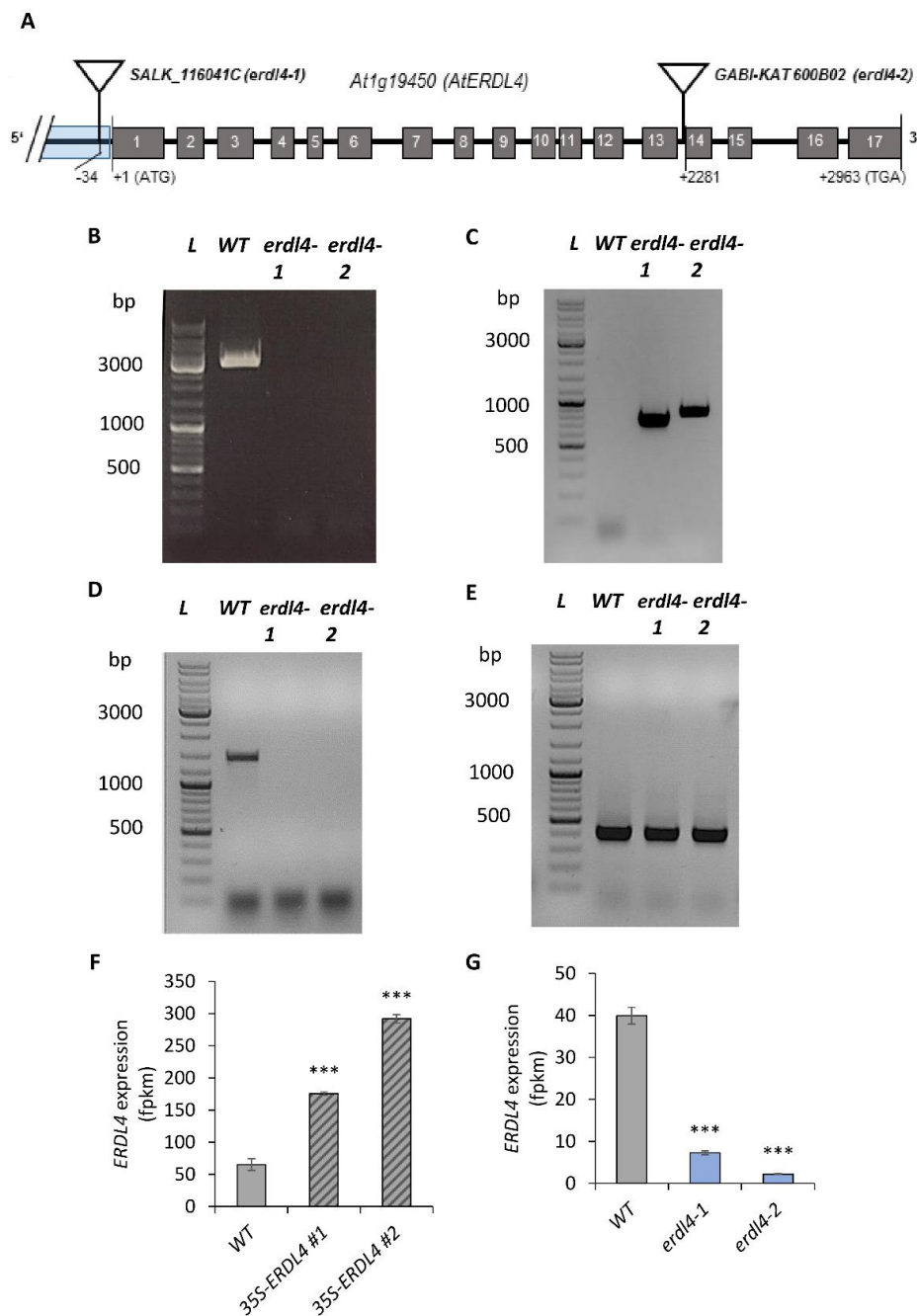


Figure 3.4. Genotyping of Arabidopsis *ERDL4* mutants. **A.** Schematic representation of *ERDL4* T-DNA insertions and promoter GUS region (blue). Boxes represent exons and lines represent introns. **B.** Amplification of *ERDL4* gene from WT and T-DNA mutants gDNA using primers (*ERDL4_F*+*ERDL4_R*) **C.** Confirmation of T-DNA insertion in WT and knockout mutants with primers (LBb1.3+RP for salk line and GK_LBP+GK_Rev for gabi-kat line). **D.** Amplification of *ERDL4* full length transcript from WT and knockout mutants cDNA with primers (*ERDL4_F* + *ERDL4_R*). **E.** Amplification of housekeeping gene (*ef1- α*) from WT and knockout plants cDNA with primers (*EF1-alpha_F*+*EF1-alpha_R*). **F.** Expression of *ERDL4* (FPKM values) in *ERDL4* overexpression lines expressed under a 35S-constitutive promoter in wild type. **G.** Expression of *ERDL4* (FPKM values) in *erd14* knockout mutants.

The expression of *AtEF1- α* was used as a control (**Figure 3.4 E**). *ERDL4* altered expression levels were also confirmed in the *35S-ERDL4* lines and T-DNA mutants with RNA-Seq results (**Figure 3.4 F, G**) which showed increased and reduced expression levels in *35S-ERDL4* and *erdl4* knockout mutants respectively.

3.1.4. Subcellular compartmentation of sugars in *ERDL4* mutants

We were interested to see how changes in *ERDL4* activity affected whole leaf sugar concentration as well as sugar compartmentation within cells. For this purpose, we calculated total glucose, fructose and sucrose contents from source leaves of five weeks old WT and *ERDL4* mutants grown in control conditions and harvested at midday. The analysis revealed that overexpression of *ERDL4* resulted in a significant increase in glucose accumulation in the leaves of *35S-ERDL4* plants (**Figure 3.5 A**). Glucose levels in *35S-ERDL4* #1 and *35S-ERDL4* #2 leaves increased more than twofold from 1.6 moles/g FW in WT to roughly 3.8 and 3.3 moles/g FW, respectively (**Figure 3.5 A**). In the leaves of *erdl4-1* and *erdl4-2* T-DNA mutant plants, glucose levels were decreased to roughly 40% and 45% of wild type levels, respectively. The fructose content of WT and *35S-ERDL4* plants, as well as WT and *erdl4* T-DNA mutants, was unaffected (**Figure 3.5 A**). Sucrose levels in the plants did not change much significantly with the exception of *35S-ERDL4* #1 plants, which had nearly 70% higher sucrose levels than WT (**Figure 3.5 A**).

To examine the subcellular sugars, we did non-aqueous fractionation (NAF) to check the sugar distribution between the chloroplast, the cytosol and the vacuole (Fürtauer et al., 2016; Patzke et al., 2019; Vu et al., 2020). It was observed that by altering *ERDL4* levels, both in the *35S-ERDL4* and the knockout mutants, lead to perturbations in sugar homeostasis between the compartments studied (**Figure 3.5 B-D**). The increase in glucose in the vacuolar and cytosolic fractions of *35S-ERDL4* lines was most noticeable, but it was not the case in the chloroplast fractions. When compared to WT levels, glucose levels in vacuoles increased 3-fold and 2 to 2.5-fold in the cytosolic fraction of *35S-ERDL4* lines. Interestingly, the faint total increase in fructose (**Figure 3.5 A**) in *35S-ERDL4* plants was limited to the cytosolic fraction rather than being distributed equally across the vacuole and the cytosol, as in the case of glucose (**Figure 3.5 C**). The distribution of sugars between compartments in *erdl4* T-DNA mutants did not differ significantly from those in WT with the exception of *erdl4-1* plants, which had much

lower fructose levels in chloroplasts than WT (**Figure 3.5 C**). The results showed that *ERDL4* overexpressing plants exhibited altered sugar transport activities at the vacuolar membrane, implying that *ERDL4* was involved in the export of the monosaccharides glucose and fructose from the vacuole to the cytosol.

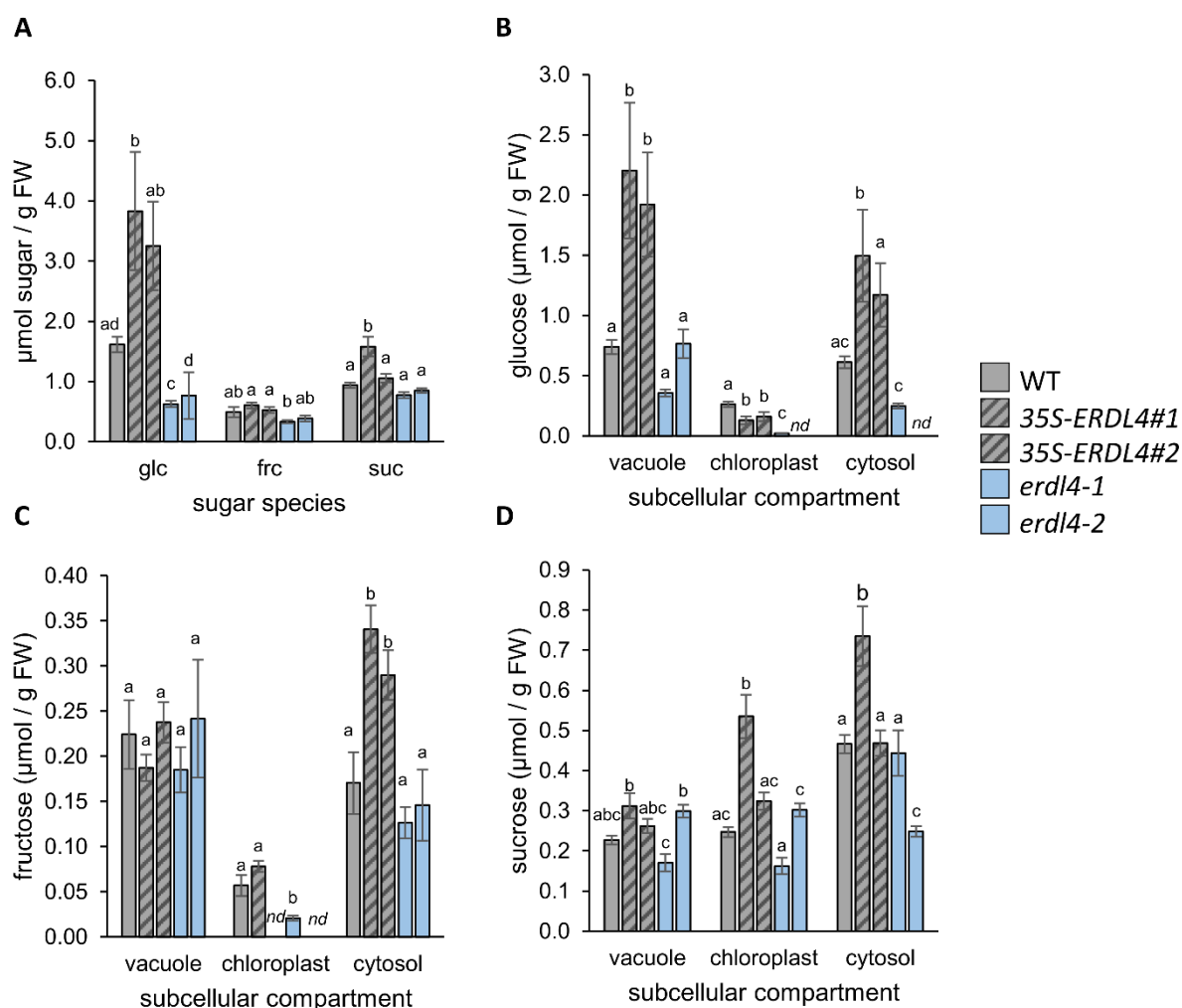


Figure 3.5. Total and subcellular sugar accumulation in WT, *ERDL4*-overexpressing and mutant plants. **A.** Contents of glucose (glc), fructose (frc), sucrose (suc) in shoots. **B-D.** subcellular contents of glucose. **B.** fructose **(C)**, sucrose **(D)** in vacuoles, chloroplast, and cytosolic fractions of shoots from WT, *ERDL4*-overexpressing and mutant plants as obtained by non-aqueous fractionation. Plants were grown in standard condition ($120 \mu\text{mol Photons m}^{-2} \text{s}^{-1}$, 10h light/14h dark, 22°C) in soil and harvested at the end of light phase. Bars represent means from $n=5$ plants \pm SE. Different letters above bars denote significant differences according to *One-Way* ANOVA with post-hoc Tukey test ($p < 0.05$). *nd* = no quantifiable amount detected.

3.1.5. Phenotypic characterization of *ERDL4* mutants

To investigate whether altered sugar compartmentation in *ERDL4* mutants can affect the growth phenotype of the plant, WT and *ERDL4* mutant plants were grown in soil and hydroponics medium for five weeks. The fresh weight of the rosettes from *35S-ERDL4* lines

was significantly increased as compared to WT while that of *erd14* mutants was significantly reduced (**Figure 3.6 A, B, C**). WT had a fresh weight of 0.37 g whereas, the weight of 35S-ERDL4 #1 and 35S-ERDL4 #2 was 0.5 g and 0.55 g respectively. Both T-DNA mutants had fresh weight of 0.3 g. Roots harvested from plants grown in hydroponics medium also showed similar changes in dry weight (**Figure 3.6 B, D**). Roots from 35S-ERDL4 lines were longer and had increased dry weight, 0.008 g and 0.01 g, as compared to WT which showed dry weight of 0.005 g. Dry weight of roots from knockout mutants was reduced to 0.003 g but it was not significant. The data showed that elevated cytosolic sugars in 35S-ERDL4 plants contribute in increased biomass.

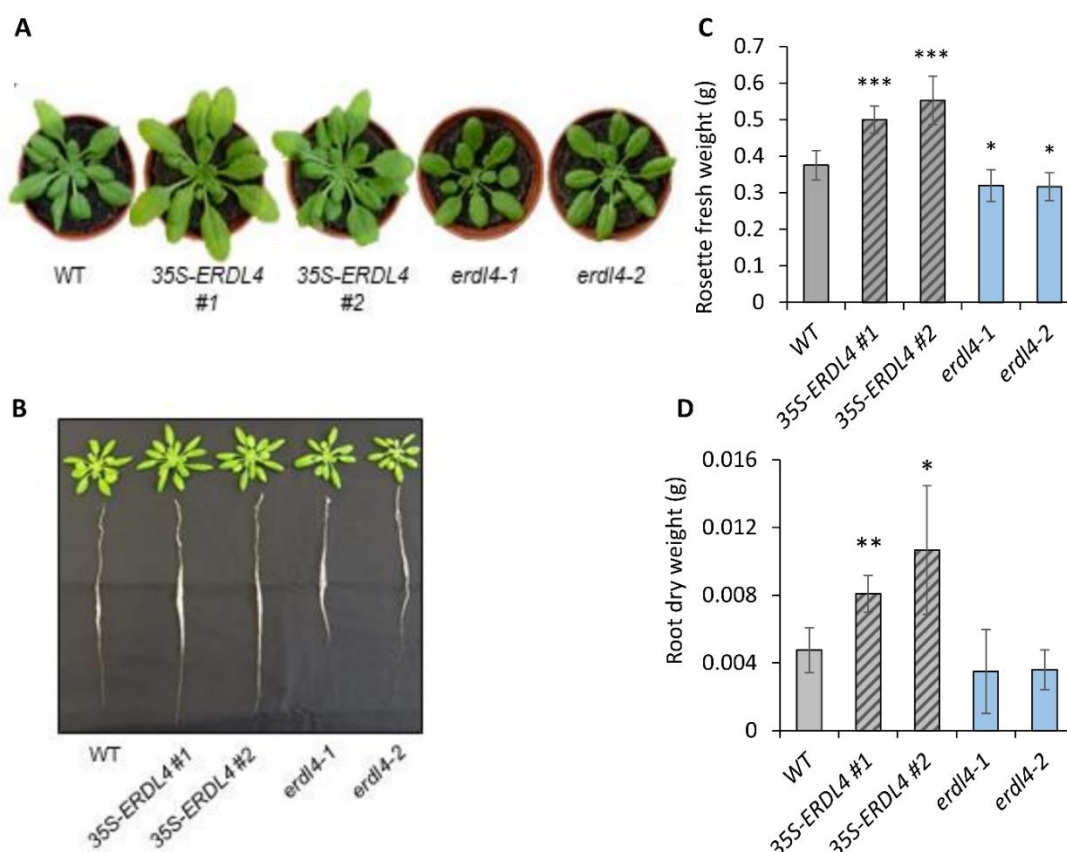


Figure 3.6. Phenotypic characterization of ERDL4 mutants. Plants were grown in soil or in hydroponic medium for 5 weeks in standard conditions ($120 \mu\text{mol Photons m}^{-2} \text{s}^{-1}$, 10 h light/14 h dark, 22°C) **A**. Rosettes of 5 weeks old ERDL4 mutants and corresponding WT. **B**. Rosettes and roots of ERDL4 mutants and WT grown in hydroponic medium **C**. Rosette fresh weight of WT and ERDL4 mutants. Data represents the mean \pm standard error from 6 biological replicates. **D**. Root dry weight of WT and ERDL4 mutants grown in hydroponics. The mean \pm standard error is shown from six biological replicates. Statistically significant differences were calculated using the one-tailed Student's t-test (* $p \leq 0.05$; ** $p \leq 0.01$; *** $p \leq 0.001$).

3.1.6. Root growth analysis from 35S-*ERDL4* lines

To examine the changes in root lengths, seeds from WT and 35S-*ERDL4* lines were placed on ½ MS agar plates (without sucrose) and plates were allowed to grow vertically. Four days after germination similar looking seedlings were transferred to new ½ MS agar plates (without sucrose) and root lengths were measured. Overexpression lines showed a significant increase in root length as compared to WT (**Figure 3.7**). Fifteen days after germination WT attained a root length of 2 cm while 35S-*ERDL4* #1 showed 3 cm and 35S-*ERDL4* #2 showed 4.1 cm increase in length.

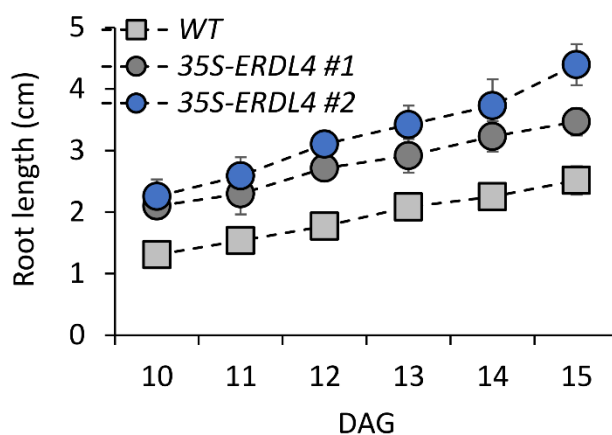


Figure 3.7. Root growth analysis of *ERDL4* overexpressors. *ERDL4* overexpressors and corresponding WT were grown under standard conditions ($120 \mu\text{mol photons m}^{-2}\text{s}^{-1}$, 10 h day/ 14 h, 22°C) on ½ MS agar plates with no additional sugars. **A.** Root length of Arabidopsis seedlings determined on the corresponding days after germination (DAG). The mean \pm standard error is shown in each case from ≥ 30 biological replicates. The mean \pm standard error is shown in each case from ≥ 30 biological replicates.

3.1.7. Analysis of phloem sugar export

Increased rosette fresh weight and root length in *ERDL4* overexpression lines due to altered vacuolar sugar transport could also be an effect of changed total sugar export via phloem to the sink organs. To investigate whether these phenotypic changes are also depicted in phloem sugar export, sugar content was quantified from the phloem exudates collected from fully developed six weeks old well-watered WT and *ERDL4* mutant plants. It was found that WT exported $0.56 \mu\text{mol sugars/g FW}$ whereas, 35S-*ERDL4* lines showed significantly increased export capacity with 0.6 and $0.7 \mu\text{mol sugars/g FW}$ exported respectively. In contrast, *erdl4* mutants exhibited significantly less sugar export with 0.38 and $0.2 \mu\text{mol sugars/g FW}$ being exported (**Figure 3.8 A**).

Increased phloem sugar export in the overexpression lines was also validated by the increased expression of phloem loading sugar transporters AtSWEET11 and AtSWEET12 which mediate sugar export from PPTCs into the apoplast (**Section 1.4**). RNA-Seq data showed 1.6 times increase in the expression of SWEET11 in both overexpressors whereas, for SWEET12 six times increase in expression was observed in *35S-ERDL4* lines as compared to WT (**Figure 3.8 B**).

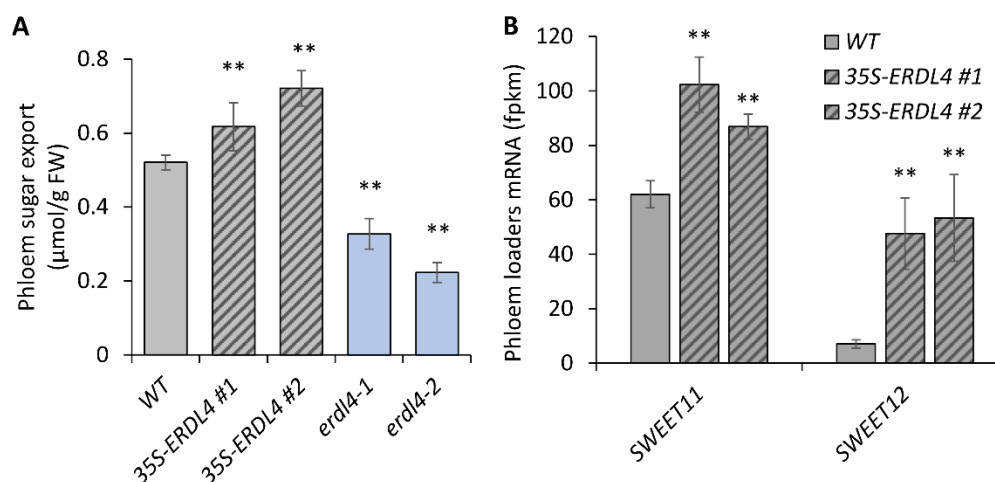


Figure 3.8. Phloem sugar export and SWEET proteins expression. Plants were grown in soil for 6 weeks in standard conditions ($120 \mu\text{mol Photons m}^{-2} \text{s}^{-1}$, 10h light/14h dark, 22°C). The leaves from well-watered plants were harvested 4h after the onset of light phase and phloem sap was collected in water for 6 hours in the dark. The sugar levels in the phloem sap were determined enzymatically. **A.** Sugar export quantified from phloem exudates Shown is the mean \pm standard error of eight biological replicates. Statistically significant differences were calculated using Student's one-tailed t-test (* $p \leq 0.05$; ** $p \leq 0.01$; *** $p \leq 0.001$). FW = fresh weight. **B.** SWEET11/12 expression analysis in *ERDL4* overexpressors and corresponding WT. FPKM values obtained from RNA-seq results. The mean \pm standard error is shown from 3 biological replicates. Statistically significant differences were calculated using Student's one-tailed t-test (* $p \leq 0.05$; ** $p \leq 0.01$; *** $p \leq 0.001$).

3.1.8. Inflorescence analysis of *35S-ERDL4* lines

Sugars are exported from source to sink tissues, inflorescences and siliques and seeds (Giaquinta et al., 1983; Haritatos et al., 2000; Durand et al., 2018). Increased sugar export via long-distance transport can influence the sink growth. To assess the potential impact of increased phloem sugar export in the overexpression lines on inflorescence and silique development fresh weight of inflorescence stems were analysed from WT and overexpression lines. The inflorescences of both overexpression lines in comparison to WT had significantly increased biomass (**Figure 3.9 A, C**). The fresh weight of the WT was 1.23 g per inflorescence, the biomass for the two *35S-ERDL4* #1 and #2 lines was 1.42 g and 1.67 g respectively. To check further effects on sink growth, development of inflorescence stem was analysed overtime. Since transfer of Arabidopsis plants from short day to long day conditions induces

bolting and increase the starch content in the leaf and sucrose in the cytosol (Corbesier et al., 1998), WT and *35S-ERDL4* plants were transferred to long day conditions after 4 weeks of growth in short day conditions to induce bolting. The results indicated that although *35S-ERDL4* plants starts bolting later but developed longer inflorescence stems when compared to WT. WT after 30 days of growth in long day conditions grew 33 cm long stem and *35S-ERDL4* plants had 38.6 and 39 cm of inflorescence stems respectively (**Figure 3.9 B**).

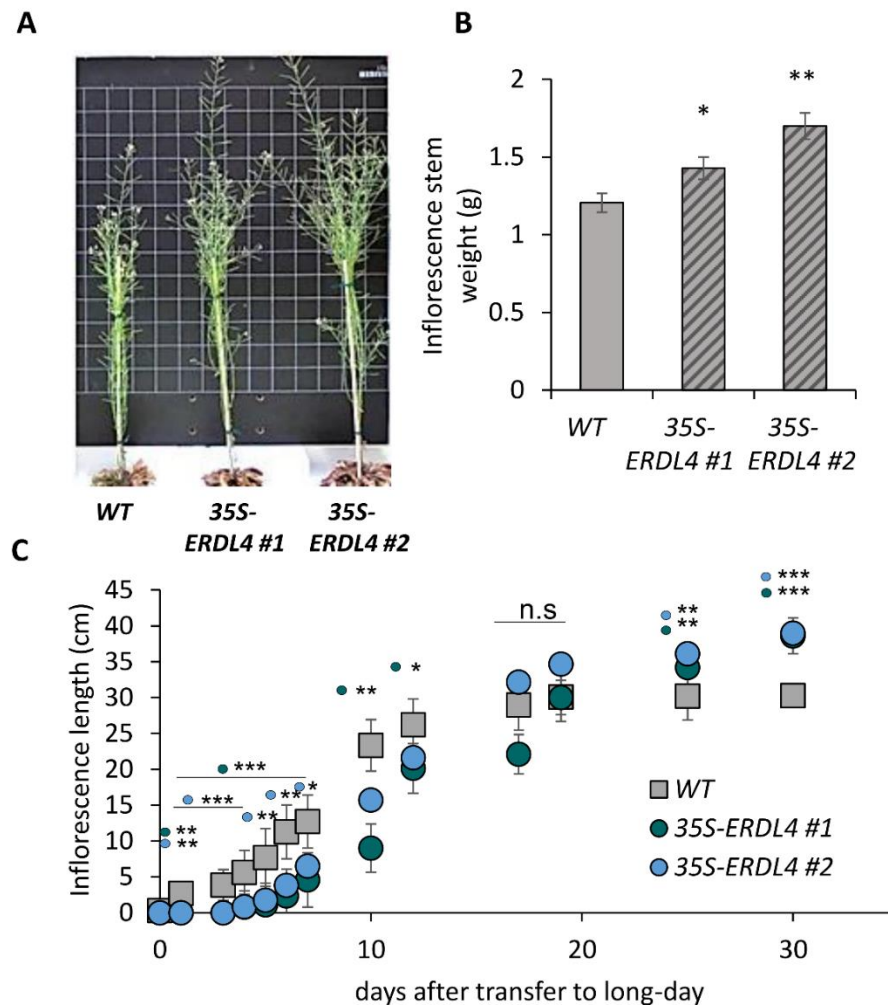


Figure 3.9. *ERDL4* overexpressors plants exhibit longer and more inflorescence stems than WT. A. Representative image of inflorescence stems of WT and *ERDL4* overexpressor plants. **B.** Inflorescence stem length of WT and *ERDL4* overexpressors. Plants were grown in control condition ($120 \mu\text{mol Photons m}^{-2} \text{s}^{-1}$, 10h light/14h dark, 22°C) in soil for 4 weeks and then transferred to long day conditions ($120 \mu\text{mol Photons m}^{-2} \text{s}^{-1}$, 14h light/10h dark, 22°C). Data collection started the first day plants started bolting and continued until the inflorescence stem length stopped to increase (~30 days after transfer to long day). Data represents the mean \pm standard error of ≥ 20 individual plants per line. **C.** Inflorescence stem fresh weight. Inflorescence stems from the corresponding plants were harvested before going to drying phase and weighed. Data represents the mean \pm standard error of ≥ 20 individual plants per line. Statistically significant differences were calculated using Student's one-tailed t-test (* $p \leq 0.05$; ** $p \leq 0.01$).

3.1.9. Silique analysis of *ERDL4* mutants

The analysis of sugar exports in section 3.8 revealed that long distance transport of sugar in *ERDL4* mutants was reduced as compared to the WT. To assess the potential impact of increased sugar export the length and the sugar composition of siliques was examined. To investigate, the silique length, fully mature and still green siliques from WT and *ERDL4* mutants were harvested. It was observed that silique length from both *35S-ERDL4* lines was slightly but significantly increased as compared to WT (**Figure 3.10 A**). The average length of the WT silique was 1.44 cm. In contrast to the WT, the silique length of both *35S-ERDL4* lines was 1.54 cm and 1.56 cm respectively. Whereas, for *erdl4* knockout mutants the silique length was significantly reduced to 1.38 cm and 1.40 cm respectively. To investigate the observed effect on the silique length in more detail sugar composition of the siliques from WT and *ERDL4* mutants was determined. Sugar extraction from the siliques showed that the WT had 37.1 $\mu\text{mol/g}$ FW of total sugars (**Figure 3.10 B**). However, the siliques from *35S-ERDL4* plants contained significantly higher sugars with the levels reaching to 60.6 $\mu\text{mol/g}$ FW and 65.8 $\mu\text{mol/g}$ FW. The sugar composition of siliques from *erdl4* T-DNA mutants was significantly reduced as compared to 18.2 $\mu\text{mol/g}$ FW and 20.5 $\mu\text{mol/g}$ FW respectively.

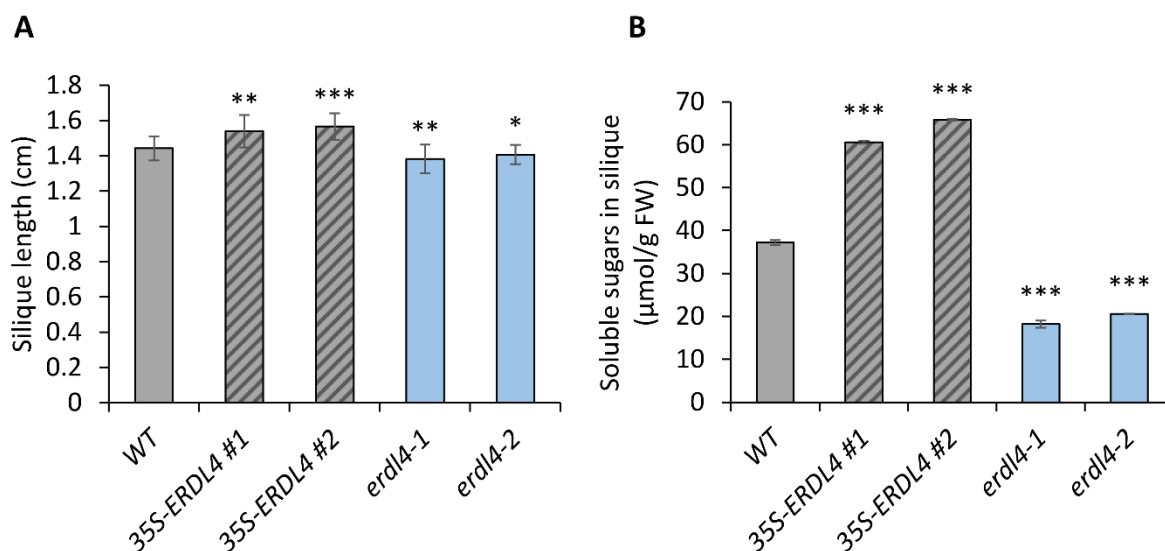


Figure 3.10. Analysis of siliques from WT and *ERDL4* mutants. **A.** Silique length of WT and *ERDL4* mutants. Mature siliques were harvested from the lower part of the inflorescence stem. For length determination 30 siliques from $n \geq 15$ plants were analyzed. **B.** Soluble sugars quantified in the siliques of *ERDL4* mutants and the WT. Siliques from inflorescence stem of the corresponding plants were harvested before the drying phase and sugars were determined enzymatically. The mean \pm standard error is shown from six biological replicates. Data represents the mean \pm standard error. Significant differences were calculated using one-tailed Student's t-test referred to WT (* $p \leq 0.05$; ** $p \leq 0.01$; *** $p \leq 0.001$).

3.1.10. Seed yield analysis from *ERDL4* mutants

All the changes observed in the sink tissues like, increased inflorescence stem length and biomass, altered silique length and sugar composition could also have a possible influence on seed development and yield. To check this, fully mature and dried siliques from WT and *ERDL4* mutant plants were carefully harvested and seeds per silique were counted. It showed that the 35S-*ERDL4* #1 had slightly less seeds per silique but there was no change in the seeds for 35S-*ERDL4* #2. However, for *erdl4* knockout mutants the number of seeds per silique was significantly reduced. WT siliques had 53 seeds per silique and the two overexpression lines possessed 52 and 54 seeds per silique respectively. The two T-DNA mutants of *ERDL4*, *erdl4-1* and *erdl4-2*, both had 44 seeds per silique (**Figure 3.11 A**). Having longer inflorescence stems and increased inflorescence biomass can lead to increased overall seed yield of the plant. Fully mature and dried seeds were harvested carefully from each plant to calculate seed yield per plant. It turned out that although 35S-*ERDL4* siliques did not show increase in seeds per silique but had more seed yield per plant. Both 35S-*ERDL4* lines had 74 and 96 seeds per plant respectively which were significantly more than the WT which had 50 seeds per plant on average (**Figure 3.11 B**).

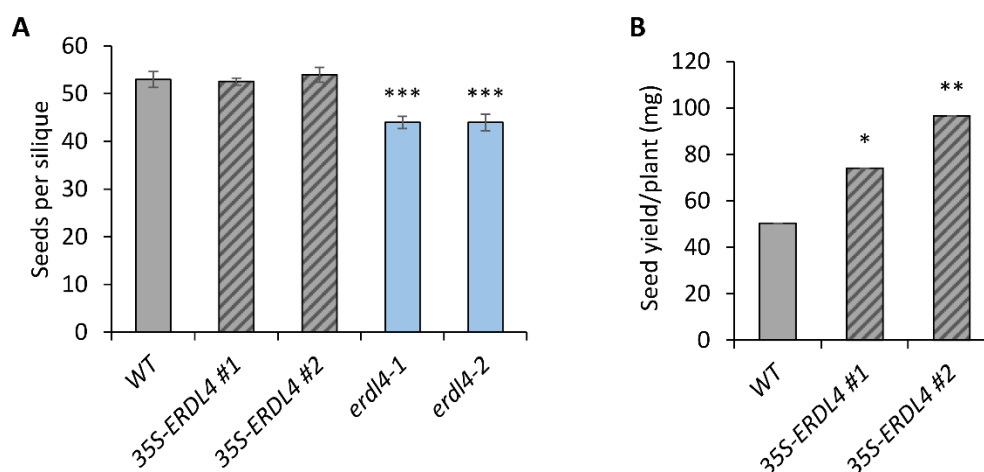


Figure 3.11. *ERDL4* overexpressors have high seed yield. **A.** Seeds counted per silique. For analysis 10 mature and dry siliques per plant from $n \geq 6$ plants were harvested and seeds were carefully extracted and counted from *ERDL4* mutants and corresponding WT plants. Data represents the mean \pm standard error. Significant differences were calculated using one-tailed Student's t-test referred to WT (* $p \leq 0.05$; ** $p \leq 0.01$; *** $p \leq 0.001$). **B.** Seed yield calculated per plant. Plants were grown for 4 weeks in short day ($120 \mu\text{mol Photons m}^{-2} \text{s}^{-1}$, 10h light/14h dark, 22°C) in soil and then transferred to long day conditions ($120 \mu\text{mol Photons m}^{-2} \text{s}^{-1}$, 14h light/10h dark, 22°C). Inflorescence stems were carefully wrapped and harvested after drying. Seeds were harvested from the inflorescence stems of the corresponding plants. The mean \pm standard error is shown from $n \geq 12$ biological replicates. Statistically significant differences were calculated using Student's one-tailed t-test (* $p \leq 0.05$; ** $p \leq 0.01$; *** $p \leq 0.001$).

3.1.11. Seed quality and physiological analysis from *ERDL4* mutants

Alterations in *ERDL4* expression had effect on siliques and seed yield. To examine if it could impact the seed quality and physiology as well, 1000 seeds were weighed from WT and *ERDL4* mutants harvested at the same time point. WT plants had a 1000 seed weight of 17.8 mg and the two *35S-ERDL4* lines showed significant increase with 20.9 mg and 23.9 mg weight for 1000 seeds. For the two T-DNA mutant lines 1000 seeds weight was significantly lower as compared to the WT. For *erdl4-1* it was found to be 15 mg whereas, for *erdl4-2* it was 11.5 mg (**Figure 3.12 A**). Arabidopsis seed weight is mainly composed of lipids and proteins (Wingenter et al., 2010; Poschet et al., 2011). To check to what extent an increased sugar export contributed towards the total lipid content of the seeds, lipids were extracted using isopropanol. The seeds from both *35S-ERDL4* lines contained 8% and 20% higher amount of lipids as compared to the WT. The two T-DNA mutant lines showed a decrease of 4% and 8% respectively as compared to WT (**Figure 3.12 B**). This change could also be depicted from a representative picture of the seeds from WT and *ERDL4* mutant lines where seeds from *35S-ERDL4* lines looks bigger and those from T-DNA mutants are wrinkled and shrunk (**Figure 3.12 C**).

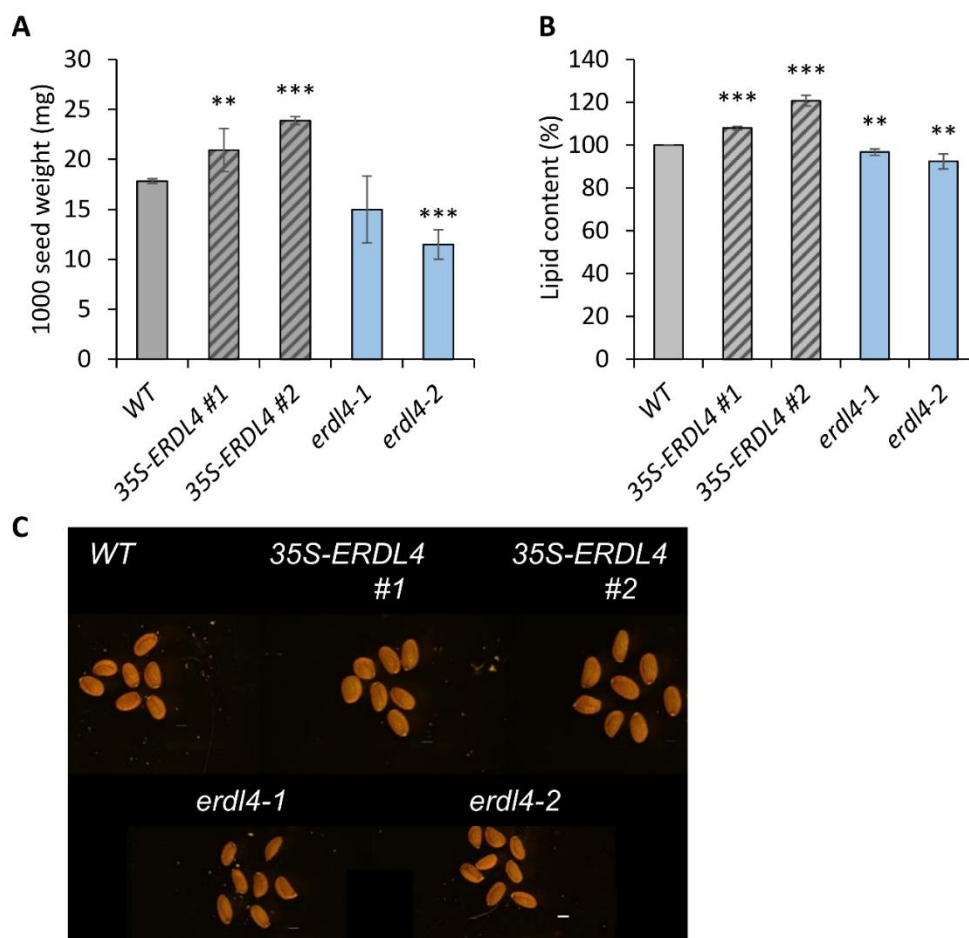


Figure 3.12. Seed quality and physiology from *ERDL4* mutants. After growing for 4 weeks in standard conditions plants were transferred to long day conditions ($120 \mu\text{mol Photons m}^{-2} \text{s}^{-1}$, 14h light/10h dark, 22°C). Fully mature and air-dried seeds were harvested from WT and *ERDL4* mutant plants. **A.** 1000 seeds weight. The mean \pm standard error is shown for three replicates (seed pool of 10 plants derived from the same harvest). **B.** Lipid quantification from 100mg of WT and *ERDL4* mutant seeds. Shown is the mean \pm standard error of 3 replicates (seed pool from 10 plants, from the same harvest). Statistically significant differences were determined using Student's one-tailed t-test calculated (* $p \leq 0.05$; ** $p \leq 0.01$; *** $p \leq 0.001$). **C.** Representative picture of seeds phenotype from WT and *ERDL4* mutants (derived from the same harvest). Bar = $200 \mu\text{m}$.

3.1.12. Differential expression analysis in 35S-*ERDL4* lines corresponds to fructose effect

NAF results pointed towards increased glucose and fructose export into the cytosol resulting in an upsurge of monosaccharide levels in the cytosol in 35S-*ERDL4* lines. To dissect the effects of glucose and fructose in the overexpression lines samples were sent for RNA-Sequencing. For this purpose, good quality RNA was extracted from WT and 35S-*ERDL4* lines harvested at midday (4 hours in light) from control conditions. Concomitantly RNA from leaf discs incubated in 1% mannitol (osmotic control), 1% glucose and 1% sucrose were also extracted and

analysed for differential gene expression. Significantly differentially expressed genes (DEGs) between WT and *35S-ERDL4* lines were identified by double sided *t*-test. Similarly, significantly differentially expressed genes between fructose/mannitol treatment and glucose/mannitol treatment were also identified using the double-sided *t*-test. Overlapping DEGs between fructose/mannitol treatment and *35S-ERDL4*/WT or glucose/mannitol and *35S-ERDL4* lines were identified using conditional analysis. Overall, 130 and 155 DEGs were found common between *35S-ERDL4* or fructose treatment and between *35S-ERDL4* or glucose treatment respectively (**Figure 3.13 A, B**). Correlation analysis was performed using the log₂ fold changes for the corresponding DEGs found common between *35S-ERDL4* and fructose treatment and likewise, between *35S-ERDL4* and glucose treatment. The analysis showed Pearson coefficients of $r = 0.48$ ($r^2 = 0.23$) for *35S-ERDL4* and fructose DEGs and $r = 0.15$ ($r^2 = 0.0225$) for *35S-ERDL4* and glucose DEGs (**Figure 3.13 C, D**). Altogether comparing *ERDL4*-overexpression and fructose-dependent gene expression changes to *ERDL4*-overexpressing and glucose-dependent gene expression changes, the analysis revealed a ten-fold higher correlation with fructose rather than glucose indicating that the transcriptional changes observed in *ERDL4*-overexpressors were caused by altered fructose signalling rather than altered glucose signalling.

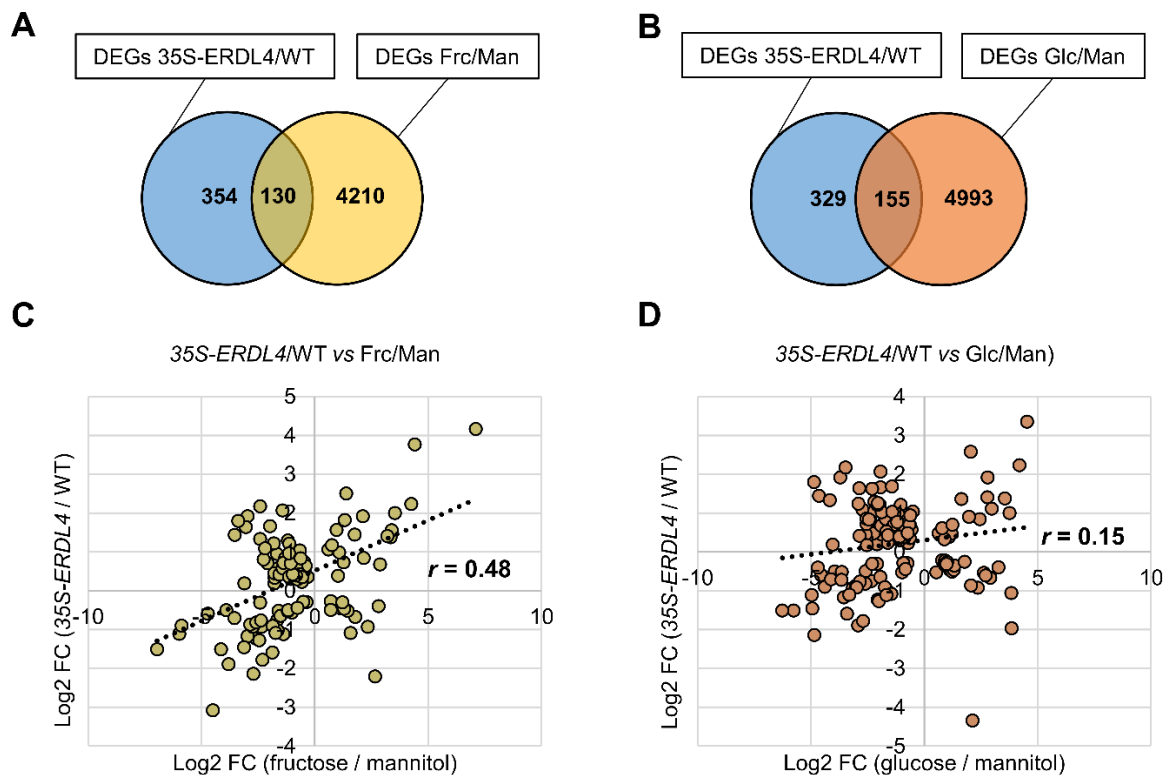


Figure 3.13. Venn-diagram and correlation analysis. Venn-diagram and correlation analysis between differentially expressed genes (DEGs) from *ERDL4*-overexpressing and WT plants and from fructose (Frc) or glucose (Glc) and mannitol (Man = control) incubated leaf discs. **A**) and **B**) show Venn-diagrams of DEGs. Numbers within circles represent the number of DEGs (significant at $p < 0.001$ according to the double-sided *t*-test of three replicates). There were 484 *35S-ERDL4*-dependent DEGs, 4340 Frc-dependent DEGs, and 5148 Glc-dependent DEGs. **A**) Diagram showing overlap of DEGs from *35S-ERDL4* and Frc-treatment. There were 130 DEGs regulated by both *ERDL4*-overexpression and Frc **B**) Diagram showing overlap of DEGs from *35S-ERDL4* and Glc-treatment. There were 155 DEGs regulated by both *ERDL4*-overexpression and Glc **C**) Correlation between relative expression (based on log₂-fold-change) of 130 DEGs between *35S-ERDL4* (against WT) and Frc (against Man). r = Pearson coefficient calculated from *ERDL4*/WT and Frc/Man matrices **D**) Correlation between relative expression (based on log₂-fold-change) of 155 DEGs between *35S-ERDL4* (against WT) and Glc (against Man). r = Pearson coefficient calculated from *ERDL4*/WT and Glc/Man matrices. (Data is kindly provided by Dr. Benjamin Pommerrenig, TU KL).

To gain deeper insight into the differential regulation observed in *35S-ERDL4* overexpression lines is due to glc or frc we identified the 10 most induced genes in presence of frc but at the same time reduced in presence of glucose. Similarly, the 10 most induced genes in presence of glc were identified which are reduced in presence of fructose. We then determined the expression pattern of these genes in *35S-ERDL4* overexpression lines. The results supported our idea that *ERDL4* overexpression lines showed similar regulation for the frc induced genes whereas, for glc induced genes they showed downregulation which is in agreement with the frc response (**Figure 3.14**). These results also give much weightage to the previous observations that *ERDL4* is more specific for fructose efflux from the vacuole rather than

glucose and the physiological changes observed in *ERDL4* mutants are probably the fructose specific effects.

| Identifier | gene symbol | description | involved in cellular process | frc/man (log2FC) | glc/man (log2FC) | 35S-ERDL4 #1/ WT (log2FC) | 35S-ERDL4 #2/ WT (log2FC) |
|---|-------------|---|------------------------------|------------------|------------------|---------------------------|---------------------------|
| <i>genes induced by fructose but repressed by glucose</i> | | | | | | | |
| AT4G15210 | BAM5 | BETA AMYLASE 5 | starch degradation | 3.85 | -1.21 | 1.16 | 1.81 |
| AT2G34850 | UXE2 | UDP-D-xylose 4-epimerase | galactose metabolism | 2.90 | -0.44 | 2.95 | 3.25 |
| AT3G57240 | BG3 | putative pathogenesis-related endo-1,3-beta-glucosidase | response to pathogen | 2.72 | -0.87 | -2.51 | -5.19 |
| AT1G24070 | CSLA10 | CELLULOSE SYNTHASE-LIKE | cellulose biosynthesis | 2.59 | -1.25 | 4.77 | 5.72 |
| AT2G47780 | SRP2 | SMALL RUBBER PARTICLE PROTEIN 2 | growth promotion | 2.57 | -0.62 | 2.44 | 2.21 |
| AT5G60930 | KIN4c | kinesin motor protein | cell cycle | 2.27 | -0.27 | 1.43 | 1.72 |
| AT3G27250 | AITR1 | ABA-INDUCED TRANSCRIPTION REPRESSOR | ABA signaling | 1.64 | -0.83 | 4.58 | 4.20 |
| AT4G01060 | ETC3 | R3-MYB transcription factor | cell differentiation | 1.53 | -0.80 | 3.25 | 3.27 |
| AT5G59220 | SAG113 | ABA-INDUCED PP2C GENE 1 | protein phosphorylation | 1.50 | -0.31 | 5.23 | 5.70 |
| AT2G39800 | P5CSA | DELTA1-PYRROLINE-5-CARBOXYLATE SYNTHASE 1 | proline biosynthesis | 1.10 | -1.03 | 2.53 | 2.10 |
| AT4G21650 | SBT3.13 | SUBTILASE 3.13 | protein degradation | 1.08 | -2.51 | 2.43 | 1.89 |
| <i>genes induced by glucose but repressed by fructose</i> | | | | | | | |
| AT5G05440 | PYL5 | Abscisic acid receptor | ABA signaling | -0.65 | 2.09 | -2.49 | -2.72 |
| AT2G43140 | BHLH129 | Basic helix-loop-helix DNA-binding protein | DNA binding | -0.81 | 2.49 | -1.09 | -1.35 |
| AT1G76600 | - | uncharacterized protein | response to fungus | -0.46 | 1.86 | -1.37 | -1.18 |
| AT1G08930 | ERD6 | EARLY RESPONSE TO DEHYDRATION 6 | vacuolar sugar transport | -0.28 | 1.77 | -2.19 | -2.51 |
| AT4G21870 | HSP15.4 | class V heat shock protein | heat response | -1.58 | 1.57 | -1.71 | -2.18 |
| AT1G76650 | CML38 | CALCIUM-BINDING CALMODULIN-LIKE 38 | nitrate signaling | -0.25 | 1.48 | -2.47 | -0.89 |
| AT2G26560 | PLA2-lia | Patatin-containing phospholipase A | oxylipin production | -0.97 | 1.22 | -1.90 | -2.54 |
| AT5G42830 | - | BAHD-type acyl-transferase family protein | response to pathogen | -0.98 | 1.21 | -1.97 | -3.01 |
| AT2G36950 | HIPP05 | metallochaperone-like protein | heavy metal detoxification | -0.58 | 1.15 | -0.26 | -0.19 |
| AT5G24570 | HMP20 | HEAVY METAL PROTEIN 20 | heavy metal detoxification | -0.62 | 1.09 | -1.43 | -1.61 |
| | | | | -5.19 | log2FC | 5.72 | |

Figure 3.14. List of DEGs oppositely regulated by frc or glc ranked after their Log2FCs. The upper part of the table lists the 10 most strongly frc-induced genes that were at the same time repressed by glc and the lower part the 10 most strongly glc-induced genes that were at the same time repressed by frc (Log2FCs cutoff ≤ 0.25). (Data is kindly provided by Dr. Benjamin Pommerrenig, TU KL).

3.1.13. Sugar transporters are diurnally regulated

Dynamics of vacuolar sugar metabolism are linked to diurnal rhythm (Nägele et al., 2010) and vacuolar sugar transporters steer subcellular sugar compartmentation (Wormit et al., 2006; Poschet et al., 2011; Vu et al., 2020). It is therefore reasonable to check whether *ERDL4* and other vacuolar sugar transporters are regulated in a diurnal manner. To check the diurnal regulation of the transporters WT plants were grown in a 10 h light, 14 h dark cycle (short day) conditions and harvested plant material at two-hour intervals to measure diurnal gene expression. In addition to *ERDL4*, we looked at the expression of TST1 and TST2 (Wormit et

al., 2006; Schulz et al., 2011), which catalyze sugar transport into the vacuolar lumen, and ERDL6 (Poschet et al., 2011), which catalyzes glucose/proton symport from the vacuolar lumen into the cytosol (**Figure 3.15**).

With the start of the light phase, *ERDL4* mRNA levels declined steadily throughout the day (**Figure 3.15 A**), reaching a minimum at the end of the day, with around 16-fold less mRNA than the first recorded value of the day. *ERDL4* mRNA levels steadily climbed during the dark phase until they achieved their maximum at the start of the day. On the other hand, the expression patterns of the *ERDL6*, *TST1*, and *TST2* genes were quite similar, and their mRNA levels quickly increased throughout the light phase, peaking near to the end of the light phase. The mRNA levels of these three genes rapidly declined with the onset of the dark phase, reaching their minimum expression throughout the night phase (**Figure 3.15 B-D**). The results suggested that like photosynthesis sugar transporters are also tightly diurnally regulated and *ERDL4* essentially follow a distinct diurnal rhythm which does not overlap with *TSTs* and its closest homolog *ERDL6*.

At EOD and EON time points, diurnal expression of the various transporter genes correlated with changing fructose to glucose ratios. While the *frc/glc* ratio of WT plants was about 0.44 at EOD, it shifted to about 0.12 at EON, indicating that fructose was released from vacuoles and used for metabolic processes during the night (**Figure 3.15 E**). However, *35S-ERDL4* lines did not follow this night-time fructose export pattern rather at EOD, the *frc* to *glc* ratio of *35S-ERDL4*-overexpressing plants was considerably lower than that of WT plants, but not at EON (**Figure 3.15 E**). Increased *ERDL4* activity during the day therefore enhanced glucose accumulation and promoted fructose export from the vacuole. This result is in line with the NAF result, which corroborated midday sugar accumulation investigation (**Figure 3.5**).

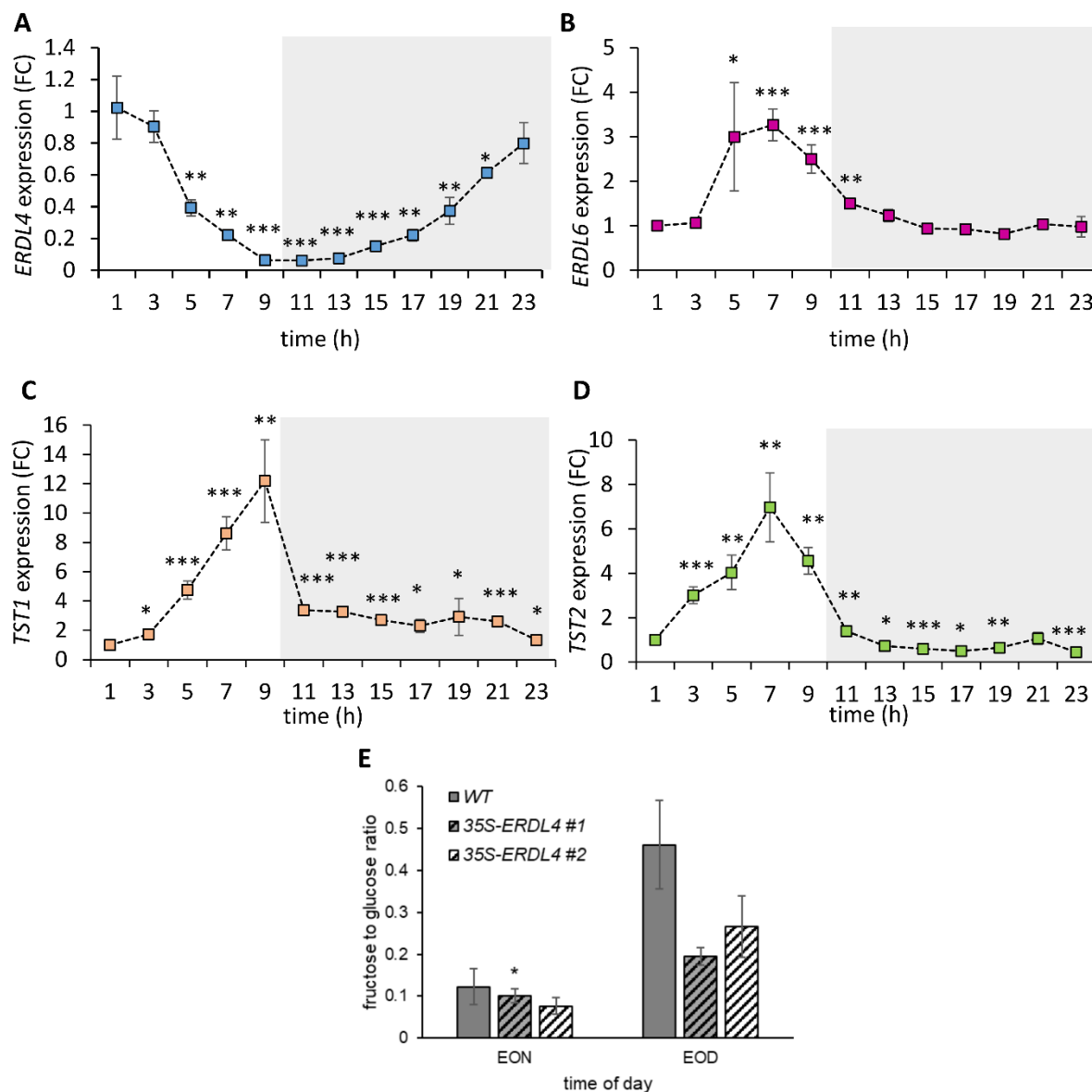


Figure 3.15. Diurnal expression of transporters. **A.** Diurnal expression profile of *ERDL4*. 6 weeks old WT plants were harvested at given time points grown under standard condition ($120 \mu\text{mol Photons m}^{-2} \text{s}^{-1}$, 10h light/14h dark, 22°C). **B.** Diurnal expression profile of *ERDL6*. **C.** Diurnal expression profile of *TST1*. **D.** Diurnal expression profile of *TST2*. Expression is normalized to *Actin*. Grey-shaded areas indicate values recorded at night-time (without illumination). Data represents mean \pm standard error from three biological replicates. Statistically significant differences were calculated using Student's one-tailed t-test (* $p \leq 0.05$; ** $p \leq 0.01$; *** $p \leq 0.001$). **E.** Fructose to glucose ratio determined from sugar levels quantified at end of night (EON) and end of day (EOD). Data represents mean \pm standard error from five biological replicates. Statistically significant differences were calculated using Student's one-tailed t-test (* $p \leq 0.05$; ** $p \leq 0.01$; *** $p \leq 0.001$).

3.1.14. Expression analysis of vacuolar sugar transporters in *ERDL4* mutants

Previous findings using NAF, RNA-Seq, and diurnal mRNA measurements suggested that *ERDL4* may function as a vacuolar sugar transporter, accelerating the release of fructose from

vacuoles into the cytosol and inducing fructose-specific gene expression responses. If *ERDL4* had such a function how could *35S-ERDL4* plants produce the observed high accumulation of glucose in the vacuole? To address this question, we checked the expression of other sugar transporters present on the vacuolar membrane. WT and *35S-ERDL4* plants grown in control conditions were harvested at midday for subsequent RNA preparation. It was found that *TST2*, *VGT1* and *VGT2* expression was upregulated in *35S-ERDL4* plants. For *TST2* it is considered to contribute towards vacuolar monosaccharide pool (Wormit et al., 2006). Although the physiological function of *VGT2* is unknown, its structural similarities to *VGT1* suggests that it resides in tonoplast and functions as a Glc/H⁺ antiporter like *VGT1* (Aluri & Büttner, 2007). *TST2* expression was found to be 2.5-fold and 3-fold increase in *35S-ERDL4* #1 and #2 respectively. For *VGT2* it was 1.6-fold and 2-fold increase in *35S-ERDL4* plants (**Figure 3.16 A, B**).

Vacuolar glucose exporters *ERDL6*, *SWEET16* and *SWEET17* were downregulated in *35S-ERDL4* plants (Poschet et al., 2011; Klemens et al., 2013; Chardon et al., 2013). *ERDL6* levels were 1.42 times reduced in *35S-ERDL4* plants and *SWEET16* levels were reduced to 1.81 times and 1.42 times in *35S-ERDL4* #1 and #2 respectively. *SWEET17* levels did not change significantly. Platidic sugar exporter *pSUT* (Patzke et al., 2019) was used as a control which was not differentially regulated among WT and *35S-ERDL4* lines. Altogether vacuolar importers were found to be upregulated and exporters primarily mediating glucose export were downregulated (**Figure 3.16 A-H**).

Expression levels of these transporters were also checked in *erd14* T-DNA mutants. Where it was on contrary, the vacuolar importers were downregulated, and exporters were upregulated (**Figure 3.16 I-L**). *TST1* levels did not change significantly while *TST2* levels in *erd14-1* and *erd14-2* were found to be 1.4 times and 2.5 times reduced. *SWEET16* was 4.8 times and 4 times upregulated in the *erd14-1* and *erd14-2* respectively. Whereas *ERDL6* was 2.6 times and 2.1 times upregulated in the corresponding T-DNA lines. The results depicted that the observed glucose accumulation in *35S-ERDL4* lines was a result of *TST2* sugar/proton antiport into vacuoles which did not occur in the same manner in *erd14* knockouts where *TST* expression was unaltered or even reduced.

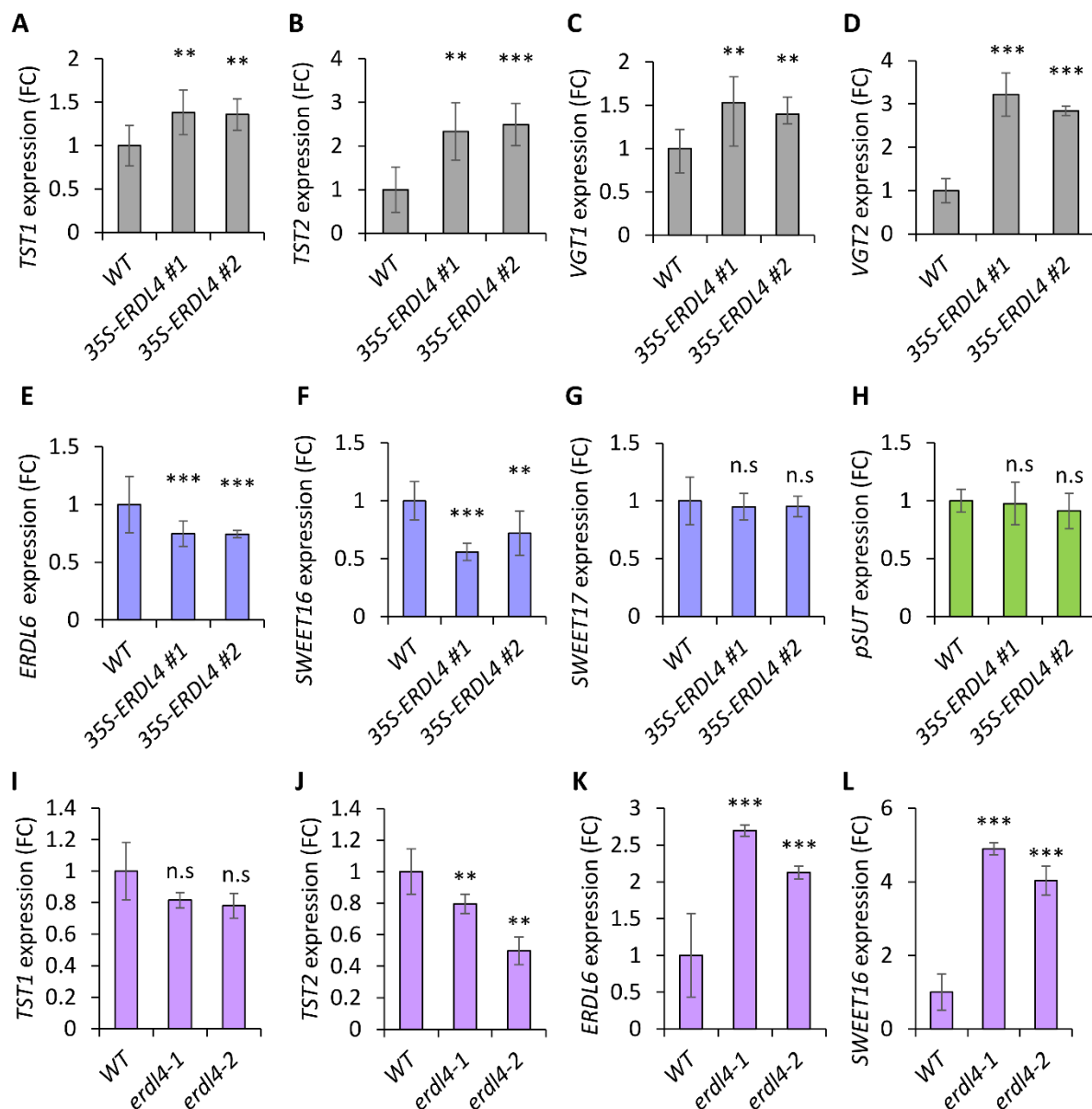


Figure 3.16. Expression of vacuolar sugar transporters in *ERDL4* mutants. Expression of vacuolar sugar importers in 35S-*ERDL4* lines and corresponding WT. **A-D.** Expression values of *TST1*, *TST2*, *VGT1* and *VGT2*. Expression of vacuolar and plastidic sugar exporters in 35S-*ERDL4* lines and corresponding WT. **E-H.** Expression values of *SWEET16*, *SWEET17*, *ERDL6* and *pSUT*. Expression of vacuolar sugar importers and exporters in *erdl4* knockout lines and corresponding WT. **I-L.** Expression values of *TST1*, *TST2*, *ERDL6* and *SWEET16*. Plants grown for 6 weeks in standard condition ($120 \mu\text{mol Photons m}^{-2} \text{s}^{-1}$, 10h light/14h dark, 22°C) were harvested 4 hours after onset of light. Data represents mean \pm standard error from three biological replicates. Statistically significant differences were calculated using Student's one-tailed t-test (* $p \leq 0.05$; ** $p \leq 0.01$; *** $p \leq 0.001$).

3.1.15. Sugar quantification from *tst-ERDL4* lines

To check whether sugar accumulation 35S-*ERDL4* overexpression lines is due to increase TSTs expression we overexpressed *ERDL4* in background of *tst1/2* double knock-out plants which are known to have greatly reduced vacuolar monosaccharide levels (Wormit et al., 2006;

Schulz et al., 2011) and checked whether *ERDL4* can still accumulate sugars or not (**Figure 3.17**

A).

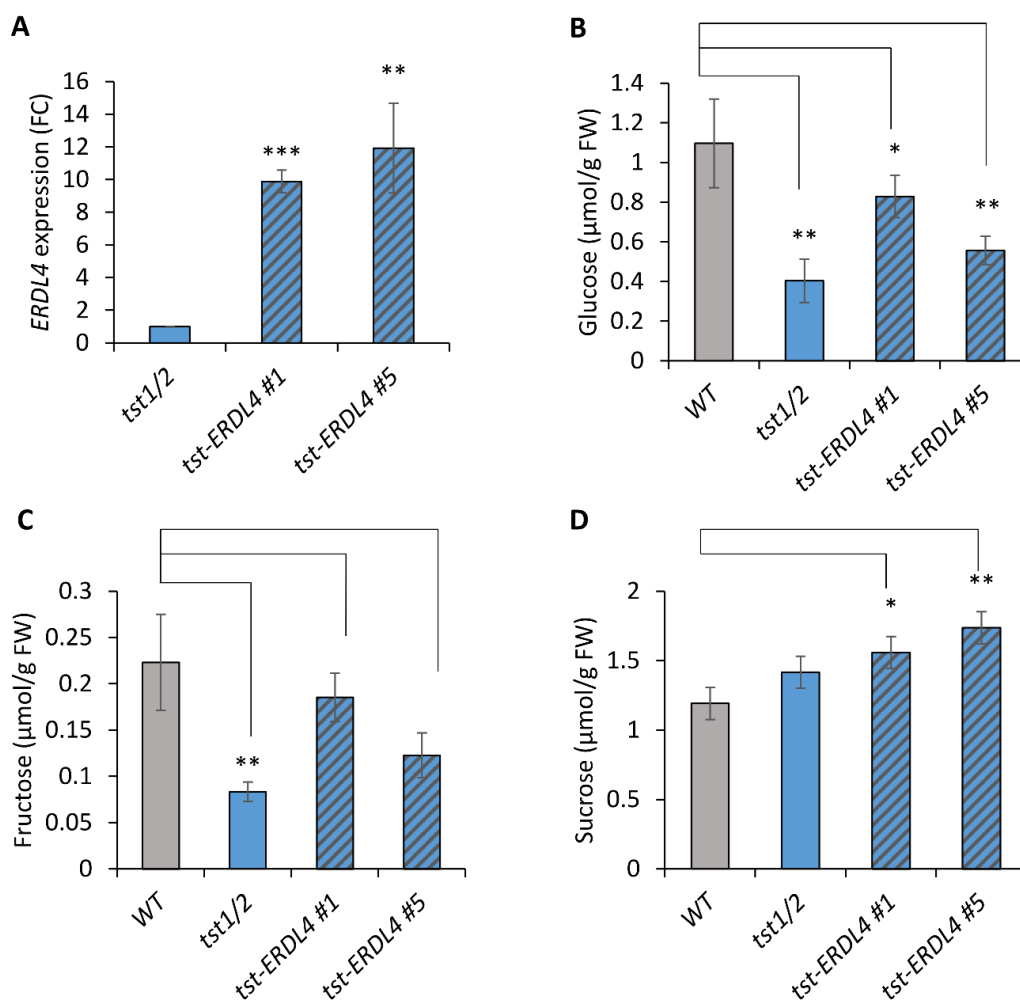


Figure 3.17. Soluble sugar content in *tst-ERDL4* overexpressors. **A.** Expression of *ERDL4* in 4 weeks old *tst-ERDL4* overexpressor plants. Expression levels are normalized to *Actin*. The mean \pm standard error is shown from five biological replicates. Statistically significant differences were calculated using Student's one-tailed t-test (* $p \leq 0.05$; ** $p \leq 0.01$; *** $p \leq 0.001$). **B-D.** Soluble sugar quantification from WT, *tst1/2* and *tst-ERDL4* overexpressor. Plants were grown for 4 weeks in standard condition ($120 \mu\text{mol Photons m}^{-2} \text{s}^{-1}$, 10h light/14h dark, 22°C) and harvested 4 hours after onset of light. Data represents mean \pm standard error from six biological replicates. Statistically significant differences were calculated using Student's one-tailed t-test (* $p \leq 0.05$; ** $p \leq 0.01$; *** $p \leq 0.001$).

Therefore, plants were harvested at midday after 4 weeks of growth in control conditions and processed for sugar quantification. The results revealed that the corresponding twofold increase in glucose levels in *35S-ERDL4* plants from NAF results was absent in *tst-ERDL4* plants as compared to WT (**Figure 3.17 B**). WT showed $1.1 \mu\text{mol glucose/g FW}$ and for the two *tst-ERDL4* overexpression lines it was $0.8 \mu\text{mol glucose/g FW}$ and $0.58 \mu\text{mol glucose/g FW}$ respectively.

Although glucose level in *tst1/2* double knockout was significantly less as compared to WT, 0.39 μmol glucose/g FW, there was a weak increase in *tst-ERDL4* glucose levels when compared to *tst1/2* double knockout (**Figure 3.17 B**). For fructose all the mutant lines showed reduced levels of fructose as compared to WT but in comparison to *tst1/2* double knockout *tst-ERDL4* overexpressors showed a slight increase, but it was not significant (**Figure 3.17 C**). Sucrose levels were not significantly altered between WT and *tst1/2* double knockout. WT showed 1.3 μmol sucrose/g FW and the double mutant had 1.4 μmol sucrose/g FW. The two lines of *tst-ERDL4* overexpressors showed a significant increase in sucrose content with 1.5 μmol sucrose/g FW and 1.6 μmol sucrose/g FW respectively (**Figure 3.17 D**). The results confirmed that the sugar build up in *35S-ERDL4* lines was a result of sugar importers upregulation which diminished in *tst-ERDL4* lines due to lack of *TSTs* transporters.

3.2. Fructose: A key signalling factor for vacuolar sugar homeostasis

The above data indicated that expression of vacuolar transport components like *TST2* or *ERDL4* depended on cytosolic fructose levels. However, activity of the transport proteins has been shown to be regulated by their phosphorylation patterns and activity of specific kinases as well like *VIK* (Wingenter et al., 2011) or *CIPK6* (J. Xu et al., 2006; Lee et al., 2007; Cheong et al., 2007; Deng et al., 2020). Recently CBL2-CIPK6-TST2 pathway was identified, responsible for sugar homeostasis in cotton providing increased stress resistance by increased sugar levels. To raise knowledge about the sequence homology and the evolutionary relationship between *GhCIPK6* and *AtCIPKs*, sequence alignment was carried out using the protein sequences of *CIPK6* from *Arabidopsis* and cotton and an unrooted phylogenetic tree was constructed using sequences from 26 *AtCIPKs* and *GhCIPK6*. The results showed a 72% of sequence identity between *CIPK6* protein from 2 species (**Figure 3.18 A**) and the data from evolutionary analysis exhibited that among all the 26 *AtCIPKs*, *GhCIPK6* was most similar or closely related to *AtCIPK6* with a reliability factor of 1.0. The arrow in the figure indicates towards *CIPK6* from both species that they are close neighbours within the tree (**Figure 3.18 B**).

Furthermore, increase in fructose has also been associated to induce cytosolic Ca^{2+} levels by activating voltage-gated Ca^{2+} channels on the plasma membrane (Furuichi et al., 2001). This rise in Ca^{2+} levels might initiate downstream Ca^{2+} signalling leading to expression of genes

RESULTS

responsible for sugar homeostasis like CBL-CIPK pathway. To raise knowledge on sugar dependent induction of CIPKs, we analysed their expression in response to glucose and fructose, as well as in *35S-ERDL4* lines (**Figure 3.19 A**).

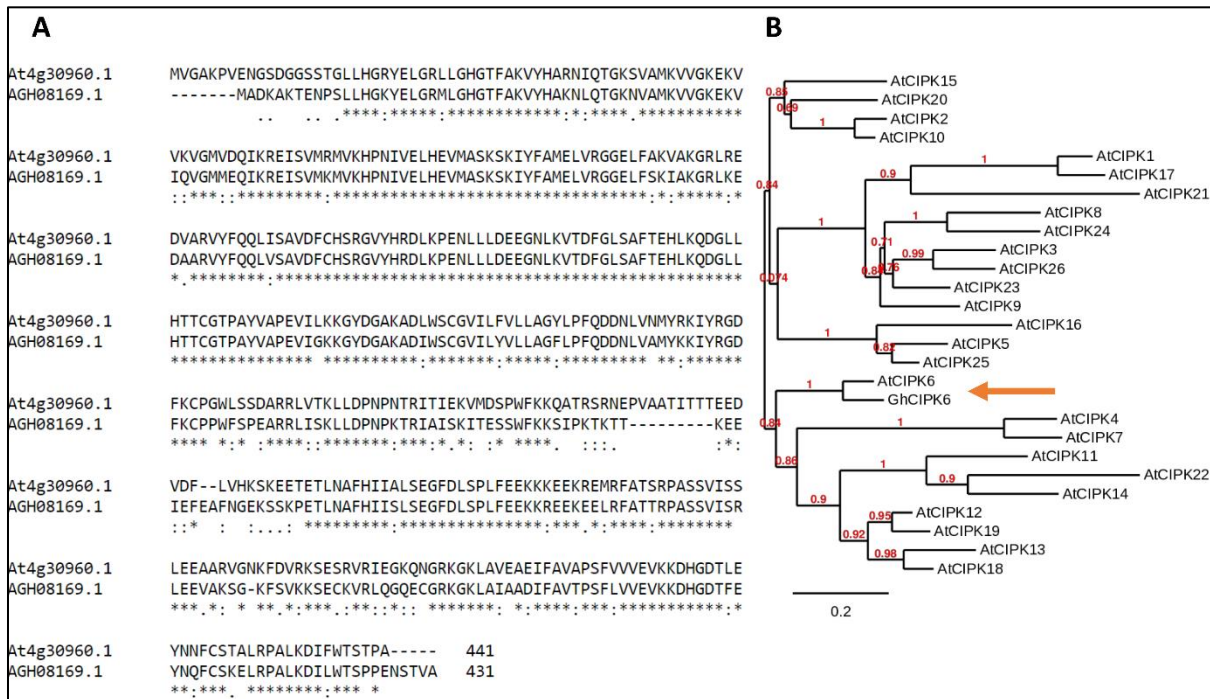


Figure 3.18. Sequence alignment and evolutionary relationship between CIPKs. Protein sequences of both *AtCIPK6* and *GhCIPK6* were used to check sequence homology between the two **A**. Protein sequence alignment of *AtCIPK6* and *GhCIPK6*. **B**. Unrooted tree showing evolutionary relationship between *GhCIPK6* and the 26 *AtCIPKs*. Arrowhead points towards the CIPK6 from both species. In red are the branch support values (reliability factor) and branch length corresponds to 0.2. (Data for the tree is kindly provided by Dr. Benjamin Pommerrenig, TU KL).

Log2 fold changes from RNA-Sequencing data indicated that six *AtCIPKs* were highly regulated in presence of glucose and fructose relative to mannitol (control) (**Figure 3.19 A**). Two of them, *AtCIPK9* and *AtCIPK20* were downregulated in presence of both glucose and fructose and were similarly regulated in *35S-ERDL4* lines (**Figure 3.19 A**). In contrast, *AtCIPK7* and *AtCIPK25* were upregulated in the two sugars as well as in *35S-ERDL4* #1 and *35S-ERDL4* #2 (**Figure 3.19 A**). Only *AtCIPK5* and *AtCIPK6* showed fructose specific upregulation and were also induced in *ERDL4* overexpression lines (**Figure 3.19 A**). On the other hand, *AtCIPK6* is more abundantly expressed in plants as compared to *AtCIPK5* which makes *AtCIPK6* a more likely target, responsible for TST2 phosphorylation and activation (**Figure 3.19 B**). We further confirmed RNA-Seq results by checking *AtCIPK6* expression in *35S-ERDL4* lines via qRT-PCR (**Figure 3.19**

C). As expected, in comparison to WT *AtCIPK6* levels were found 2.3 fold and 2.5 fold upregulated in 35S-*ERDL4* #1 and 35S-*ERDL4* #2 respectively (Figure 3.19 C).

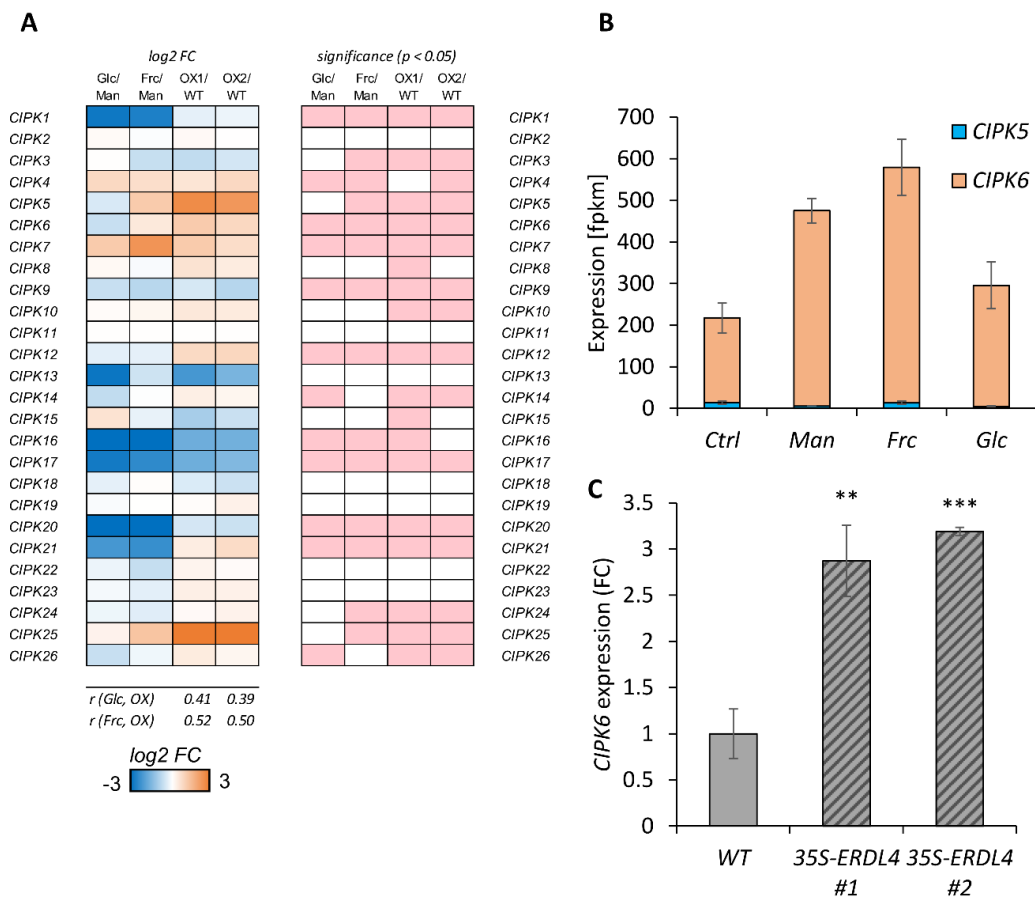


Figure 3.19. Sugar and *ERDL4* dependent expression of CIPKs. **A.** The heat map representation on the left side indicates log₂ fold-changes of the expression of different CIPKs in fructose/mannitol treatment, glucose/mannitol and in 35S-*ERDL4* lines. On the right side is the heatmap representation of the corresponding significance values (p-values) for each corresponding log₂ fold change. Pearson coefficient *r* indicates the correlation between CIPKs expression in glucose treatment/35S-*ERDL4* lines and CIPKs expression in fructose/35S-*ERDL4* lines. **B.** *CIPK5* and *CIPK6* fpkm values indicating their expression abundance in plants. **C.** Relative expression levels of *CIPK6* checked via qRT-PCR in WT and 35S-*ERDL4* lines. (Heat map data is kindly provided Dr. Benjamin Pommerrenig, TU KL).

3.3. Role of *ERDL4* in abiotic stresses

3.3.1. *ERDL4* expression in response to cold

Plants increase their overall sugar content in leaves dramatically after being exposed to cold temperatures for a short period of time, typically one to three days, known as cold acclimation (Klemens et al., 2013; Rodrigues et al., 2020; Ho et al., 2020). Cold acclimation is linked to gene expression changes and a substantial cold-dependent rise in monosaccharides in vacuoles (Vu et al., 2020). TSTs other than sugars also respond to stimuli like cold (Wormit et al., 2006).

During cold temperatures TST1 and TST2 help plants to efficiently accumulate vacuolar sugars which is a critical metabolic process in cold for developing frost tolerance (Pommerrenig et al., 2018). To identify the possible role of *ERDL4* in cold, its expression was checked in plants exposed to cold (4°C) for 24 hours. *ERDL4* levels increased markedly upto 18 fold after cold exposure (**Figure 3.20 A**). *ERDL4_{prom}:GUS* plants were used to check if there are differences in tissue specific expression due to cold exposure. It showed that in cold *ERDL4* expression was increased both in the source leaves and roots. In control conditions (20°C) *GUS* activity was visible not in the mesophyll cells of source leaves but only in shoot apical meristem (SAM) and in the roots only expressed in cortex and endodermis as shown in the corresponding cross-section (**Figure 3.20 B, C left panel**). Upon exposure to cold, expression in the source leaves extended to the petiole and in the leaf vasculature while in roots cross-section it appeared to spread to the vascular cylinder (xylem and phloem) (**Figure 3.20 B, C right panel**).

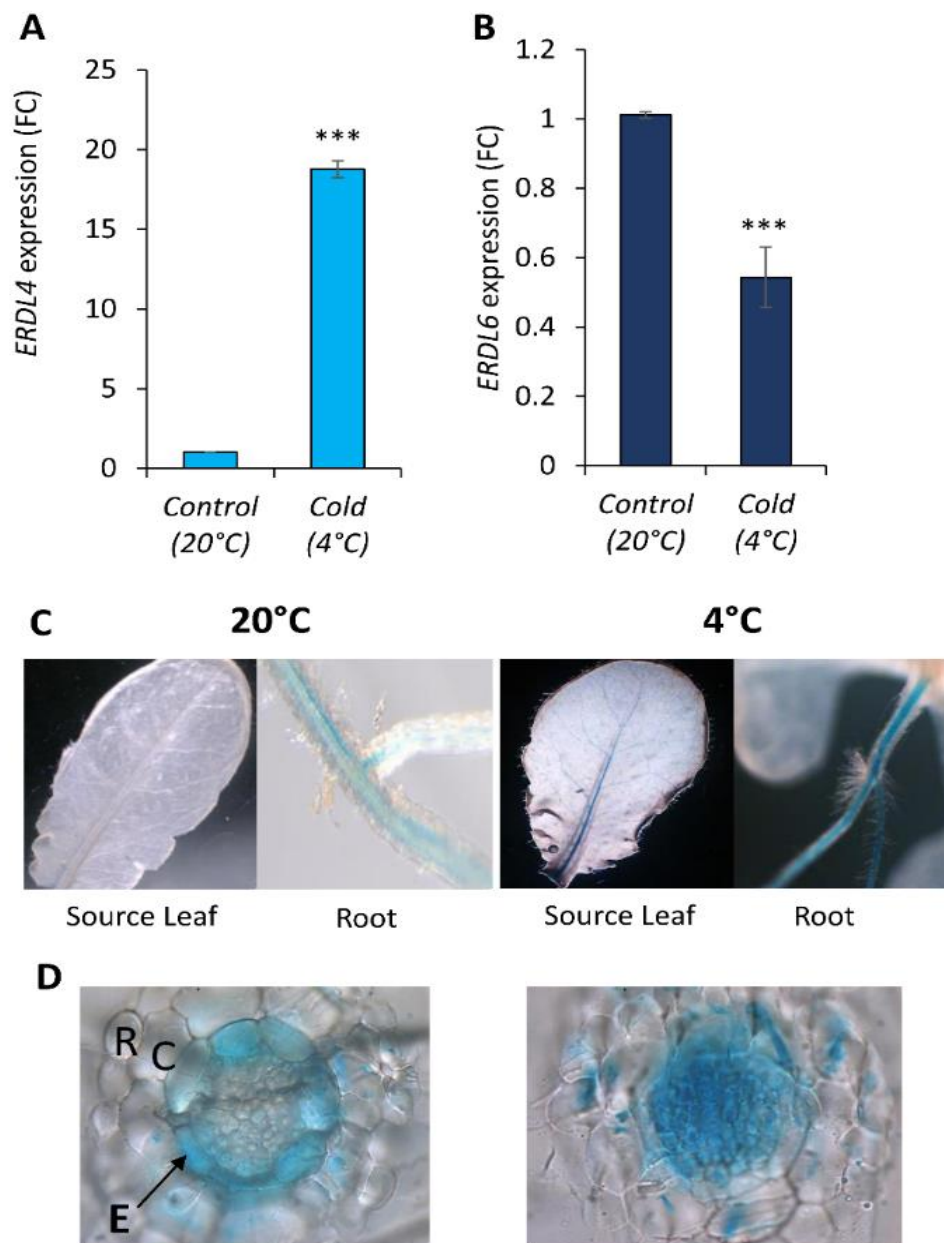


Figure 3.20. Cold induced changes in expression of *ERDL4* and *ERDL6*. **A-B.** Expression of *ERDL4* and *ERDL6* in response to cold (4°C). WT plants were placed in cold at 4°C for 1 day. Expression is normalized to *PP2A* and *SAND*. Data represents mean \pm standard error from three biological replicates. Statistically significant differences were calculated using Student's one-tailed t-test (* $p \leq 0.05$; ** $p \leq 0.01$; *** $p \leq 0.001$). **C.** Representative picture of 2 weeks old leaf and root from control and cold conditions used for GUS staining. **D.** Root cross-sections from control condition (20°C) and cold (4°C). Plants were grown for 2 weeks in $\frac{1}{2}$ MS agar plates supplemented with 0.5% sucrose. For cold treatment plates were transferred to cold (4°C) for 3 days and then used for GUS staining. R represents rhizodermis, C represents cortex and E represents endodermis. Stained tissues were fixed with 2% glutaraldehyde and embedded in Technovit® 7100 resin before making the 5 μ m thin cross-sections with microtome.

3.3.2. *ERDL4* influences cold acclimation and freezing tolerance

ERDL4 mutants already showed differences in vacuolar sugar accumulation due to altered sugar homeostasis in control conditions. Keeping in view *ERDL4* cold specific induction it was interesting to check how it effects sugar accumulation in cold. Cold acclimated plants (3 days in 4°C) showed significantly higher levels of glucose, fructose and sucrose in their leaves (**Figure 3.21 A-C**). Similar to control conditions *ERDL4* mutants also showed variations in sugar accumulation in cold. When compared to WT (16.3 $\mu\text{mol/g FW}$), 35S-*ERDL4* #1 and #2 lines accumulated the most glucose (22.3 and 22.9 $\mu\text{mol/ FW}$) (**Figure 3.21 A**). Plants from *erdl4-1* and *erdl4-2* T-DNA lines accumulated only around 75 % (12 $\mu\text{mol/g FW}$) and 87 % (14.1 $\mu\text{mol/g FW}$), respectively as compared to WT (**Figure 3.21 A**). Fructose levels remained the same in plants from 35S-*ERDL4* lines and WT but were reduced in *erdl4* knockout plants to 70% (*erdl4-1*) and 82 % (*erdl4-2*) as compared to WT levels (**Figure 3.21 B**). Sucrose levels did not show a significant change in all the lines (**Figure 3.21 C**). Differences in sugar accumulation in *ERDL4* mutants also contributed towards altered frost tolerance. This was examined by determining the temperatures at which leaves from WT and the mutant lines lost 50 % of their electrolytes. It was found that 35S-*ERDL4* leaves when exposed to freezing temperatures did not show significant difference to that of WT. WT leaves lost 50 % of their electrolytes at -5.3 °C whereas the two 35S-*ERDL4* lines (#1 and #2) had LT50% of -5.2 °C and -5.4 °C respectively (**Figure 3.21 D**). In contrast the two *erdl4* knockout lines exhibited LT50% of -3.5 °C and -3.7 °C (**Figure 3.21 D**). The results suggested that *erdl4-1* and *erdl4-2* accumulated less sugars which made them less tolerant towards freezing as they lost 50 % of their electrolytes earlier than the WT.

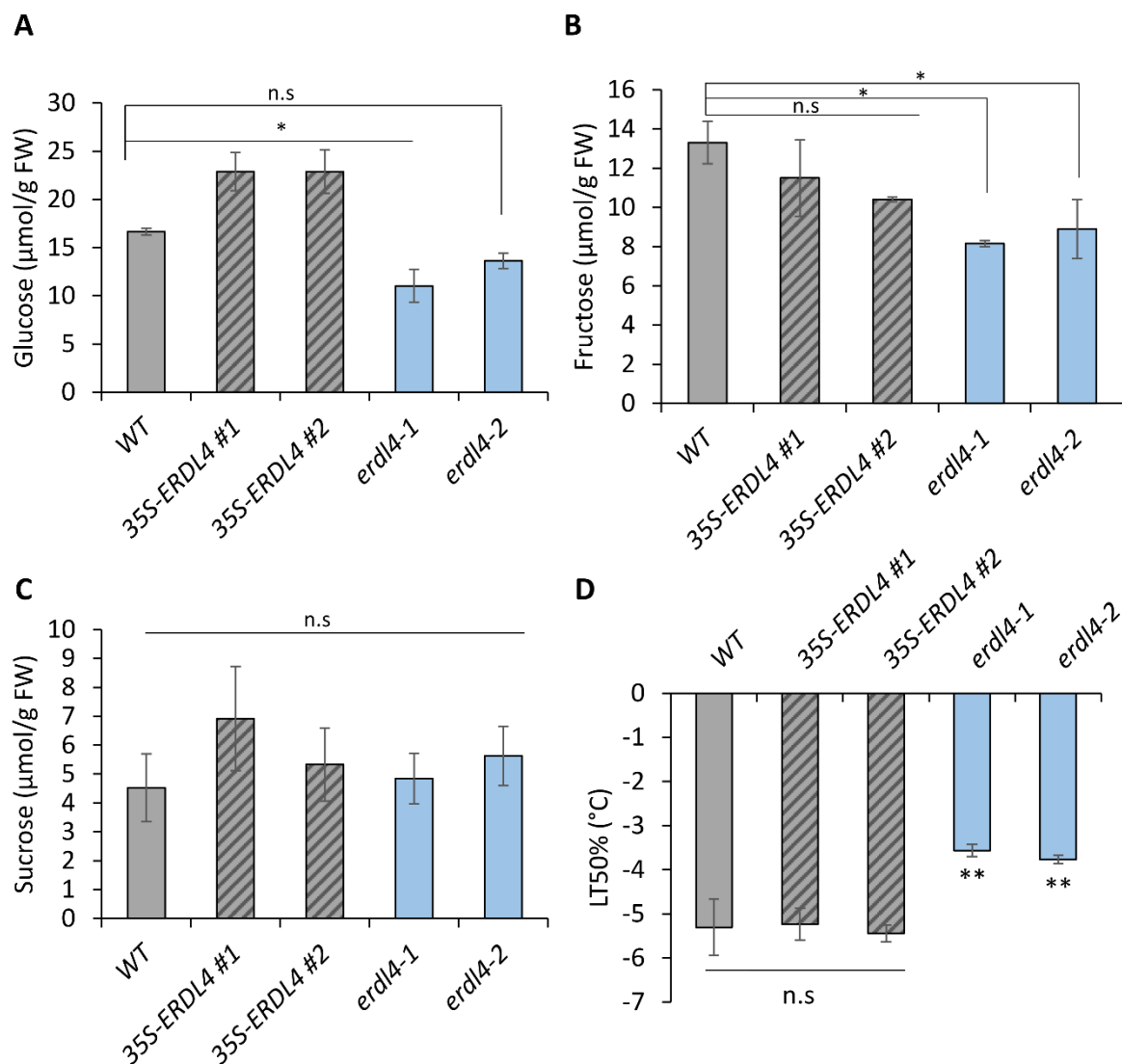


Figure 3.21. Soluble sugars in cold acclimated plants and freezing tolerance. Sugars were quantified from rosettes harvested after 3 days of cold exposure. **A-C.** Glucose, fructose and sucrose content in WT and *ERDL4* mutants. Plants were grown in soil for four weeks in control conditions ($120 \mu\text{mol Photons m}^{-2} \text{s}^{-1}$, 10h light/14h dark, 22°C) and then transferred to cold conditions ($120 \mu\text{mol Photons m}^{-2} \text{s}^{-1}$, 10h light/14h dark, 4°C) for another four weeks. Plants were harvested at mid-day and sugars were quantified enzymatically. Data represents mean \pm standard error from 5-6 biological replicates. Statistically significant differences were calculated using Student's one-tailed t-test (* $p \leq 0.05$; ** $p \leq 0.01$; *** $p \leq 0.001$).

3.3.3. *ERDL4* response to long-term cold

Upon exposure to low temperatures plants show immediate drop in photosynthesis which is followed by sugar accumulation. However, cold-tolerant *Arabidopsis* plants can adapt to long term cold and recover photosynthesis and resume growth after weeks of exposure to low temperatures (Strand et al., 1999, 2003). But it requires help from low temperature induced

anthocyanins which fight against the developing oxidative stress and hence act as antioxidants.

Thus, to gain insight into a putative role of *ERDL4* in growth under long term cold conditions we cultivated WT and *ERDL4* mutants for 4 weeks in control conditions and then transferred them to cold conditions for 2 weeks. Subsequently, we observed growth and quantified anthocyanin accumulation in plants. We also determined sugar levels of cold adapted plants (**Figure 3.22**). After two weeks of growth at 4°C WT contained a fresh weight of 1.1 g. 35S-*ERDL4* #1 had a fresh weight of 1.3 g and 35S-*ERDL4* #2 showed on average a fresh weight of 1.4 g.

The two knockout lines, *erd14-1* and *erd14-2* showed significantly less fresh weight of 0.85 g and 0.65 g respectively. The mutants also showed marked differences in anthocyanin accumulation. The two overexpression lines showed 1.4 fold and 1.7 fold increase in anthocyanin levels whereas, the two knockout lines showed a significant decrease as compared to WT (**Figure 3.22 A-C**). Since the mutants showed changes in anthocyanin accumulation. We checked the expression of anthocyanin biosynthesis genes in WT and 35S-*ERDL4* lines. It turned out that genes like Chalcone synthase (*CHS*), Dihydroflavonol 4-reductase (*DFRA*) and Leucoanthocyanidin dioxygenase (*LDOX*) were upregulated in the presence of sugars as well as in 35S-*ERDL4* lines (**Figure 3.22 D**).

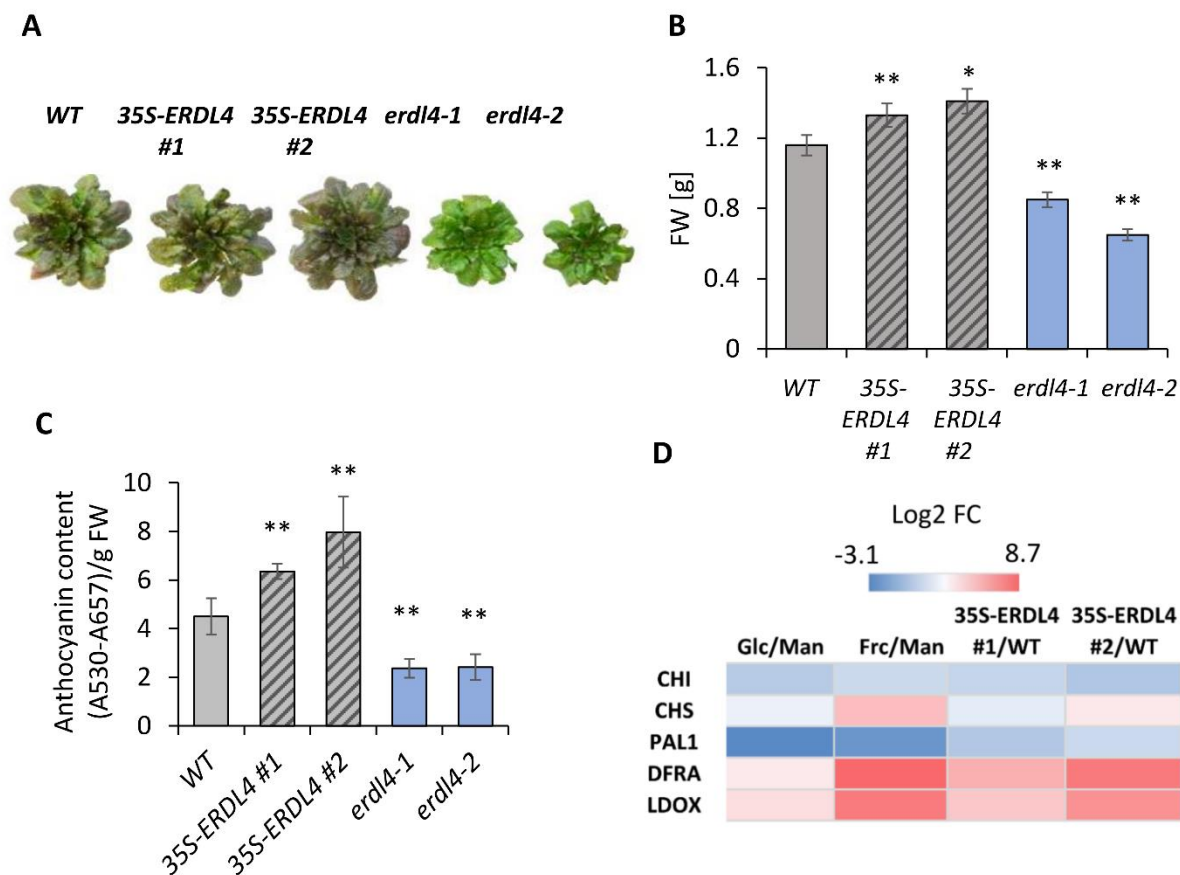


Figure 3.22. Long-term cold adaptation. Analysis of WT and *ERDL4* mutant plants after four weeks of cold exposure. Plants were grown in control conditions ($120 \mu\text{mol Photons m}^{-2} \text{s}^{-1}$, 10h light/14h dark, 22°C) for 4 weeks and then transferred to cold conditions ($120 \mu\text{mol Photons m}^{-2} \text{s}^{-1}$, 10h light/14h dark, 4°C) for another four weeks. **A.** Phenotype of WT and *ERDL4* mutant plants after 4 weeks in cold (4°C). **B.** Rosette fresh weight of WT and *ERDL4* mutants after 4 weeks in cold. **C.** Anthocyanin content in rosettes harvested at mid-day. **D.** Heat map of log2 fold changes of anthocyanin biosynthesis related genes differentially expressed in *ERDL4* overexpressors in comparison with WT. Data represents mean \pm standard error from 5-6 biological replicates. Statistically significant differences were calculated using Student's one-tailed t-test (* $p \leq 0.05$; ** $p \leq 0.01$; *** $p \leq 0.001$).

To analyse whether long term cold adaptation would influence the sugar compartmentation, soluble sugar content from WT and *ERDL4* mutants was determined. The metabolite data indicated that sugar accumulation in cold adapted plants was different as compared to cold acclimation. Here *erdl4* knockout lines showed higher levels of both glucose and fructose as compared to WT and *35S-ERDL4* lines but significantly lower levels of sucrose (**Figure 3.23 A, B, C**). The results suggested that knockout lines failed to export glucose and fructose followed by their accumulation. Sucrose was less because most of it is hydrolysed by the activity of vacuolar invertases into glucose and fructose.

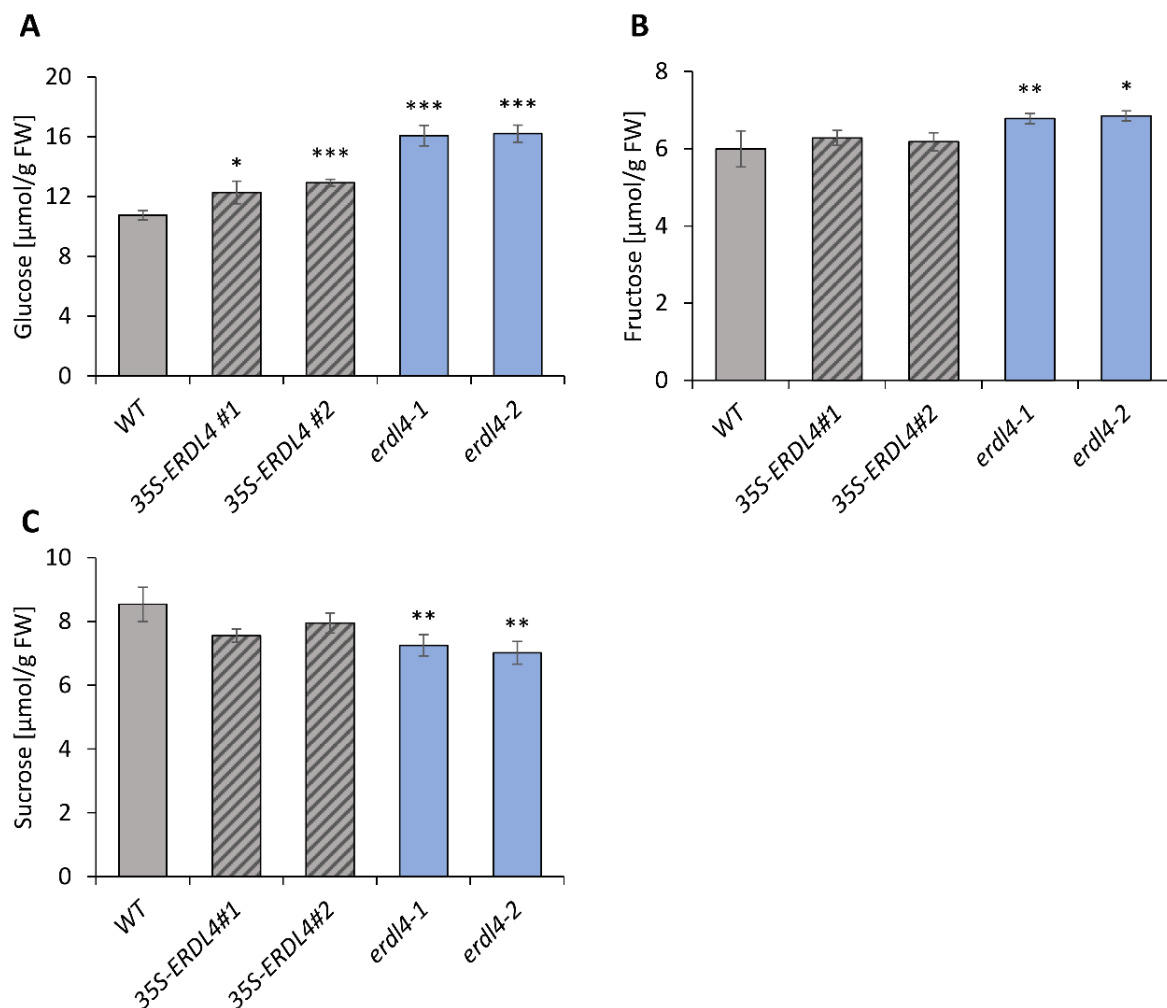


Figure 3.23. Soluble sugars in cold adapted plants. Sugars were quantified from rosettes harvested after 4 weeks of cold exposure. **A-C.** Glucose, fructose and sucrose content in WT and *ERDL4* mutants. Plants were grown in soil for four weeks in control conditions ($120 \mu\text{mol Photons m}^{-2} \text{s}^{-1}$, 10h light/14h dark, 22°C) and then transferred to cold conditions ($120 \mu\text{mol Photons m}^{-2} \text{s}^{-1}$, 10h light/14h dark, 4°C) for another four weeks. Plants were harvested at mid-day and sugars were quantified enzymatically. Data represents mean \pm standard error from 5-6 biological replicates. Statistically significant differences were calculated using Student's one-tailed t-test (* $p \leq 0.05$; ** $p \leq 0.01$; *** $p \leq 0.001$).

3.3.4. Role of *ERDL4* in dark induced senescence

Under conditions where carbohydrates are scarce (continuous dark) plants need alternative sources of energy, proteins and lipids, for the sink tissues to develop (Kunz et al., 2009; Kamranfar et al., 2018). This is accomplished by sacrificing source leaves and causing internal organs such as chloroplasts, mitochondria, and nucleus to degrade in order to recycle carbon and nitrogen supplies. (Fischer & Gan, 2007; Goldman et al., 2010). Since in the promoter region of *ERDL4*, cis-regulatory elements responsible for light responses account for 8% of the promoter region. It was interesting to check how continuous export of monosaccharides from vacuole into the cytosol during dark, influences plant growth. To achieve this *ERDL4* mutants

and the corresponding WT plants were cultivated in control conditions for 5 weeks and then transferred to continuous dark for another 5 days. Samples were collected each day to check *ERDL4* expression over the course of dark period. After 5 days of dark, samples were harvested to check the expression of senescence markers and the corresponding sugar levels. Plants were then placed in control conditions for a week to check the survival rate of the plants. The results exhibited that *ERDL4* levels were found to be markedly lowered throughout the dark treatment (**Figure 3.24 C**). Glucose levels in *35S-ERDL4* lines were upregulated while that in the knockouts were downregulated as compared to WT. Fructose levels in all the lines did not change while sucrose levels reduced significantly in all the lines (**Figure 3.24 E**). Extent of senescence was also analysed by determining the expression of senescence marker genes. From previous studies both *SAG13* and *DIN2* are known to be sugar repressed and positive regulators of senescence (Fujiki et al., 2001; Dhar et al., 2020). Expression of *SAG13* and *DIN2* was found to be significantly reduced in *35S-ERDL4* lines while in the *erdl4-1* and *erdl4-2* was upregulated (**Figure 3.24 F**). Altogether the results showed that sugar export in *35S-ERDL4* lines into the cytosol helps the plant to survive the dark phase. This was also confirmed by the survival rate of the dark treated plants. WT plants showed a survival rate of 88% whereas, *35S-ERDL4* #1 and *35S-ERDL4* #2 exhibited 96% and 100% survival rate. On the contrary, *erdl4* knockout lines had significantly reduced survival rates, 76% and 77% respectively as compared to WT (**Figure 3.24**).

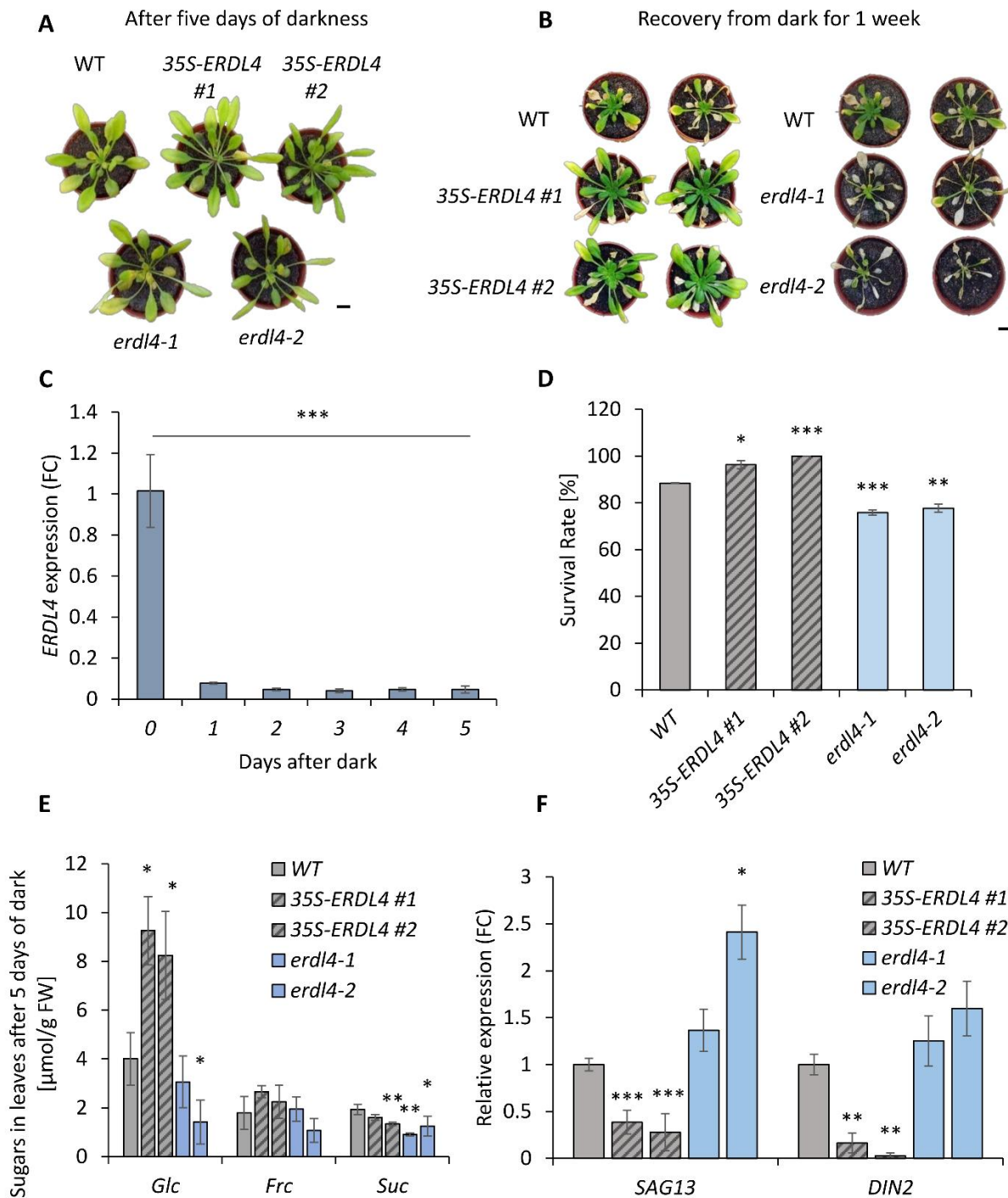


Figure 3.24. Analysis of WT and *ERDL4* mutants after dark treatment. Plants were grown for 5 weeks in standard conditions ($120 \mu\text{mol Photons m}^{-2} \text{s}^{-1}$, 10h light/14h dark, 22°C) in soil and then transferred to complete dark for five days. After dark treatment plants were again placed in standard conditions for recovery (7 days). **A.** Phenotype of WT and *ERDL4* mutants after 5 days in dark. **B.** Phenotype of WT and *ERDL4* mutants after 7 days of dark recovery. **C.** Expression of *ERDL4* in dark over the course of 5 days. Expression is normalized to *Actin*. Data represents mean \pm standard error from 4 biological replicates. **D.** Survival rate of WT and *ERDL4* mutants determined after 7 days of dark recovery in light. Data represents mean \pm standard error from 15 biological replicates. **E.** Level of soluble sugars analysed from WT and *ERDL4* mutants. Data represents mean \pm standard error from 5 biological replicates. **F.** Expression analysis of *AtSAG13* and *AtDIN2* (senescence markers) dark treated WT and *ERDL4* mutants. Samples were collected after five days in dark. Data represents mean \pm standard error from 3 biological replicates. Statistically significant differences were calculated using Student's one-tailed t-test (* $p \leq 0.05$; ** $p \leq 0.01$; *** $p \leq 0.001$)

4. Discussion

Plants often suffer environmental conundrum and have successfully adapted to cope with them. Sugar transport pathways, as well as the proteins that mediate them, are becoming increasingly important. A growing body of research is devoted to deciphering the many sugar transporters and determining their transport specificity and characteristics. Only then would it be feasible to create plants that can better cope with stress while maintaining their yield. However, it presents numerous difficulties, and obtaining a complete image of a sugar transporter in all aspects is far more difficult than anticipated. This research intends to characterize *ERDL4*, a sugar transporter belonging to the MST family, in order to bridge the gap between sugar homeostasis in plants and how it affects plant growth. The findings are explored in the context of altered sugar metabolism and its role in abiotic stresses to provide a better understanding of its function.

4.1. Outcomes of regulated vacuolar sugar export

4.1.1. *ERDL4* is homologous to *ERDL6* but essentially quite different

Analysis of ERD6-like transporters reveal their early emergence and conservation among the plant kingdom. Both *AtERDL4* and *AtERDL6* express constitutively in almost all organs (Slawinski et al., 2021). Protein sequence and evolutionary analysis revealed that the two genes are homologous and closely related (**Figure 3.1 A, B**) having the same secondary structure of 12 transmembrane domains and sharing common sugar motifs (**Figure 3.1 C**). However, expression and functional analysis of the two proteins is on the contrary. In response to varying day and night light conditions the two genes are regulated differently. Expression of *ERDL4* start increasing at the onset of night and is maximum at dawn whereas, *ERDL6* levels are maximum at midday and in the evening (**Figure 3.15 B, D**) suggesting different roles for the two genes. Diurnal expression of *ERDL4* with its exporter function. Since at night the stored sugars in the vacuole need to be mobilized for growth at night (Gordon et al., 1980). Many genes are known to be triggered by low sugars or which are involved in photosynthesis peak at the end of night and those involved in carbon distribution or sucrose synthesis are induced at the end of day (Bläsing et al., 2005). *ERDL6* diurnal expression pattern supports its

role in cellular carbon distribution being a vacuolar glucose exporter. Diel expression analysis of vacuolar sugar importers, TST1 and TST2, also supports the notion that during daytime, sugars are being accumulated in the vacuole for which induction of sugar importers is essential. This is supported by the observation that levels of TST1 and TST2 rise during the day and decline at night-time (**Figure 3.15 F, H**).

In terms of regulation during abiotic stresses like cold and dark the two transporters showed opposite regulation. *ERDL4* is upregulated during cold stress (**Figure 3.20 A, B**) and downregulated in dark (**Figure 3.24 C**) whereas, for *ERDL6* it is vice versa (Poschet et al., 2011). Vacuolar sugar accumulation in cold is well documented (Wormit et al., 2006; Poschet et al., 2011; Klemens et al., 2013). During cold temperatures TST1 and TST2 help plants to efficiently accumulate vacuolar sugars which is a critical metabolic process in cold for developing frost tolerance (Pommerrenig et al., 2018). Upon exposure to different stresses, sugar export out of the vacuole has also been studied supporting synthesis of molecules acting as an osmoprotectant and stabilizing membranes (Ruan et al., 2010). Hence cold induced increase in *ERDL4* levels is in line with its export function.

Analysis of cis-acting elements in the promoter region (1000 bp upstream of the start ATG) of *ERDL4* provided more insights into the gene regulation (**Figure 3.2**). Presence of cold-specific DRE (dehydration responsive element), CRT (C-repeat) elements and LTRE (low temperature responsive element) elements confirms its role in cold signalling (Chinnusamy et al., 2006; Yamaguchi-Shinozaki & Shinozaki, 2006). Among the other predominant cis-elements found in the promoter of *ERDL4* were that of light responsive BOX4 cis-element (Lam & Chua, 1989), ERE (ethylene response element) involved in stress and defense related processes (Itzhaki et al., 1994), WUN (wounding and pathogen response) (Pastuglia et al., 1997) and drought responsive elements MYB and MYC suggesting its participation in different stresses. MYB proteins regulate primary and secondary metabolism, seed and floral development, cell destiny and identity, defense, and stress responses in plants, among other biological activities (Dubos et al., 2010). MYC controls ABA responsive gene expression which is also evident from the *frc* specific regulation observed in *35S-ERDL4* overexpression lines. Some of the commonly regulated genes between fructose and overexpressors also accounts for ABA related gene expression (**Figure 3.14**) (Abe et al., 1997, 2003).

4.1.2. *ERDL4* is a vacuolar protein and resides in the tonoplast

Many studies have been conducted to determine the subcellular localization of ERDLs in Arabidopsis. All of them have been found to reside in the vacuolar membrane, the tonoplast. These include GFP-fusions of ERD6, ERDL3, ERDL6, and ERDL7/ZIF2 (Yamada et al., 2010; Poschet et al., 2011; Remy et al., 2014). Because of the presence of chloroplast transit peptides, membrane targeting prediction implies that two other members, ERDL10 and ERDL12, also localize to the tonoplast, while ERDL14 and ERDL15 may target to plastids. (Pommerrenig et al., 2018). ERDL4 localization has also been studied previously and isolated as a vacuolar membrane protein (Endler et al., 2006; Jaquinod et al., 2007; Schulze et al., 2011). In addition, ERDL4, ERDL7, ERDL8 have also been detected in tonoplast membrane fractions by proteomic LC-MS/MS-based analysis (Pertl-Obermeyer et al., 2016). The transient expression of ERDL4-GFP fusion protein in Arabidopsis mesophyll protoplasts clearly suggested that ERDL4 localizes to the tonoplast (**Figure 3.3**) corroborating results obtained from proteomic analysis of tonoplast proteins (Jaquinod et al., 2007; Pertl-Obermeyer et al., 2016).

4.1.3. *ERDL4* mediates vacuolar fructose export influencing plant organ development

The fact that *ERDL4* is related to MSTs, as well as its fundamental structure and the usual sugar-binding motifs in its amino acid sequence (**Figure 3.1 C**) suggested a sugar transporter function. Since the opinion that MST members with similar biochemical features tend to phylogenetically cluster together and form functional subfamilies (Pommerrenig et al., 2018), it is possible that *ERDL4*, like its closest homolog ERDL6, functions as an H⁺/Glu symporter. It was difficult to study the biochemical transport features of the ERDL4 protein via uptake assays of radiolabelled substrates or electrophysiology due to likely targeting of ERDL4 protein to internal membranes of *Xenopus laevis* oocyte cells or yeast cells (**Figure 7.3, 7.4**). However, NAF analysis of plants with increased and reduced *ERDL4* activity provided substantial evidence for the altered subcellular sugar distribution (**Figure 3.6**). Furthermore, it not only indicated that *ERDL4* is a sugar exporter, but also suggested fructose as a preferred export substrate as compared to glucose. This observation can be supported by the uneven distribution of monosaccharides in the vacuole and cytosol of *35S-ERDL4* plants.

Overexpression of *ERDL4* leads to high cytosolic fructose levels while glucose levels increase correspondingly both in the vacuolar and cytosolic fractions. Sugar accumulation patterns in the cold provided additional evidence that *ERDL4* worked as a vacuolar fructose exporter. Plants that are cold-stressed are prone to cold dependent rise of monosaccharides in their vacuoles (Klemens et al., 2013; Rodrigues et al., 2020; Ho et al., 2020; Vu et al., 2020). After three days in the cold, we observed a comparable response in the WT, 35S-*ERDL4*, and *erd14* knockout lines in our cold acclimation study (**Figure 3.20**). However, under these conditions, these lines stored sugars at varying degrees. It is worth noting that the drop in glucose and fructose in *erd14-1* and *erd14-2* knockouts occurred proportionally, whereas the increase in these sugars in 35S-*ERDL4* plants did not. In the cold, monosaccharide build-up in vacuoles is nearly entirely due to sucrose import by TST proteins and subsequent breakdown by vacuolar enzymes (Klemens et al., 2013; Vu et al., 2020). This results in a proportional increase in glucose and fructose fractions. In conclusion, *erd14* knockout lines collected less monosaccharides in the cold, but their frc to glc ratio remained unchanged when compared to WT cells (**Figure 3.20**). The frc to glc ratio was clearly lower in *ERDL4*-overexpressing plants even though these plants accumulated monosaccharides at higher quantities than WT plants. The non-proportional increase in glucose and fructose in 35S-*ERDL4* plants compared to WT plants suggested that fructose was released from vacuoles of 35S-*ERDL4* plants in the cold to a greater extent than glucose, confirming the hypothesis that *ERDL4* acts as a fructose rather than glucose transporter.

Manipulations in cellular sugar homeostasis led to changes in growth and development. Sugars can play a variety of regulatory roles in physiological processes, and the plant's developmental stage determines how it responds to sugars (Rolland et al., 2006; Eveland & Jackson, 2012; Horacio & Martinez-Noel, 2013). The phenotypic differences of *ERDL4* mutant plants can be explained by the suggested fructose export capacity of *ERDL4* and the subsequent rise in cytosolic sugars (**Figure 3.6**). The free fructose in the cytosol can contribute to the provision of carbon skeletons which can serve as a fuel in glycolysis. Since cytosolic hexoses need to be phosphorylated before they are utilized in metabolic pathways (Dennis & Blakeley, 2000), this purpose might be served by a cytosolic HXK or FRK. Fructose-6-phosphate (F6P) is a primary precursor of glycolysis which results in the formation of transport sugar sucrose, a non-reducing disaccharide (Dennis & Blakeley, 2000). Since 35S-*ERDL4* lines also

showed increased cytosolic sugar levels which is depicted by downregulation of CAB1 and upregulation of GPT2 (**Figure 7.5**) it is tempting to speculate that free fructose which is exported out by ERDL4 might be phosphorylated by HXK2 and PFK7 which are upregulated in *ERDL4* overexpression lines (**Figure 7.5**) resulting in elevated sugar levels which is then exported to the sinks. Very recently PFK7 is also observed as a key player for maintaining Arabidopsis leaf sugar homeostasis and source to sink transport and reduced levels of PFK7 are linked to reduced shoot growth (Perby et al., 2022).

Increased transport to the sinks is associated with stimulated development of inflorescences and seed production (Wingenter et al., 2010). It is of significance that balance between sucrose/hexose ratio is maintained for initiation of flowering (Wingler, 2018). 35S-*ERDL4* lines show elevated phloem sugar export (**Figure 3.8 A**) and is confirmed by induced expression of SWEET11 and SWEET12 transporters (**Figure 3.8 B**). The two proteins are key players in sugar efflux and phloem loading. Double mutant of *sweet11;12* shows reduce phloem loading and elevated leaf sugar levels (Chen et al., 2012). Furthermore, it is reported that reduced sucrose sink supply also decreases seed lipid content (Chen et al., 2015). Hence, increased sugar export in 35S-*ERDL4* lines is contributing towards longer inflorescences with more branches (**Figure 3.9 B, C**). Seed properties are also visibly affected with 35S-*ERDL4* lines possessing bigger and heavier seeds whereas, *erdl4* knockout lines show wrinkled and smaller seeds indicating reduced seed filling. Thus, increased source to sink transport is required for better seed yield, seed size and lipid content (**Figure 3.11**) (**Figure 3.12 A, B**).

Roots also represent a strong sink tissue. Reduced sugar export via phloem also effects the provision of assimilates to the roots and correspondingly root growth. Differences in root growth mediated by altered *ERDL4* levels in the mutants also depicts the significance of maintaining proper sugar efflux. *ERDL4* overexpressors show strong sink strength by possessing longer roots as compared to WT and *erdl4* knockouts (**Figure 3.6 B, D**) (**Figure 3.7**).

4.1.4. *ERDL4* overexpression correlates with cytosolic fructose

Induction

Although not much is known about the fructose related effects on global gene expression, our RNA-Seq analysis with sugar feeding data provides some information but still, most of the

genes are regulated in the same manner by both fructose and glucose (**Figure 7.6**). Dissection of fructose specific induction in *35S-ERDL4* lines from glucose points out towards the signalling role of fructose more than the glucose in *35S-ERDL4* plants (**Figure 3.13**) which confirms the fructose export mediated by *ERDL4*, increasing cytosolic fructose levels and initiating fructose related gene regulation responses (**Figure 3.13 E**). The results showed that many genes which are highly induced by fructose but reduced by glucose were also regulated in the same manner in *35S-ERDL4* overexpressors and vice versa (**Figure 3.13 E**). Sugar homeostasis in plants is also tightly diurnally regulated. Sugar was found to be more important than light or water stress in daily gene expression oscillations, and it was concluded that sugars and the circadian clock are the two most important inputs to rhythmic regulation of transcripts (Bläsing et al., 2005). The significance of transport in circadian behaviour cannot be assumed solely based on transcriptional control of transporters (Covington & Harmer, 2007) oscillations in the fluxes and concentrations of the transported solutes must also be considered. Sucrose is synthesized during the day and is cleaved by invertases into glucose and fructose for night-time energy metabolism. Thus, it is reasonable to believe that night-time elevation in fructose levels could be an indication of invertase activity and a drop in sucrose levels (Zhong et al., 2020). Like sugar transporter1 (*STP1*) and *SWEET1* (Cordoba et al., 2015; Sherson et al., 2000; Chen et al., 2010), *ERDL4*, *ERDL6* and *TSTs* also follow a diurnal rhythm and this regulation is also observed in the oscillations of fructose levels mediated by overexpression of *ERDL4* as depicted by frc/glc ratios at the EON and EOD (**Figure 3.15**).

Furthermore, presence of glucose and sucrose at low concentrations promote root growth whereas, fructose even at very low concentrations restricts growth (Zhong et al., 2020). Because of such an inhibitory effect it cannot be neglected that plants have endogenous mechanisms to cope with such inappropriate conditions. Modifying sugar homeostasis by changing sugar transporter levels has been shown to cause differential regulation of other sugar transporters, presumably to preserve the internal sugar balance (Sun et al., 2019; Zhu et al., 2021). Similar regulation is also observed in *ERDL4* overexpressing plants where high cytosolic fructose levels result in differential regulation of other importers and exporters (**Figure 3.15**). Since the sugar accumulation effect in *ERDL4* overexpressing lines is mainly due to *TST2* differential regulation and fructose is known to modulate *TST2* levels (Wormit et al., 2006), the focus of current work is on endogenous fructose homeostasis.

Previously it was known that sugar transport is controlled via protein phosphorylation, and various putative phosphorylation sites were identified but the respective kinases responsible were still unknown. Identification of mitogen-activated triple kinase-like protein kinase (VIK) provided new insights in the post-translational control of TST1 sugar/proton antiporter function (Wingenter et al., 2011). Post-translational control of AtSUC2 by WALL-ASSOCIATED KINASE-LIKE8 (*AtWAKL8*) has recently been established (Q. Xu et al., 2020), acting as a positive regulator of *SUC2* activity and promoting growth. It is known that activity of *TST2* is also regulated via phosphorylation increasing its import strength (Hedrich et al., 2015). This phosphorylation can be triggered either by the Arabidopsis protein kinase VIK1 (Wingenter et al., 2011) or the cotton protein Calcineurin B-like protein (CBL) interacting protein kinase 6 (CIPK6) (Deng et al., 2020). In cotton TST2, Ser⁴⁴⁸ has been found as a target amino acid being phosphorylated by *GhCIPK6* (Deng et al., 2020). Interestingly this Ser⁴⁴⁸ residue is conserved in barley, rice and Arabidopsis TST2 proteins (**Figure 7.7**) (Dhungana & Braun, 2021; Hunter, 2020) suggesting conservation of this Ca⁺ and phosphorylation signalling resulting in sugar accumulation across these species. Sequence and phylogenetic analysis of *GhCIPK6* and *AtCIPK6* (**Figure 3.18**) revealed that the two kinases are very similar and closely related pointing towards the possible regulation of AtTST2 also by *AtCIPK6*. Further analysis of *AtCIPKs* with a focus on sugar specific induction reveals that both TST2 and CIPK6 are specifically fructose induced (**Figure 3.19**). Therefore, it is conceivable that cytosolic fructose presence in *ERDL4* overexpressing lines mediates *CIPK6* activity which in turn phosphorylates TST2 facilitating vacuolar glucose sequestration.

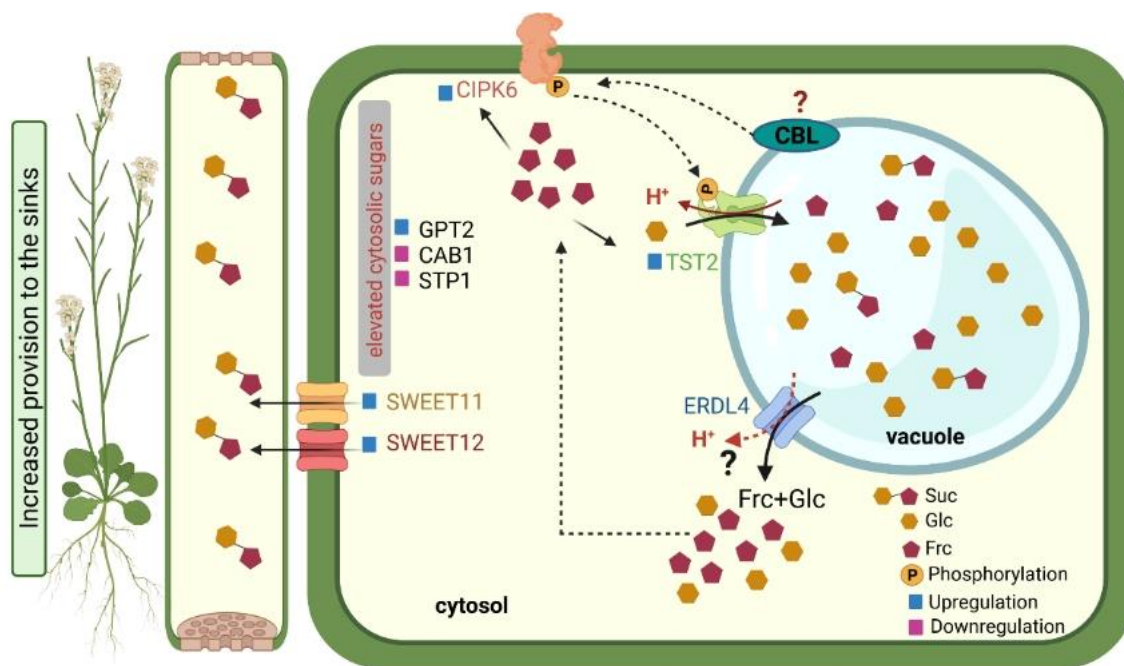


Figure 4.1. Schematic overview of *ERDL4* mediated processes. *ERDL4* mediates glc/frc release from the vacuole. Increased cytosolic fructose levels causes induction of CIPK6 which is recruited by an unknown CBL protein to the tonoplast phosphorylating TST2 which mediates glucose import back into the vacuole. High cytosolic sugars cause upregulation of GPT2 and downregulation of CAB1 and STP1, serving as cytosolic sugar sensors. Sugars are being exported and loaded into apoplast via SWEET11 and SWEET12 transporters suggesting increased provision of sugars to the sink. *This figure was created with BioRender.com.*

4.1.5. *ERDL4* and cold response

Plants reprogram gene expression and metabolic fluxes during cold stress to adjust their metabolism and development (Stitt & Hurry, 2002; Yamaguchi-Shinozaki & Shinozaki, 2006; Chinnusamy et al., 2006; Miura & Furumoto, 2013). Since the promoter region of *ERDL4* contains LTRE motifs which provides binding site for CBF/DREB1 transcription factor, we can expect a cold specific response from *ERDL4*. Overexpression of these transcription factors provide increased cold acclimation and an elevated frost tolerance (Jaglo-Ottosen et al., 1998; Cook et al., 2004). CBF genes are also regulated by inducer of CBF expression1 (ICE1) transcription factor which binds to MYC motif in the promoter region. *ERDL4* promoter also contains 2 of this MYC motifs. TST2 promoter is also known to possess several of these motifs in its promoter region and *ice1* mutant plants show less induction of *TST2* during cold (Chinnusamy et al., 2003). Also, soluble sugars are the key players in enhancing plant tolerance to cold stress (Nägele & Heyer, 2013). This is achieved by direct interaction of sugar moieties with the membrane phospholipids and hence decreasing membrane permeability (Strauss & Hauser, 1986; Ruelland & Collin, 2011). Arabidopsis plants are known to accumulate sugars

during acclimation process which increases their frost tolerance (Wanner & Junttila, 1999; Klemens et al., 2013; Vu et al., 2020). Being a vacuolar sugar transporter and having cold specific cis-elements *ERDL4* levels also fluctuate during cold stress showing a dramatic cold dependent increase (**Figure 3.20**). Considering the cold dependent differential regulation of other soluble sugar transporters, particularly the Tonoplast Monosaccharide Transporters (TMTs) (Wormit et al., 2006) and Sugars Will Eventually Be Exported Transporters (SWEETs) (Klemens et al., 2013), it is perceivable that both vacuolar importers and exporters are required to cope up with the cold response. During cold acclimation *ERDL4* overexpression mediates cold dependent uneven monosaccharide accumulation. There is a build-up of glucose but not fructose suggesting fructose export via *ERDL4* whereas *erd14* knockout lines after three days of cold exposure do not show significant differences as compared to WT but accumulated in total less monosaccharides (**Figure 3.21**) subsequently effecting plant frost tolerance (**Figure 3.21 D**). Here it is noticeable that monosaccharide accumulation in vacuoles in the cold occurs almost exclusively via sucrose import by TST proteins and successive hydrolysis by vacuolar invertases (Klemens et al., 2013; Vu et al., 2020) resulting in proportional increase in glucose and fructose moieties however, this was not the case in *ERDL4* overexpressing lines pointing more towards fructose export rather than glucose.

In contrast to short time acclimation responses, plants transit to an adaptation phase after prolong exposure to environmental stress. During long term cold adaptation, the metabolic processes in plants are different to acclimation. Here the plants must fight against the developing oxidative stress and the resulting reactive oxygen species (ROS) build up. This is achieved by the accumulation of anthocyanins acting as osmoprotectant of cellular compounds (Havaux & Kloppstech, 2001); Hernández et al., 2009). *ERDL4* mutants when expose to cold adaptation show varying responses (**Figure 3.22**). *35S-ERDL4* overexpressing lines accumulate anthocyanins more than the WT which was obvious by their purple coloration and show better growth. On the other hand, *erd14* knockout plants accumulated less anthocyanins and had less fresh weight. Coming to the sugar profiles, the overexpression lines again show uneven build-up of monosaccharides with fructose not accumulated to significant levels as compared to glucose. It is interesting to note here that knockouts also show increased monosaccharides which would indicate their failure to export vacuolar sugars which in the cytosol can be used for anthocyanin production (**Figure 3.23**).

Hence, upregulation of *ERDL4* transcript levels during cold are required for sugar build-up in the cytosol to protect against frost damage (Weizmann et al., 2018) and for growth promotion during cold stress.

4.1.6. *ERDL4* and dark induced senescence

Plants sessile nature has made them exceedingly sensitive and adaptable to the constantly changing environment, especially light and dark. Because they are photoautotrophs, they are largely reliant on light for photosynthesis, yet they have mechanisms in place to withstand brief periods of darkness. The plant's metabolism is radically reprogrammed during dark-induced senescence to extend its lifespan by switching from anabolic to catabolic cellular reactions. In *Arabidopsis* photoreceptors, phytochromes, have a central role in both shade sensing and shade avoidance. When a plant experiences shade, it mobilizes its resources to accelerate stem and hypocotyl extension to escape this competition for light (de Wit et al., 2016). The principal effect of darkness is a termination of photosynthesis. To survive in such a scenario plant needs a continuous supply of energy via glycolysis and TCA cycle and to keep these running, degradation and recycling of proteins, lipids and sugars take place (Zhu et al., 2022). Therefore, to access cellular energy stores it is reasonable for a plant to induce vacuolar sugar exporters like in case of *ERDL6* to make sugars available in the cytosol (Poschet et al., 2011). Phytochrome mutants *phy*, also show increased accumulation of hexose pool possibly because they cannot activate the vacuolar sugar transporter genes controlled by phytochromes to mobilize vacuolar sugars resulting in decreased biomass (Krahmer et al., 2021). Promoter of *ERDL4* also contains some light responsive motifs specific to phytochrome response (**Figure 3.2**). To investigate further the role of *ERDL4* during prolonged darkness, WT, *ERDL4* overexpression and knockout plants were subjected to 5 days of complete darkness. Surprisingly, *ERDL4* transcript levels were reduced in the WT and stayed low over the course of five days (**Figure 3.24 C**). Despite this *35S-ERDL4* lines showed a better dark tolerance and increased survival rate of almost 100% as compared to the WT (**Figure 3.24 D**). For the *erdl4* knockouts it was expected to perform like the WT, because of the induction of *ERDL6* transporter in dark, but on the contrary knockouts showed even less dark tolerance and lower survival rates than the WT (**Figure 3.24 B, D**).

Differential response of the mutants is probably related to the altered sugar homeostasis in the cytosol. Increased soluble sugars can also be measured from *35S-ERDL4* plants after 5 days of the dark with glucose showing most prominent increase. While the knockouts have overall less sugars (**Figure 3.24 E**). Since sugar phosphates (glucose-6-phosphate and glucose-1-phosphate) are known inhibitors of leaf senescence (Toroser et al., 2000; Zhang et al., 2009; Piattoni et al., 2011; Nunes et al., 2013), export of fructose and glucose into the cytosol by *ERDL4* overexpressing plants and their subsequent phosphorylation by *HXK* or *FRK* provides an advantage over the WT and can fuel sugar metabolism, promoting growth and repressing senescence (Baena-González et al., 2007). Conversely *erdl4* knockout plants because of having less cytosolic sugars, initiated autophagy and senescence leading to degradation of subcellular organs and proteins indicated by induced expression of senescence marker genes (Dhar et al., 2020; Fujiki et al., 2001) (**Figure 3.24 F**). This is also obvious from the plants after 7 days of recovery. *35S-ERDL4* lines recovered faster and better because of the subcellular organs still intact while *erdl4* knockout plants struggle with recovery having most of the cells already degraded.

Hence, it raises a question that why in nature *ERDL4* transcript content is not upregulated in the dark-stressed WT plants (**Figure 3.24 C**), although such a regulation can support prolong dark survival? One possible explanation would be that plants only generate alternative responses to a particular stress depending on how often they must experience similar stress situations and in nature such long periods of complete darkness are never occurring phenomenon (Des Marais & Juenger, 2010). Plants have naturally occurring shade avoidance program in which they accelerate their growth towards the light source to escape the shade (Morelli & Ruberti, 2002). Another perception also prevails that plants only produce expensive phenotypes when needed (Collins et al., 2008). So instead of spending energy resources in inducing multiple response factors during energy starved conditions to survive, they spend energy on rapid growth to avoid shade. In summary, dark stress response requires a regulated sugar homeostasis mediated by movement of vacuolar sugar pool via tonoplast localized sugar transporters.

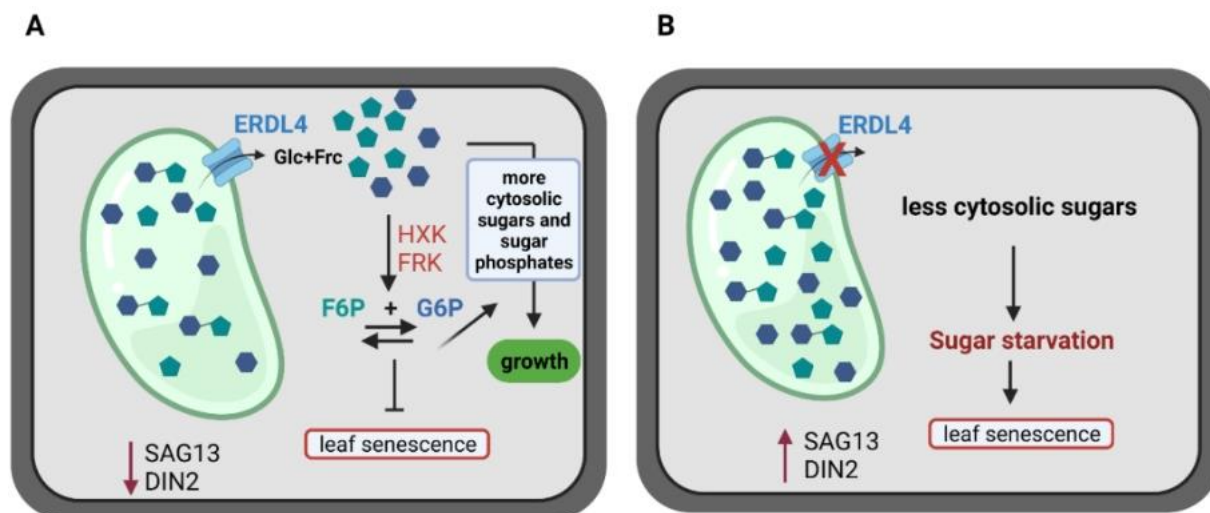


Figure 4.2. Overview of ERDL4 in dark induced senescence. **A.** Export of monosaccharides via *ERDL4* elevates cytosolic sugar levels. The free sugars can be phosphorylated by HXK and FRK to form G6P and F6P respectively. F6P can be successively converted to G6P which is the precursor for growth related processes and inhibits senescence. **B.** In *erdl4* knockout plants the sugars are trapped inside the vacuole resulting in less cytosolic sugars available for growth promoting senescence. *This figure was created with BioRender.com.*

4.2. Conclusion

The data collected as part of this dissertation showed an influence of the vacuolar sugar exporter *ERDL4* on the sugar homeostasis of Arabidopsis, demonstrating that *ERDL4* mediates glucose and more specifically fructose efflux out of the vacuole. Overexpression of this transporter leads to high cytosolic sugar levels prompting increased phloem sugar export leading to better growth of sink tissues. Overexpression plants exhibit better shoot and root growth and increased seed yield and seed filling. Additionally seeds also have higher lipid content. Whereas, the knockouts have less shoot and root growth, and less sugar export results in lower seed yields, smaller and wrinkled seeds. Knocking out *ERDL4* also lead to reduced seed lipid content. Furthermore, increased fructose export in the cytosol also induced other vacuolar sugar importer genes notably TST2 which results in elevated vacuolar glucose accumulation. Moreover, high cytosolic fructose concentration also increases *CIPK6* levels which is responsible for the phosphorylation of TST2 mediating vacuolar sugar import.

ERDL4 also plays crucial role in different stress responses of Arabidopsis. In cold stress *ERDL4* mediates glucose accumulation in the vacuole but promotes fructose export to the cytosol. The knockouts of *ERDL4* show less frost tolerance due to reduced sugar levels. In long term cold adaptation response sugar export mediated by *ERDL4* overexpressors show its

significance in synthesis and accumulation of anthocyanins useful to fight against developing ROS stress and help plants to grow. On the other hand, *ERDL4* overexpression-dependent high cytosolic monosaccharide accumulation promote growth under induced darkness ensuring plant survival and recovery during periods of low light intensity. Absence of *ERDL4* during dark has drastic effects on the knockout plants with least survival and slowest recovery rates. So far there are still some ambiguities, such as glucose and fructose export directly regulate these processes in detail, or they become a part of certain pathway to change glucose or sucrose-mediated signalling. For the biochemical transport indication to check whether the transport is proton coupled or is it working as a symporter or facilitator the gap remains to be filled. Overall, this work provided the first indication of *ERDL4* function in a plant-physiological context which can form the basis for further investigations.

4.3. Outlook

ERDL4 is a sugar transporter, it would be interesting and advantageous to determine its transport characteristics whether the transport is proton coupled and if it is working as a symporter or a facilitator. Since it is a vacuolar protein and localize on tonoplast (**Section 3.1.3**) making it a tough target for uptake studies using heterologous systems. Some attempts have already been done to check the ^{14}C labelled glucose and sucrose uptake using *Xenopus* oocytes expression system (Bröer et al., 1999; Klemens et al., 2013) but it failed to show high uptake counts both in the control and *ERDL4* expressing oocytes in case of all the sugars. Although the difference between control and *ERDL4* expressing oocytes is higher in case of ^3H Frc (**Figure 7.4**). One possible explanation could be that the protein is not localized to the plasma membrane or only a very small amount expresses on the plasma membrane.

In yeast heterologous system also *ERDL4* depicts tonoplast localization (**Figure 7.3**). Currently efforts are being done to change the tonoplast localization of the protein to plasma membrane by mutating the putative di-leucine motif (EGRNDL) to two Alanines (GCTGCT) (Yamada et al., 2010). In another approach N-terminal truncated *ERDL4*-GFP protein is also constructed and fused to GFP. Both GFP constructs are expressed in yeast which shows high expression in cytosol and probably endoplasmic reticulum, and we expect that some part might also go to the plasma membrane. With such a possibility, *ERDL4* might help the yeast mutated in plasma membrane hexose transporters, EBY.VW-4000, to grow on glucose or fructose as a sole carbon

source. Uptake studies on isolated vacuoles from *35S-ERDL4* plants would also provide an insight into its transport characteristics (Wormit et al., 2006).

ERDL4 is also tightly diurnally regulated (**Figure 3.15 A**). It might be possible that the altered clock genes levels in *35S-ERDL4* plants results in different sugar accumulation patterns at different time points since molecular clock and carbon fluxes in plants closely interact with each other (Haydon et al., 2011). Insight into diurnal sugar accumulation patterns would also provide details on how *ERDL4* contribute towards maintenance of diel cellular sugar homeostasis.

Furthermore, gene expression of *ERDL4* is downregulated in *Arabidopsis* during drought stress (eFP browser: Winter et al., 2007), presumably to protect the membranes by keeping sugars inside the vacuole and so to avoid osmotic imbalance. Soluble sugars often reduce protein denaturation during drought stress. To preserve protein structure and function, the free hydroxyl groups of soluble sugars compensate for those of water (Kaur et al., 2021). Increased sugar metabolism, transport, and distribution results in a higher root-shoot ratio, which improved drought tolerance (Du et al., 2020). Since *35S-ERDL4* plants already show increased root length due to increase sugar export (**Figure 3.6 B**) we expect that during drought stress it would prove to be beneficial for the plants. Drought stress can be applied depending upon the soil field capacity (Valifard et al., 2021) and plants can be studied for their respective phenotypes and survival rate.

5. Summary

Soluble sugars play an important role in plant growth and development and are synthesized via photosynthesis in chloroplast and cytosol and are stored in the vacuole. Maintenance of sugar homeostasis between different cellular compartments and cytosol is of critical importance. *ERDL4* is a tonoplast localized transporter mediating glucose and with more specificity fructose efflux into the cytosol. To investigate and characterize the transporter functionally we altered the gene's level in plants both by overexpressing it in Arabidopsis and using the knockout lines. Overexpression of this transporter lead to accumulation of sugars predominantly glucose and faintly fructose. While the knockout lines showed reduced sugar levels. Detailed sub cellular sugar compartmentation analysis showed that glucose levels were increased both in the vacuole and cytosol while the fructose levels were elevated solely in the cytosol of *35S-ERDL4* lines. This high cytosolic sugar levels lead to increase in long distance sugar transport providing more carbon to the sinks which had a positive effect on shoot and root growth and also significantly improved seed size and lipid content. This observation demonstrates an influence of *ERDL4* on vacuolar sugar accumulation. In summary, it could be shown that *ERDL4* mediates fructose and glucose export from vacuole to cytosol with improved long-distance transport.

To investigate the increased glucose levels inside the vacuole expression levels of *TST2* along with other vacuolar sugar importers were found upregulated in *35S-ERDL4* lines. To confirm the results and to check whether this differential regulation in *35S-ERDL4* lines corresponds more to glucose effects or is it a fructose specific effect, we send samples for RNA-Seq from WT and *35S-ERDL4* lines as well as WT incubated in different sugars. With the help of correlation analysis, it was confirmed that overexpressors show more fructose specific regulation rather than glucose. This also confirms our observation that high cytosolic fructose levels lead to induction of *TST2* and CIPK6 kinase known to phosphorylate *TST2* which subsequently opens the path for vacuolar glucose accumulation.

ERDL4 also plays a significant role when it comes to different abiotic stresses in Arabidopsis. It could be shown in this work that low vacuolar sugar content in *erd14* knockouts lead to less frost tolerance while long term cold exposure gave overexpressors an advantage over WT and knockout plants by developing more osmoprotectants like anthocyanins to fight against

developing ROS and showed better growth. In prolonged dark treatment sugar efflux mediated by *35S-ERDL4* lines proved beneficial for the survival and recovery of the overexpressor plants. Overall, within the framework of the dissertation, important information for clarifying the importance of sugar homeostasis mediated by *ERDL4* was gained, which forms the basis for further investigations.

6. Bibliography

- Abe, H., Urao, T., Ito, T., Seki, M., Shinozaki, K., & Yamaguchi-Shinozaki, K. (2003). Arabidopsis AtMYC2 (bHLH) and AtMYB2 (MYB) function as transcriptional activators in abscisic acid signaling. *The Plant Cell*, *15*(1), 63–78.
- Abe, H., Yamaguchi-Shinozaki, K., Urao, T., Iwasaki, T., Hosokawa, D., & Shinozaki, K. (1997). Role of arabidopsis MYC and MYB homologs in drought- and abscisic acid-regulated gene expression. *The Plant Cell*, *9*(10), 1859–1868.
- Aguero, T., Newman, K., & King, M. Lou. (2018). Microinjection of *Xenopus* oocytes. *Cold Spring Harbor Protocols*, *2018*(2), pdb-prot096974.
- Ahuja, I., de Vos, R. C. H., Bones, A. M., & Hall, R. D. (2010). Plant molecular stress responses face climate change. *Trends in Plant Science*, *15*(12), 664–674.
- Aluri, S., & Büttner, M. (2007). Identification and functional expression of the Arabidopsis thaliana vacuolar glucose transporter 1 and its role in seed germination and flowering. *Proceedings of the National Academy of Sciences*, *104*(7), 2537–2542.
- Amemiya, T., Kanayama, Y., Yamaki, S., Yamada, K., & Shiratake, K. (2006). Fruit-specific V-ATPase suppression in antisense-transgenic tomato reduces fruit growth and seed formation. *Planta*, *223*(6), 1272–1280.
- Anchordoguy, T. J., Rudolph, A. S., Carpenter, J. F., & Crowe, J. H. (1987). Modes of interaction of cryoprotectants with membrane phospholipids during freezing. *Cryobiology*, *24*(4), 324–331.
- Baena-González, E., Rolland, F., Thevelein, J. M., & Sheen, J. (2007). A central integrator of transcription networks in plant stress and energy signalling. *Nature*, *448*(7156), 938–942.
- Baker, A., Graham, I. A., Holdsworth, M., Smith, S. M., & Theodoulou, F. L. (2006). Chewing the fat: β -oxidation in signalling and development. *Trends in Plant Science*, *11*(3), 124–132.
- Baker, R. F., Leach, K. A., & Braun, D. M. (2012). SWEET as sugar: new sucrose effluxers in plants. *Molecular Plant*, *5*(4), 766–768.
- Becker, D., Kemper, E., Schell, J., & Masterson, R. (1992). New plant binary vectors with selectable markers located proximal to the left T-DNA border. *Plant Molecular Biology*, *20*(6), 1195–1197.
- Berthiaume, E. P., Medina, C., & Swanson, J. A. (1995). Molecular size-fractionation during endocytosis in macrophages. *The Journal of Cell Biology*, *129*(4), 989–998.
- Bläsing, O. E., Gibon, Y., Günther, M., Höhne, M., Morcuende, R., Osuna, D., Thimm, O., Usadel, B., Scheible, W.-R., & Stitt, M. (2005). Sugars and circadian regulation make major contributions to the global regulation of diurnal gene expression in Arabidopsis. *The Plant Cell*, *17*(12), 3257–3281.
- Bogdanović, J., Mojović, M., Milosavić, N., Mitrović, A., Vučinić, Ž., & Spasojević, I. (2008). Role

- of fructose in the adaptation of plants to cold-induced oxidative stress. *European Biophysics Journal*, 37(7), 1241–1246.
- BRÖER, S., BRÖER, A., SCHNEIDER, H.-P., STEGEN, C., HALESTRAP, A. P., & DEITMER, J. W. (1999). Characterization of the high-affinity monocarboxylate transporter MCT2 in *Xenopus laevis* oocytes. *Biochemical Journal*, 341(3), 529–535.
- Bullock, Wo. (1987). XL1-Blue: a high efficiency plasmid transforming recA *Escherichia coli* strain with beta-galactosidase selection. *Bio Techniques*, 5, 376–379.
- Büttner, M. (2007). The monosaccharide transporter (-like) gene family in *Arabidopsis*. *FEBS Letters*, 581(12), 2318–2324.
- Carter, C., Pan, S., Zouhar, J., Avila, E. L., Girke, T., & Raikhel, N. V. (2004). The vegetative vacuole proteome of *Arabidopsis thaliana* reveals predicted and unexpected proteins. *The Plant Cell*, 16(12), 3285–3303.
- Chae, L., Pandey, G. K., Luan, S., Cheong, Y. H., & Kim, K.-N. (2009). Protein kinases and phosphatases for stress signal transduction in plants. In *Abiotic stress adaptation in plants* (pp. 123–163). Springer.
- Chardon, F., Bedu, M., Calenge, F., Klemens, P. A. W., Spinner, L., Clement, G., Chietera, G., Lérans, S., Ferrand, M., & Lacombe, B. (2013). Leaf fructose content is controlled by the vacuolar transporter SWEET17 in *Arabidopsis*. *Current Biology*, 23(8), 697–702.
- Chen, J.-G., & Jones, A. M. (2004). AtRGS1 function in *Arabidopsis thaliana*. *Methods in Enzymology*, 389, 338–350.
- Chen, L.-Q., Hou, B.-H., Lalonde, S., Takanaga, H., Hartung, M. L., Qu, X.-Q., Guo, W.-J., Kim, J.-G., Underwood, W., & Chaudhuri, B. (2010). Sugar transporters for intercellular exchange and nutrition of pathogens. *Nature*, 468(7323), 527–532.
- Chen, L.-Q., Lin, I. W., Qu, X.-Q., Sosso, D., McFarlane, H. E., Londoño, A., Samuels, A. L., & Frommer, W. B. (2015). A cascade of sequentially expressed sucrose transporters in the seed coat and endosperm provides nutrition for the *Arabidopsis* embryo. *The Plant Cell*, 27(3), 607–619.
- Chen, L.-Q., Qu, X.-Q., Hou, B.-H., Sosso, D., Osorio, S., Fernie, A. R., & Frommer, W. B. (2012). Sucrose efflux mediated by SWEET proteins as a key step for phloem transport. *Science*, 335(6065), 207–211.
- Chen, Z., Zhou, L., Jiang, P., Lu, R., Halford, N. G., & Liu, C. (2021). Genome-wide identification of sucrose nonfermenting-1-related protein kinase (SnRK) genes in barley and RNA-seq analyses of their expression in response to abscisic acid treatment. *BMC Genomics*, 22(1), 1–16.
- Cheng, W.-H., Endo, A., Zhou, L., Penney, J., Chen, H.-C., Arroyo, A., Leon, P., Nambara, E., Asami, T., & Seo, M. (2002). A unique short-chain dehydrogenase/reductase in *Arabidopsis* glucose signaling and abscisic acid biosynthesis and functions. *The Plant Cell*, 14(11), 2723–2743.
- Cheong, Y. H., Pandey, G. K., Grant, J. J., Batistic, O., Li, L., Kim, B., Lee, S., Kudla, J., & Luan, S.

- (2007). Two calcineurin B-like calcium sensors, interacting with protein kinase CIPK23, regulate leaf transpiration and root potassium uptake in *Arabidopsis*. *The Plant Journal*, *52*(2), 223–239.
- Chinnusamy, V., Ohta, M., Kanrar, S., Lee, B., Hong, X., Agarwal, M., & Zhu, J.-K. (2003). ICE1: a regulator of cold-induced transcriptome and freezing tolerance in *Arabidopsis*. *Genes & Development*, *17*(8), 1043–1054.
- Chinnusamy, V., Zhu, J., & Zhu, J. (2006). Gene regulation during cold acclimation in plants. *Physiologia Plantarum*, *126*(1), 52–61.
- Chiou, T.-J., & Bush, D. R. (1996). Molecular cloning, immunochemical localization to the vacuole, and expression in transgenic yeast and tobacco of a putative sugar transporter from sugar beet. *Plant Physiology*, *110*(2), 511–520.
- Cho, L.-H., Pasriga, R., Yoon, J., Jeon, J.-S., & An, G. (2018). Roles of sugars in controlling flowering time. *Journal of Plant Biology*, *61*(3), 121–130.
- Cho, Y.-H., & Yoo, S.-D. (2011). Signaling role of fructose mediated by FINS1/FBP in *Arabidopsis thaliana*. *PLoS Genetics*, *7*(1), e1001263.
- Cho, Y.-H., Yoo, S.-D., & Sheen, J. (2006). Regulatory functions of nuclear hexokinase1 complex in glucose signaling. *Cell*, *127*(3), 579–589.
- Coello, P., Hirano, E., Hey, S. J., Muttucumar, N., Martinez-Barajas, E., Parry, M. A. J., & Halford, N. G. (2012). Evidence that abscisic acid promotes degradation of SNF1-related protein kinase (SnRK) 1 in wheat and activation of a putative calcium-dependent SnRK2. *Journal of Experimental Botany*, *63*(2), 913–924.
- Collins, N. C., Tardieu, F., & Tuberosa, R. (2008). Quantitative trait loci and crop performance under abiotic stress: where do we stand? *Plant Physiology*, *147*(2), 469–486.
- Cook, D., Fowler, S., Fiehn, O., & Thomashow, M. F. (2004). A prominent role for the CBF cold response pathway in configuring the low-temperature metabolome of *Arabidopsis*. *Proceedings of the National Academy of Sciences*, *101*(42), 15243–15248.
- Corbesier, L., Lejeune, P., & Bernier, G. (1998). The role of carbohydrates in the induction of flowering in *Arabidopsis thaliana*: comparison between the wild type and a starchless mutant. *Planta*, *206*(1), 131–137.
- Cordoba, E., Aceves-Zamudio, D. L., Hernández-Bernal, A. F., Ramos-Vega, M., & León, P. (2015). Sugar regulation of SUGAR TRANSPORTER PROTEIN 1 (STP1) expression in *Arabidopsis thaliana*. *Journal of Experimental Botany*, *66*(1), 147–159.
- Covington, M. F., & Harmer, S. L. (2007). The circadian clock regulates auxin signaling and responses in *Arabidopsis*. *PLoS Biology*, *5*(8), e222.
- Crowe, J. H., Crowe, L. M., Carpenter, J. F., Rudolph, A. S., Wistrom, C. A., Spargo, B. J., & Anchooguy, T. J. (1988). Interactions of sugars with membranes. *Biochimica et Biophysica Acta (BBA)-Reviews on Biomembranes*, *947*(2), 367–384.
- de Wit, M., Keuskamp, D. H., Bongers, F. J., Hornitschek, P., Gommers, C. M. M., Reinen, E.,

- Martínez-Cerón, C., Fankhauser, C., & Pierik, R. (2016). Integration of phytochrome and cryptochrome signals determines plant growth during competition for light. *Current Biology*, 26(24), 3320–3326.
- Deng, J., Yang, X., Sun, W., Miao, Y., He, L., & Zhang, X. (2020). The calcium sensor CBL2 and its interacting kinase CIPK6 are involved in plant sugar homeostasis via interacting with tonoplast sugar transporter TST2. *Plant Physiology*, 183(1), 236–249.
- Dennis, D., & Blakeley, S. (2000). Carbohydrate metabolism In: Biochemistry & molecular biology of plants. Ed. By BB Buchanans, W. Gruissem and RL Jones. American Society of Plant Physiologists, Rock Vile, Md., USA.
- Des Marais, D. L., & Juenger, T. E. (2010). Pleiotropy, plasticity, and the evolution of plant abiotic stress tolerance. *Annals of the New York Academy of Sciences*, 1206(1), 56–79.
- Dhar, N., Caruana, J., Erdem, I., Subbarao, K. V, Klosterman, S. J., & Raina, R. (2020). The Arabidopsis SENESCENCE-ASSOCIATED GENE 13 regulates dark-induced senescence and plays contrasting roles in defense against bacterial and fungal pathogens. *Molecular Plant-Microbe Interactions*, 33(5), 754–766.
- Dhungana, S. R., & Braun, D. M. (2021). Sugar transporters in grasses: Function and modulation in source and storage tissues. *Journal of Plant Physiology*, 266, 153541.
- Drozdowicz, Y. M., & Rea, P. A. (2001). Vacuolar H⁺ pyrophosphatases: from the evolutionary backwaters into the mainstream. *Trends in Plant Science*, 6(5), 206–211.
- Du, Y., Zhao, Q., Chen, L., Yao, X., Zhang, W., Zhang, B., & Xie, F. (2020). Effect of drought stress on sugar metabolism in leaves and roots of soybean seedlings. *Plant Physiology and Biochemistry*, 146, 1–12.
- Dubey, R. S., & Singh, A. K. (1999). Salinity induces accumulation of soluble sugars and alters the activity of sugar metabolising enzymes in rice plants. *Biologia Plantarum*, 42(2), 233–239.
- Dubos, C., Stracke, R., Grotewold, E., Weisshaar, B., Martin, C., & Lepiniec, L. (2010). MYB transcription factors in Arabidopsis. *Trends in Plant Science*, 15(10), 573–581.
- Durand, M., Mainson, D., Porcheron, B., Maurousset, L., Lemoine, R., & Pourtau, N. (2018). Carbon source–sink relationship in Arabidopsis thaliana: the role of sucrose transporters. *Planta*, 247(3), 587–611.
- Endler, A., Meyer, S., Schelbert, S., Schneider, T., Weschke, W., Peters, S. W., Keller, F., Baginsky, S., Martinoia, E., & Schmidt, U. G. (2006). Identification of a vacuolar sucrose transporter in barley and Arabidopsis mesophyll cells by a tonoplast proteomic approach. *Plant Physiology*, 141(1), 196–207.
- Endler, A., Reiland, S., Gerrits, B., Schmidt, U. G., Baginsky, S., & Martinoia, E. (2009). In vivo phosphorylation sites of barley tonoplast proteins identified by a phosphoproteomic approach. *Proteomics*, 9(2), 310–321.
- Eom, J.-S., Chen, L.-Q., Sosso, D., Julius, B. T., Lin, I. W., Qu, X.-Q., Braun, D. M., & Frommer, W. B. (2015). SWEETs, transporters for intracellular and intercellular sugar translocation.

- Current Opinion in Plant Biology*, 25, 53–62.
- Eveland, A. L., & Jackson, D. P. (2012). Sugars, signalling, and plant development. *Journal of Experimental Botany*, 63(9), 3367–3377.
- Fischer, A. M., & Gan, S. (2007). Nutrient remobilization during leaf senescence. *Annual Reviews of Senescence Processes in Plants*, 26, 87–107.
- Fleurat-Lessard, P., Frangne, N., Maeshima, M., Ratajczak, R., Bonnemain, J.-L., & Martinoia, E. (1997). Increased expression of vacuolar aquaporin and H⁺-ATPase related to motor cell function in *Mimosa pudica* L. *Plant Physiology*, 114(3), 827–834.
- Fujiki, Y., Yoshikawa, Y., Sato, T., Inada, N., Ito, M., Nishida, I., & Watanabe, A. (2001). Dark-inducible genes from *Arabidopsis thaliana* are associated with leaf senescence and repressed by sugars. *Physiologia Plantarum*, 111(3), 345–352.
- Fürtauer, L., Küstner, L., Weckwerth, W., Heyer, A. G., & Nägele, T. (2019). Resolving subcellular plant metabolism. *The Plant Journal*, 100(3), 438–455.
- Fürtauer, L., Weckwerth, W., & Nägele, T. (2016). A benchtop fractionation procedure for subcellular analysis of the plant metabolome. *Frontiers in Plant Science*, 7, 1912.
- Furuichi, T., Cunningham, K. W., & Muto, S. (2001). A putative two pore channel AtTPC1 mediates Ca²⁺ flux in *Arabidopsis* leaf cells. *Plant and Cell Physiology*, 42(9), 900–905.
- Gallagher, S. R., & Chang, D. C. (1992). Novel applications of electroporation. *Guid to Electroporation and Electrofusion*, 411–425.
- Gamboa, M. C., Baltierra, F., Leon, G., & Krauskopf, E. (2013). Drought and salt tolerance enhancement of transgenic *Arabidopsis* by overexpression of the vacuolar pyrophosphatase 1 (EVP1) gene from *Eucalyptus globulus*. *Plant Physiology and Biochemistry*, 73, 99–105.
- Giaquinta, R. T., Lin, W., Sadler, N. L., & Franceschi, V. R. (1983). Pathway of phloem unloading of sucrose in corn roots. *Plant Physiology*, 72(2), 362–367.
- Gietz, R. D., & Schiestl, R. H. (2007). Quick and easy yeast transformation using the LiAc/SS carrier DNA/PEG method. *Nature Protocols*, 2(1), 35–37.
- Gill, P. K., Sharma, A. D., Singh, P., & Bhullar, S. S. (2001). Effect of various abiotic stresses on the growth, soluble sugars and water relations of sorghum seedlings grown in light and darkness. *Bulg J Plant Physiol*, 27(1–2), 72–84.
- Gleave, A. P. (1992). A versatile binary vector system with a T-DNA organisational structure conducive to efficient integration of cloned DNA into the plant genome. *Plant Molecular Biology*, 20(6), 1203–1207.
- Goetz, M., Godt, D. E., Guivarc'h, A., Kahmann, U., Chriqui, D., & Roitsch, T. (2001). Induction of male sterility in plants by metabolic engineering of the carbohydrate supply. *Proceedings of the National Academy of Sciences*, 98(11), 6522–6527.
- Goldman, S. J., Taylor, R., Zhang, Y., & Jin, S. (2010). Autophagy and the degradation of

- mitochondria. *Mitochondrion*, 10(4), 309–315.
- Gong, D., Guo, Y., Schumaker, K. S., & Zhu, J.-K. (2004). The SOS3 family of calcium sensors and SOS2 family of protein kinases in Arabidopsis. *Plant Physiology*, 134(3), 919–926.
- Gordon, A. J., Ryle, G. J. A., Powell, C. E., & Mitchell, D. (1980). Export, mobilization, and respiration of assimilates in unicultum barley during light and darkness. *Journal of Experimental Botany*, 31(2), 461–473.
- Granot, D., David-Schwartz, R., & Kelly, G. (2013). Hexose kinases and their role in sugar-sensing and plant development. *Frontiers in Plant Science*, 4, 44.
- Grant, S. G., Jessee, J., Bloom, F. R., & Hanahan, D. (1990). Differential plasmid rescue from transgenic mouse DNAs into Escherichia coli methylation-restriction mutants. *Proceedings of the National Academy of Sciences*, 87(12), 4645–4649.
- Grodzinski, B., Jiao, J., & Leonardos, E. D. (1998). Estimating photosynthesis and concurrent export rates in C3 and C4 species at ambient and elevated CO₂, 2. *Plant Physiology*, 117(1), 207–215.
- Guo, W.-J., Nagy, R., Chen, H.-Y., Pfrunder, S., Yu, Y.-C., Santelia, D., Frommer, W. B., & Martinoia, E. (2014). SWEET17, a facilitative transporter, mediates fructose transport across the tonoplast of Arabidopsis roots and leaves. *Plant Physiology*, 164(2), 777–789.
- Halford, N. G., & Hey, S. J. (2009). Snf1-related protein kinases (SnRKs) act within an intricate network that links metabolic and stress signalling in plants. *Biochemical Journal*, 419(2), 247–259.
- Hanahan, D. (1983). Studies on transformation of Escherichia coli with plasmids. *Journal of Molecular Biology*, 166(4), 557–580.
- Haritatos, E., Ayre, B. G., & Turgeon, R. (2000). Identification of phloem involved in assimilate loading in leaves by the activity of the galactinol synthase promoter. *Plant Physiology*, 123(3), 929–938.
- Havaux, M., & Kloppstech, K. (2001). The protective functions of carotenoid and flavonoid pigments against excess visible radiation at chilling temperature investigated in Arabidopsis npq and tt mutants. *Planta*, 213(6), 953–966.
- Haydon, M. J., Bell, L. J., & Webb, A. A. R. (2011). Interactions between plant circadian clocks and solute transport. *Journal of Experimental Botany*, 62(7), 2333–2348.
- Hedrich, R., Sauer, N., & Neuhaus, H. E. (2015). Sugar transport across the plant vacuolar membrane: nature and regulation of carrier proteins. *Current Opinion in Plant Biology*, 25, 63–70.
- Henderson, P. J. F. (1991). Sugar transport proteins. *Current Opinion in Structural Biology*, 1(4), 590–601.
- Hernández, I., Alegre, L., Van Breusegem, F., & Munné-Bosch, S. (2009). How relevant are flavonoids as antioxidants in plants? *Trends in Plant Science*, 14(3), 125–132.

- Hey, S. J., Byrne, E., & Halford, N. G. (2009). The interface between metabolic and stress signalling. *Annals of Botany*, *105*(2), 197–203.
- Ho, L.-H., Rode, R., Siegel, M., Reinhardt, F., Neuhaus, H. E., Yvin, J.-C., Pluchon, S., Hosseini, S. A., & Pommerrenig, B. (2020). Potassium application boosts photosynthesis and sorbitol biosynthesis and accelerates cold acclimation of common plantain (*Plantago major* L.). *Plants*, *9*(10), 1259.
- Horacio, P., & Martinez-Noel, G. (2013). Sucrose signaling in plants: a world yet to be explored. *Plant Signaling & Behavior*, *8*(3), e23316.
- Hrabak, E. M., Chan, C. W. M., Gribskov, M., Harper, J. F., Choi, J. H., Halford, N., Kudla, J., Luan, S., Nimmo, H. G., & Sussman, M. R. (2003). The Arabidopsis CDPK-SnRK superfamily of protein kinases. *Plant Physiology*, *132*(2), 666–680.
- Huber, S. C., & Huber, J. L. (1996). Role and regulation of sucrose-phosphate synthase in higher plants. *Annual Review of Plant Biology*, *47*(1), 431–444.
- Hunter, K. (2020). *CBL2-CIPK6-TST2-mediated regulation of sugar homeostasis*. American Society of Plant Biologists.
- Itzhaki, H., Maxson, J. M., & Woodson, W. R. (1994). An ethylene-responsive enhancer element is involved in the senescence-related expression of the carnation glutathione-S-transferase (GST1) gene. *Proceedings of the National Academy of Sciences*, *91*(19), 8925–8929.
- Jaglo-Ottosen, K. R., Gilmour, S. J., Zarka, D. G., Schabenberger, O., & Thomashow, M. F. (1998). Arabidopsis CBF1 overexpression induces COR genes and enhances freezing tolerance. *Science*, *280*(5360), 104–106.
- Jang, J.-C., León, P., Zhou, L., & Sheen, J. (1997). Hexokinase as a sugar sensor in higher plants. *The Plant Cell*, *9*(1), 5–19.
- Jänkänpää, H. J., Mishra, Y., Schröder, W. P., & Jansson, S. (2012). Metabolic profiling reveals metabolic shifts in Arabidopsis plants grown under different light conditions. *Plant, Cell & Environment*, *35*(10), 1824–1836.
- Jaquinod, M., Villiers, F., Kieffer-Jaquinod, S., Hugouvieux, V., Bruley, C., Garin, J., & Bourguignon, J. (2007). A proteomics dissection of Arabidopsis thaliana vacuoles isolated from cell culture. *Molecular & Cellular Proteomics*, *6*(3), 394–412.
- Jiao, J., & Grodzinski, B. (1996). The effect of leaf temperature and photorespiratory conditions on export of sugars during steady-state photosynthesis in *Salvia splendens*. *Plant Physiology*, *111*(1), 169–178.
- Jung, B., Ludewig, F., Schulz, A., Meissner, G., Woestefeld, N., Fluegge, U.-I., Pommerrenig, B., Wirsching, P., Sauer, N., & Koch, W. (2015). Identification of the transporter responsible for sucrose accumulation in sugar beet taproots. *Nature Plants*, *1*(1), 1–6.
- Kamranfar, I., Xue, G., Tohge, T., Sedaghatmehr, M., Fernie, A. R., Balazadeh, S., & Mueller-Roeber, B. (2018). Transcription factor RD 26 is a key regulator of metabolic reprogramming during dark-induced senescence. *New Phytologist*, *218*(4), 1543–1557.

- Karimi, M., Inzé, D., & Depicker, A. (2002). GATEWAY™ vectors for Agrobacterium-mediated plant transformation. *Trends in Plant Science*, 7(5), 193–195.
- Kaur, H., Manna, M., Thakur, T., Gautam, V., & Salvi, P. (2021). Imperative role of sugar signaling and transport during drought stress responses in plants. *Physiologia Plantarum*, 171(4), 833–848.
- Kiyosue, T., Abe, H., Yamaguchi-Shinozaki, K., & Shinozaki, K. (1998). ERD6, a cDNA clone for an early dehydration-induced gene of Arabidopsis, encodes a putative sugar transporter. *Biochimica et Biophysica Acta (BBA)-Biomembranes*, 1370(2), 187–191.
- Klemens, P. A. W., Patzke, K., Deitmer, J., Spinner, L., Le Hir, R., Bellini, C., Bedu, M., Chardon, F., Krapp, A., & Neuhaus, H. E. (2013). Overexpression of the vacuolar sugar carrier AtSWEET16 modifies germination, growth, and stress tolerance in Arabidopsis. *Plant Physiology*, 163(3), 1338–1352.
- Klemens, P. A. W., Patzke, K., Trentmann, O., Poschet, G., Büttner, M., Schulz, A., Marten, I., Hedrich, R., & Neuhaus, H. E. (2014). Overexpression of a proton-coupled vacuolar glucose exporter impairs freezing tolerance and seed germination. *New Phytologist*, 202(1), 188–197.
- Klotke, J., Kopka, J., Gatzke, N., & Heyer, A. G. (2004). Impact of soluble sugar concentrations on the acquisition of freezing tolerance in accessions of Arabidopsis thaliana with contrasting cold adaptation—evidence for a role of raffinose in cold acclimation. *Plant, Cell & Environment*, 27(11), 1395–1404.
- Koncz, C., & Schell, J. (1986). The promoter of TL-DNA gene 5 controls the tissue-specific expression of chimaeric genes carried by a novel type of Agrobacterium binary vector. *Molecular and General Genetics MGG*, 204(3), 383–396.
- Krahmer, J., Abbas, A., Mengin, V., Ishihara, H., Romanowski, A., Furniss, J. J., Moraes, T. A., Krohn, N., Annunziata, M. G., & Feil, R. (2021). Phytochromes control metabolic flux, and their action at the seedling stage determines adult plant biomass. *Journal of Experimental Botany*, 72(8), 3263–3278.
- Krueger, S., Giavalisco, P., Krall, L., Steinhauser, M.-C., Büssis, D., Usadel, B., Flügge, U.-I., Fernie, A. R., Willmitzer, L., & Steinhauser, D. (2011). A topological map of the compartmentalized Arabidopsis thaliana leaf metabolome. *PLoS One*, 6(3), e17806.
- Kühn, C., Quick, W. P., Schulz, A., Riesmeier, J. W., Sonnewald, U., & Frommer, W. B. (1996). Companion cell-specific inhibition of the potato sucrose transporter SUT1. *Plant, Cell & Environment*, 19(10), 1115–1123.
- Kunz, H.-H., Scharnewski, M., Feussner, K., Feussner, I., Flügge, U.-I., Fulda, M., & Gierth, M. (2009). The ABC transporter PXA1 and peroxisomal β -oxidation are vital for metabolism in mature leaves of Arabidopsis during extended darkness. *The Plant Cell*, 21(9), 2733–2749.
- Lam, E., & Chua, N.-H. (1989). Light to dark transition modulates the phase of antenna chlorophyll protein gene expression. *Journal of Biological Chemistry*, 264(34), 20175–20176.

- Lee, S. C., Lan, W.-Z., Kim, B.-G., Li, L., Cheong, Y. H., Pandey, G. K., Lu, G., Buchanan, B. B., & Luan, S. (2007). A protein phosphorylation/dephosphorylation network regulates a plant potassium channel. *Proceedings of the National Academy of Sciences*, *104*(40), 15959–15964.
- Li, L., Li, M., Yu, L., Zhou, Z., Liang, X., Liu, Z., Cai, G., Gao, L., Zhang, X., & Wang, Y. (2014). The FLS2-associated kinase BIK1 directly phosphorylates the NADPH oxidase RbohD to control plant immunity. *Cell Host & Microbe*, *15*(3), 329–338.
- Li, P., Wind, J. J., Shi, X., Zhang, H., Hanson, J., Smeekens, S. C., & Teng, S. (2011). Fructose sensitivity is suppressed in Arabidopsis by the transcription factor ANAC089 lacking the membrane-bound domain. *Proceedings of the National Academy of Sciences*, *108*(8), 3436–3441.
- Li, X., Chanroj, S., Wu, Z., Romanowsky, S. M., Harper, J. F., & Sze, H. (2008). A distinct endosomal Ca²⁺/Mn²⁺ pump affects root growth through the secretory process. *Plant Physiology*, *147*(4), 1675–1689.
- Liman, E. R., Tytgat, J., & Hess, P. (1992). Subunit stoichiometry of a mammalian K⁺ channel determined by construction of multimeric cDNAs. *Neuron*, *9*(5), 861–871.
- Loqué, D., Lalonde, S., Looger, L. L., Von Wirén, N., & Frommer, W. B. (2007). A cytosolic trans-activation domain essential for ammonium uptake. *Nature*, *446*(7132), 195–198.
- Lutfiyya, L. L., Xu, N., Robert, L. D., Morrell, J. A., Miller, P. W., & Duff, S. M. G. (2007). Phylogenetic and expression analysis of sucrose phosphate synthase isozymes in plants. *Journal of Plant Physiology*, *164*(7), 923–933.
- Ma, Q., Sun, M., Lu, J., Kang, H., You, C., & Hao, Y. (2019). An apple sucrose transporter MdSUT2. 2 is a phosphorylation target for protein kinase MdCIPK22 in response to drought. *Plant Biotechnology Journal*, *17*(3), 625–637.
- Ma, S., Li, Y., Li, X., Sui, X., & Zhang, Z. (2019). Phloem unloading strategies and mechanisms in crop fruits. *Journal of Plant Growth Regulation*, *38*(2), 494–500.
- Maeshima, M. (2000). Vacuolar H⁺-pyrophosphatase. *Biochimica et Biophysica Acta (BBA)-Biomembranes*, *1465*(1–2), 37–51.
- Maeshima, M. (2001). Tonoplast transporters: organization and function. *Annual Review of Plant Biology*, *52*(1), 469–497.
- Mancinelli, A. L., Yang, C.-P. H., Lindquist, P., Anderson, O. R., & Rabino, I. (1975). Photocontrol of anthocyanin synthesis: III. The action of streptomycin on the synthesis of chlorophyll and anthocyanin. *Plant Physiology*, *55*(2), 251–257.
- Martinoia, E., Maeshima, M., & Neuhaus, H. E. (2007). Vacuolar transporters and their essential role in plant metabolism. *Journal of Experimental Botany*, *58*(1), 83–102.
- Martinoia, E., Meyer, S., De Angeli, A., & Nagy, R. (2012). Vacuolar transporters in their physiological context. *Annual Review of Plant Biology*, *63*, 183–213.
- Miura, K., & Furumoto, T. (2013). Cold signaling and cold response in plants. *International*

Journal of Molecular Sciences, 14(3), 5312–5337.

Moore, B., Zhou, L., Rolland, F., Hall, Q., Cheng, W.-H., Liu, Y.-X., Hwang, I., Jones, T., & Sheen, J. (2003). Role of the Arabidopsis glucose sensor HXK1 in nutrient, light, and hormonal signaling. *Science*, 300(5617), 332–336.

Morelli, G., & Ruberti, I. (2002). Light and shade in the photocontrol of Arabidopsis growth. *Trends in Plant Science*, 7(9), 399–404.

Nägele, T., Henkel, S., Hörmiller, I., Sauter, T., Sawodny, O., Ederer, M., & Heyer, A. G. (2010). Mathematical modeling of the central carbohydrate metabolism in Arabidopsis reveals a substantial regulatory influence of vacuolar invertase on whole plant carbon metabolism. *Plant Physiology*, 153(1), 260–272.

Nägele, T., & Heyer, A. G. (2013). Approximating subcellular organisation of carbohydrate metabolism during cold acclimation in different natural accessions of Arabidopsis thaliana. *New Phytologist*, 198(3), 777–787.

Nguyen, S. T. T., & McCurdy, D. W. (2015). High-resolution confocal imaging of wall ingrowth deposition in plant transfer cells: semi-quantitative analysis of phloem parenchyma transfer cell development in leaf minor veins of Arabidopsis. *BMC Plant Biology*, 15(1), 1–14.

Nunes, C., O'Hara, L. E., Primavesi, L. F., Delatte, T. L., Schlupepman, H., Somsen, G. W., Silva, A. B., Fevereiro, P. S., Wingler, A., & Paul, M. J. (2013). The trehalose 6-phosphate/SnRK1 signaling pathway primes growth recovery following relief of sink limitation. *Plant Physiology*, 162(3), 1720–1732.

Offler, C. E., McCurdy, D. W., Patrick, J. W., & Talbot, M. J. (2003). Transfer cells: cells specialized for a special purpose. *Annual Review of Plant Biology*, 54(1), 431–454.

Paris, N., Stanley, C. M., Jones, R. L., & Rogers, J. C. (1996). Plant cells contain two functionally distinct vacuolar compartments. *Cell*, 85(4), 563–572.

Pastuglia, M., Roby, D., Dumas, C., & Cock, J. M. (1997). Rapid induction by wounding and bacterial infection of an S gene family receptor-like kinase gene in Brassica oleracea. *The Plant Cell*, 9(1), 49–60.

Patzke, K., Prananingrum, P., Klemens, P. A. W., Trentmann, O., Rodrigues, C. M., Keller, I., Fernie, A. R., Geigenberger, P., Bölter, B., & Lehmann, M. (2019). The plastidic sugar transporter pSuT influences flowering and affects cold responses. *Plant Physiology*, 179(2), 569–587.

Perby, L. K., Richter, S., Weber, K., Hieber, A. J., Hess, N., Crocoll, C., Mogensen, H. K., Pribil, M., Burow, M., & Nielsen, T. H. (2022). Cytosolic phosphofructokinases are important for sugar homeostasis in leaves of Arabidopsis thaliana. *Annals of Botany*, 129(1), 37–52.

Pertl-Obermeyer, H., Trentmann, O., Duscha, K., Neuhaus, H. E., & Schulze, W. X. (2016). Quantitation of vacuolar sugar transporter abundance changes using QconCAT synthetic peptides. *Frontiers in Plant Science*, 7, 411.

Piattoni, C. V., Bustos, D. M., Guerrero, S. A., & Iglesias, A. Á. (2011). Nonphosphorylating

- glyceraldehyde-3-phosphate dehydrogenase is phosphorylated in wheat endosperm at serine-404 by an SNF1-related protein kinase allosterically inhibited by ribose-5-phosphate. *Plant Physiology*, 156(3), 1337–1350.
- Polge, C., & Thomas, M. (2007). SNF1/AMPK/SnRK1 kinases, global regulators at the heart of energy control? *Trends in Plant Science*, 12(1), 20–28.
- Pommerrenig, B., Ludewig, F., Cvetkovic, J., Trentmann, O., Klemens, P. A. W., & Neuhaus, H. E. (2018). In concert: orchestrated changes in carbohydrate homeostasis are critical for plant abiotic stress tolerance. *Plant and Cell Physiology*, 59(7), 1290–1299.
- Pontis, H. G. (1989). Fructans and cold stress. *Journal of Plant Physiology*, 134(2), 148–150.
- Poschet, G., Hannich, B., Raab, S., Jungkunz, I., Klemens, P. A. W., Krueger, S., Wic, S., Neuhaus, H. E., & Büttner, M. (2011). A novel Arabidopsis vacuolar glucose exporter is involved in cellular sugar homeostasis and affects the composition of seed storage compounds. *Plant Physiology*, 157(4), 1664–1676.
- Ralsler, M., Kuhl, H., Ralsler, M., Werber, M., Lehrach, H., Breitenbach, M., & Timmermann, B. (2012). The *Saccharomyces cerevisiae* W303-K6001 cross-platform genome sequence: insights into ancestry and physiology of a laboratory mutt. *Open Biology*, 2(8), 120093.
- Reiser, J., Linka, N., Lemke, L., Jeblick, W., & Neuhaus, H. E. (2004). Molecular physiological analysis of the two plastidic ATP/ADP transporters from Arabidopsis. *Plant Physiology*, 136(3), 3524–3536.
- Remy, E., Cabrito, T. R., Batista, R. A., Hussein, M. A. M., Teixeira, M. C., Athanasiadis, A., Sá-Correia, I., & Duque, P. (2014). Intron retention in the 5' UTR of the novel ZIF2 transporter enhances translation to promote zinc tolerance in Arabidopsis. *PLoS Genetics*, 10(5), e1004375.
- Riesmeier, J. W., Willmitzer, L., & Frommer, W. B. (1992). Isolation and characterization of a sucrose carrier cDNA from spinach by functional expression in yeast. *The EMBO Journal*, 11(13), 4705–4713.
- Rodrigues, C. M., Müdsam, C., Keller, I., Zierer, W., Czarnecki, O., Corral, J. M., Reinhardt, F., Nieberl, P., Fiedler-Wiechers, K., & Sommer, F. (2020). Vernalization alters sink and source identities and reverses phloem translocation from taproots to shoots in sugar beet. *Plant Cell*, 32(10), 3206–3223.
- Roitsch, T., & González, M.-C. (2004). Function and regulation of plant invertases: sweet sensations. *Trends in Plant Science*, 9(12), 606–613.
- Rolland, F., Baena-Gonzalez, E., & Sheen, J. (2006). Sugar sensing and signaling in plants: conserved and novel mechanisms. *Annu. Rev. Plant Biol.*, 57, 675–709.
- Rottmann, T., Zierer, W., Subert, C., Sauer, N., & Stadler, R. (2016). STP10 encodes a high-affinity monosaccharide transporter and is induced under low-glucose conditions in pollen tubes of Arabidopsis. *Journal of Experimental Botany*, 67(8), 2387–2399.
- Ruan, Y.-L. (2014). Sucrose metabolism: gateway to diverse carbon use and sugar signaling. *Annual Review of Plant Biology*, 65, 33–67.

- Ruan, Y.-L., Jin, Y., Yang, Y.-J., Li, G.-J., & Boyer, J. S. (2010). Sugar input, metabolism, and signaling mediated by invertase: roles in development, yield potential, and response to drought and heat. *Molecular Plant*, 3(6), 942–955.
- Ruelland, E., & Collin, S. (2011). *Plant stress physiology*.
- Schmidt, U. G., Endler, A., Schelbert, S., Brunner, A., Schnell, M., Neuhaus, H. E., Marty-Mazars, D., Marty, F., Baginsky, S., & Martinoia, E. (2007). Novel tonoplast transporters identified using a proteomic approach with vacuoles isolated from cauliflower buds. *Plant Physiology*, 145(1), 216–229.
- Schneider, S., Hulpke, S., Schulz, A., Yaron, I., Höll, J., Imlau, A., Schmitt, B., Batz, S., Wolf, S., & Hedrich, R. (2012). Vacuoles release sucrose via tonoplast-localised SUC4-type transporters. *Plant Biology*, 14(2), 325–336.
- Schulz, A., Beyhl, D., Marten, I., Wormit, A., Neuhaus, E., Poschet, G., Büttner, M., Schneider, S., Sauer, N., & Hedrich, R. (2011). Proton-driven sucrose symport and antiport are provided by the vacuolar transporters SUC4 and TMT1/2. *The Plant Journal*, 68(1), 129–136.
- Schulze, C., Sticht, H., Meyerhoff, P., & Dietrich, P. (2011). Differential contribution of EF-hands to the Ca²⁺-dependent activation in the plant two-pore channel TPC1. *The Plant Journal*, 68(3), 424–432.
- Schulze, W. X., Schneider, T., Starck, S., Martinoia, E., & Trentmann, O. (2012). Cold acclimation induces changes in Arabidopsis tonoplast protein abundance and activity and alters phosphorylation of tonoplast monosaccharide transporters. *The Plant Journal*, 69(3), 529–541.
- Sessions, A., Weigel, D., & Yanofsky, M. F. (1999). The Arabidopsis thaliana MERISTEM LAYER 1 promoter specifies epidermal expression in meristems and young primordia. *The Plant Journal*, 20(2), 259–263.
- Sheen, J., Zhou, L., & Jang, J.-C. (1999). Sugars as signaling molecules. *Current Opinion in Plant Biology*, 2(5), 410–418.
- Sherson, S. M., Hemmann, G., Wallace, G., Forbes, S., Germain, V., Stadler, R., Bechtold, N., Sauer, N., & Smith, S. M. (2000). Monosaccharide/proton symporter AtSTP1 plays a major role in uptake and response of Arabidopsis seeds and seedlings to sugars. *The Plant Journal*, 24(6), 849–857.
- Skirycz, A., & Inzé, D. (2010). More from less: plant growth under limited water. *Current Opinion in Biotechnology*, 21(2), 197–203.
- Slawinski, L., Israel, A., Paillot, C., Thibault, F., Cordaux, R., Atanassova, R., Dédaldéchamp, F., & Laloi, M. (2021). Early response to dehydration six-like transporter family: early origin in streptophytes and evolution in land plants. *Frontiers in Plant Science*, 12.
- Smith, A. M., & Stitt, M. (2007). Coordination of carbon supply and plant growth. *Plant, Cell & Environment*, 30(9), 1126–1149.
- Smith, A. M., & Zeeman, S. C. (2020). Starch: a flexible, adaptable carbon store coupled to

- plant growth. *Annual Review of Plant Biology*, 71, 217–245.
- Stadler, R., & Sauer, N. (1996). The *Arabidopsis thaliana* AtSUC2 gene is specifically expressed in companion cells. *Botanica Acta*, 109(4), 299–306.
- Stitt, M., & Hurry, V. (2002). A plant for all seasons: alterations in photosynthetic carbon metabolism during cold acclimation in *Arabidopsis*. *Current Opinion in Plant Biology*, 5(3), 199–206.
- Strand, Å., Foyer, C. H., Gustafsson, P., Gardeström, P., & Hurry, V. (2003). Altering flux through the sucrose biosynthesis pathway in transgenic *Arabidopsis thaliana* modifies photosynthetic acclimation at low temperatures and the development of freezing tolerance. *Plant, Cell & Environment*, 26(4), 523–535.
- Strand, Å., Hurry, V., Henkes, S., Huner, N., Gustafsson, P., Gardeström, P., & Stitt, M. (1999). Acclimation of *Arabidopsis* leaves developing at low temperatures. Increasing cytoplasmic volume accompanies increased activities of enzymes in the Calvin cycle and in the sucrose-biosynthesis pathway. *Plant Physiology*, 119(4), 1387–1398.
- Straub, T., Ludewig, U., & Neuhäuser, B. (2017). The kinase CIPK23 inhibits ammonium transport in *Arabidopsis thaliana*. *The Plant Cell*, 29(2), 409–422.
- Strauss, G., & Hauser, H. (1986). Stabilization of lipid bilayer vesicles by sucrose during freezing. *Proceedings of the National Academy of Sciences*, 83(8), 2422–2426.
- Sun, L., Sui, X., Lucas, W. J., Li, Y., Feng, S., Ma, S., Fan, J., Gao, L., & Zhang, Z. (2019). Down-regulation of the sucrose transporter CsSUT1 causes male sterility by altering carbohydrate supply. *Plant Physiology*, 180(2), 986–997.
- Sze, H., Li, X., & Palmgren, M. G. (1999). Energization of plant cell membranes by H⁺-pumping ATPases: regulation and biosynthesis. *The Plant Cell*, 11(4), 677–689.
- Taiz, L., Zeiger, E., Møller, I. M., & Murphy, A. (2015). *Plant physiology and development*. (Issue Ed. 6). Sinauer Associates Incorporated.
- Thao, N. P., & Tran, L.-S. P. (2012). Potentials toward genetic engineering of drought-tolerant soybean. *Critical Reviews in Biotechnology*, 32(4), 349–362.
- Toroser, D., Plaut, Z., & Huber, S. C. (2000). Regulation of a plant SNF1-related protein kinase by glucose-6-phosphate. *Plant Physiology*, 123(1), 403–412.
- Valifard, M., Le Hir, R., Müller, J., Scheuring, D., Neuhaus, H. E., & Pommerrenig, B. (2021). Vacuolar fructose transporter SWEET17 is critical for root development and drought tolerance. *Plant Physiology*, 187(4), 2716–2730.
- Volkert, K., Debast, S., Voll, L. M., Voll, H., Schießl, I., Hofmann, J., Schneider, S., & Börnke, F. (2014). Loss of the two major leaf isoforms of sucrose-phosphate synthase in *Arabidopsis thaliana* limits sucrose synthesis and nocturnal starch degradation but does not alter carbon partitioning during photosynthesis. *Journal of Experimental Botany*, 65(18), 5217–5229.
- Vu, D. P., Martins Rodrigues, C., Jung, B., Meissner, G., Klemens, P. A. W., Holtgräwe, D.,

- Fürtauer, L., Nägele, T., Nieberl, P., & Pommerrenig, B. (2020). Vacuolar sucrose homeostasis is critical for plant development, seed properties, and night-time survival in *Arabidopsis*. *Journal of Experimental Botany*, *71*(16), 4930–4943.
- Wang, L., & Ruan, Y.-L. (2016). Critical roles of vacuolar invertase in floral organ development and male and female fertilities are revealed through characterization of GhVIN1-RNAi cotton plants. *Plant Physiology*, *171*(1), 405–423.
- Wanner, L. A., & Junttila, O. (1999). Cold-induced freezing tolerance in *Arabidopsis*. *Plant Physiology*, *120*(2), 391–400.
- Webb, Y., Zhou, X., Ngo, L., Cornish, V., Stahl, J., Erdjument-Bromage, H., Tempst, P., Rifkind, R. A., Marks, P. A., & Breslow, R. (1999). Photoaffinity labeling and mass spectrometry identify ribosomal protein S3 as a potential target for hybrid polar cytodifferentiation agents. *Journal of Biological Chemistry*, *274*(20), 14280–14287.
- Weinl, S., & Kudla, J. (2009). The CBL–CIPK Ca²⁺-decoding signaling network: function and perspectives. *New Phytologist*, *184*(3), 517–528.
- Weiszmann, J., Fürtauer, L., Weckwerth, W., & Nägele, T. (2018). Vacuolar sucrose cleavage prevents limitation of cytosolic carbohydrate metabolism and stabilizes photosynthesis under abiotic stress. *The FEBS Journal*, *285*(21), 4082–4098.
- Wesley, S. V., Helliwell, C. A., Smith, N. A., Wang, M., Rouse, D. T., Liu, Q., Gooding, P. S., Singh, S. P., Abbott, D., & Stoutjesdijk, P. A. (2001). Construct design for efficient, effective and high-throughput gene silencing in plants. *The Plant Journal*, *27*(6), 581–590.
- Whiteman, S., Nühse, T. S., Ashford, D. A., Sanders, D., & Maathuis, F. J. M. (2008). A proteomic and phosphoproteomic analysis of *Oryza sativa* plasma membrane and vacuolar membrane. *The Plant Journal*, *56*(1), 146–156.
- Whiteman, S., Serazetdinova, L., Jones, A. M. E., Sanders, D., Rathjen, J., Peck, S. C., & Maathuis, F. J. M. (2008). Identification of novel proteins and phosphorylation sites in a tonoplast enriched membrane fraction of *Arabidopsis thaliana*. *Proteomics*, *8*(17), 3536–3547.
- Wieczorke, R., Krampe, S., Weierstall, T., Freidel, K., Hollenberg, C. P., & Boles, E. (1999). Concurrent knock-out of at least 20 transporter genes is required to block uptake of hexoses in *Saccharomyces cerevisiae*. *FEBS Letters*, *464*(3), 123–128.
- Wind, J., Smeekens, S., & Hanson, J. (2010). Sucrose: metabolite and signaling molecule. *Phytochemistry*, *71*(14–15), 1610–1614.
- Wingenter, K., Schulz, A., Wormit, A., Wic, S., Trentmann, O., Hoermiller, I. I., Heyer, A. G., Marten, I., Hedrich, R., & Neuhaus, H. E. (2010). Increased activity of the vacuolar monosaccharide transporter TMT1 alters cellular sugar partitioning, sugar signaling, and seed yield in *Arabidopsis*. *Plant Physiology*, *154*(2), 665–677.
- Wingenter, K., Trentmann, O., Wünsch, I., Hörmiller, I. I., Heyer, A. G., Reinders, J., Schulz, A., Geiger, D., Hedrich, R., & Neuhaus, H. E. (2011). A member of the mitogen-activated protein 3-kinase family is involved in the regulation of plant vacuolar glucose uptake. *The*

Plant Journal, 68(5), 890–900.

- Wingler, A. (2018). Transitioning to the next phase: the role of sugar signaling throughout the plant life cycle. *Plant Physiology*, 176(2), 1075–1084.
- Winter, D., Vinegar, B., Nahal, H., Ammar, R., Wilson, G. V., & Provart, N. J. (2007). An “Electronic Fluorescent Pictograph” browser for exploring and analyzing large-scale biological data sets. *PLoS One*, 2(8), e718.
- Winter, H., Robinson, D. G., & Heldt, H. W. (1994). Subcellular volumes and metabolite concentrations in spinach leaves. *Planta*, 193(4), 530–535.
- Wormit, A., Trentmann, O., Feifer, I., Lohr, C., Tjaden, J., Meyer, S., Schmidt, U., Martinoia, E., & Neuhaus, H. E. (2006). Molecular identification and physiological characterization of a novel monosaccharide transporter from Arabidopsis involved in vacuolar sugar transport. *The Plant Cell*, 18(12), 3476–3490.
- Xu, J., Li, H.-D., Chen, L.-Q., Wang, Y., Liu, L.-L., He, L., & Wu, W.-H. (2006). A protein kinase, interacting with two calcineurin B-like proteins, regulates K⁺ transporter AKT1 in Arabidopsis. *Cell*, 125(7), 1347–1360.
- Xu, Q., Ren, Y., & Liesche, J. (2019). Studying Phloem Loading with EDTA-Facilitated Phloem Exudate Collection and Analysis. In *Phloem* (pp. 125–133). Springer.
- Xu, Q., Yin, S., Ma, Y., Song, M., Song, Y., Mu, S., Li, Y., Liu, X., Ren, Y., & Gao, C. (2020). Carbon export from leaves is controlled via ubiquitination and phosphorylation of sucrose transporter SUC2. *Proceedings of the National Academy of Sciences*, 117(11), 6223–6230.
- Yamada, K., Osakabe, Y., Mizoi, J., Nakashima, K., Fujita, Y., Shinozaki, K., & Yamaguchi-Shinozaki, K. (2010). Functional analysis of an Arabidopsis thaliana abiotic stress-inducible facilitated diffusion transporter for monosaccharides. *Journal of Biological Chemistry*, 285(2), 1138–1146.
- Yamaguchi-Shinozaki, K., & Shinozaki, K. (2006). Transcriptional regulatory networks in cellular responses and tolerance to dehydration and cold stresses. *Annu. Rev. Plant Biol.*, 57, 781–803.
- Yanagisawa, S., Yoo, S.-D., & Sheen, J. (2003). Differential regulation of EIN3 stability by glucose and ethylene signalling in plants. *Nature*, 425(6957), 521–525.
- Zhang, X., Henriques, R., Lin, S.-S., Niu, Q.-W., & Chua, N.-H. (2006). Agrobacterium-mediated transformation of Arabidopsis thaliana using the floral dip method. *Nature Protocols*, 1(2), 641–646.
- Zhang, Y., Primavesi, L. F., Jhurreea, D., Andralojc, P. J., Mitchell, R. A. C., Powers, S. J., Schluemann, H., Delatte, T., Wingler, A., & Paul, M. J. (2009). Inhibition of SNF1-related protein kinase1 activity and regulation of metabolic pathways by trehalose-6-phosphate. *Plant Physiology*, 149(4), 1860–1871.
- Zhao, H., Guan, J., Liang, Q., Zhang, X., Hu, H., & Zhang, J. (2021). Effects of cadmium stress on growth and physiological characteristics of sassafras seedlings. *Scientific Reports*, 11(1), 1–11.

- Zhong, Y., Xie, J., Wen, S., Wu, W., Tan, L., Lei, M., Shi, H., & Zhu, J. (2020). TPST is involved in fructose regulation of primary root growth in *Arabidopsis thaliana*. *Plant Molecular Biology*, *103*(4), 511–525.
- Zhu, F., Alseekh, S., Koper, K., Tong, H., Nikoloski, Z., Naake, T., Liu, H., Yan, J., Brotman, Y., & Wen, W. (2022). Genome-wide association of the metabolic shifts underpinning dark-induced senescence in *Arabidopsis*. *The Plant Cell*, *34*(1), 557–578.
- Zhu, L., Li, B., Wu, L., Li, H., Wang, Z., Wei, X., Ma, B., Zhang, Y., Ma, F., & Ruan, Y.-L. (2021). MdERDL6-mediated glucose efflux to the cytosol promotes sugar accumulation in the vacuole through up-regulating TSTs in apple and tomato. *Proceedings of the National Academy of Sciences*, *118*(1).

7. Supplementary information

7.1. Supplementary figures

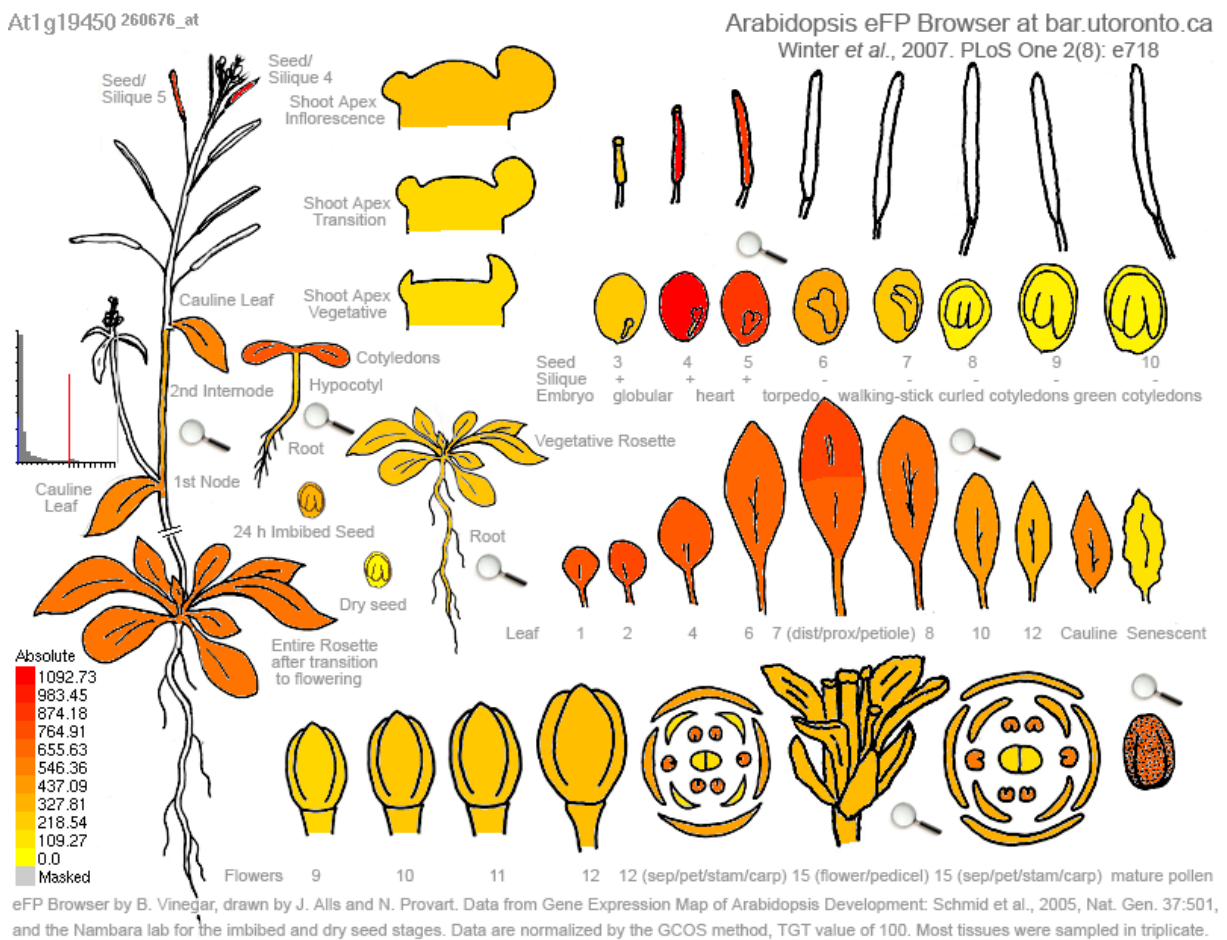


Figure 7.1. Expression pattern of *ERDL4* (At1g19450) in Arabidopsis during different developmental stages in the eFP browser (Arabidopsis electronic fluorescent pictograph; Winter et al. 2007).

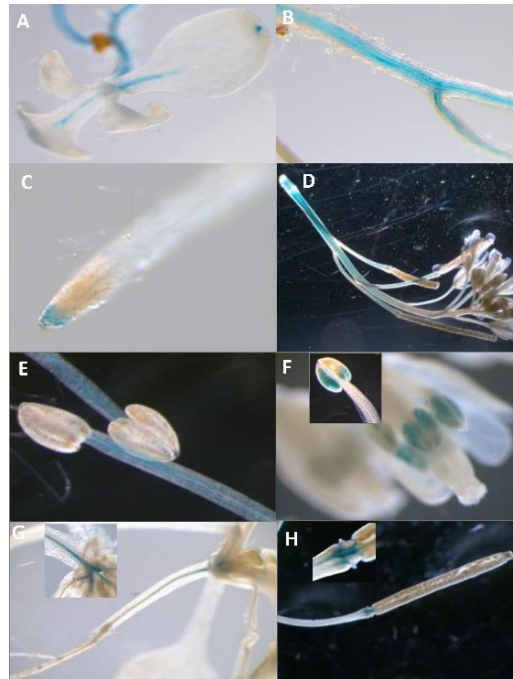


Figure 7.2. Tissue specific expression of *ERDL4*. *ERDL4_{Pro}::GUS* fusion protein was transformed into WT Col-0 plants and subjected to histochemical GUS staining. **A, B.** In two weeks old plants *ERDL4* expression was mainly found in the vasculature of leaf and roots. **C, D.** GUS staining in root tip and inflorescence. **E, F.** GUS staining was observed in anthers and strongly in pollens. **G.** GUS staining in shoot apical meristem region and hypocotyl **H.** GUS staining in silique pedicel.

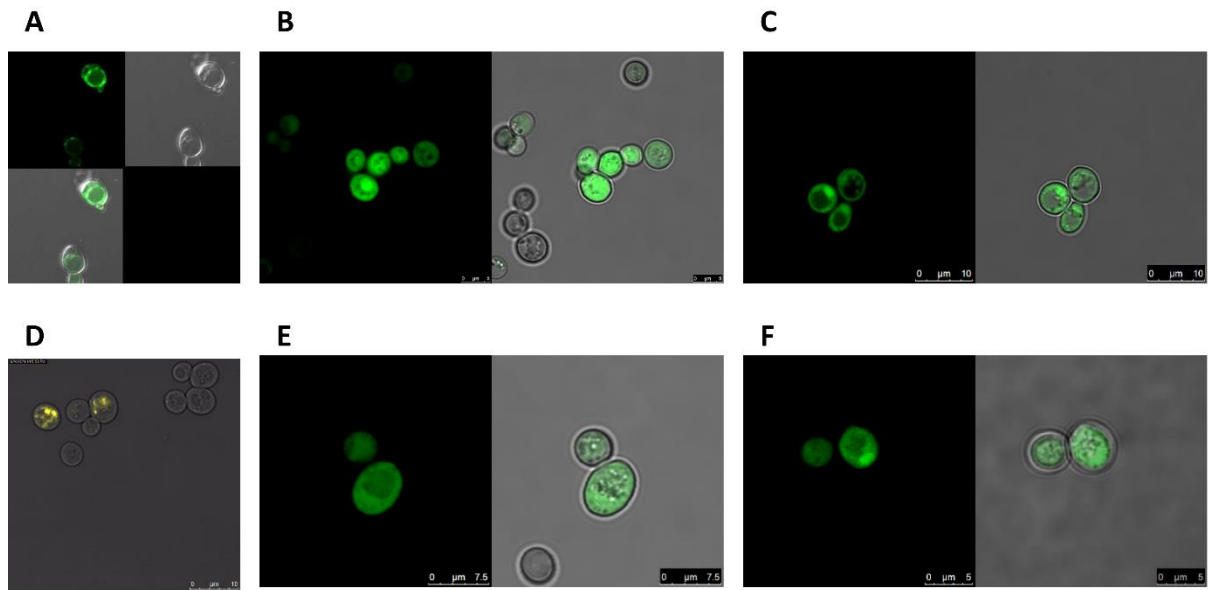


Figure 7.3. Native and mutated *ERDL4* localization in different yeast strains. Native and mutated *ERDL4* fused with C-terminal GFP constructs were expressed in W303 and EBY.VW-4000 yeast strains. **A.** Native *ERDL4* expression in W303 yeast. **B.** Mutated AA-*ERDL4* fused with GFP and expressed in W303. **C.** Truncated ΔN-*ERDL4* fused with GFP and expressed in W303. **D.** Native *ERDL4* expressed in the vacuole and in cytosol in EBY.VW-4000. **E.** Mutated AA-*ERDL4* fused with GFP and expressed in EBY.VW-4000. **F.** Truncated ΔN-*ERDL4* fused with GFP and expressed in EBY.VW-4000. Bar=10µm.

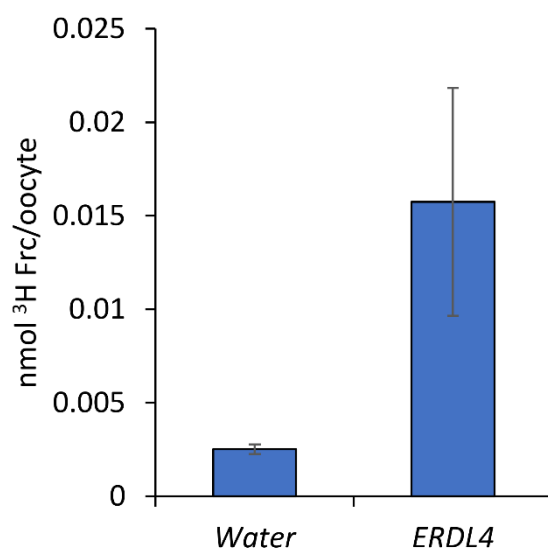


Figure 7.4. ^3H fructose uptake via *Xenopus* oocytes expressing ERDL4. Fructose uptake activity of water or ERDL4 expressing oocytes was determined using 2.5 μCi ^3H -labelled Frc as described in material and methods section. Values are means of \pm sd (n=6)

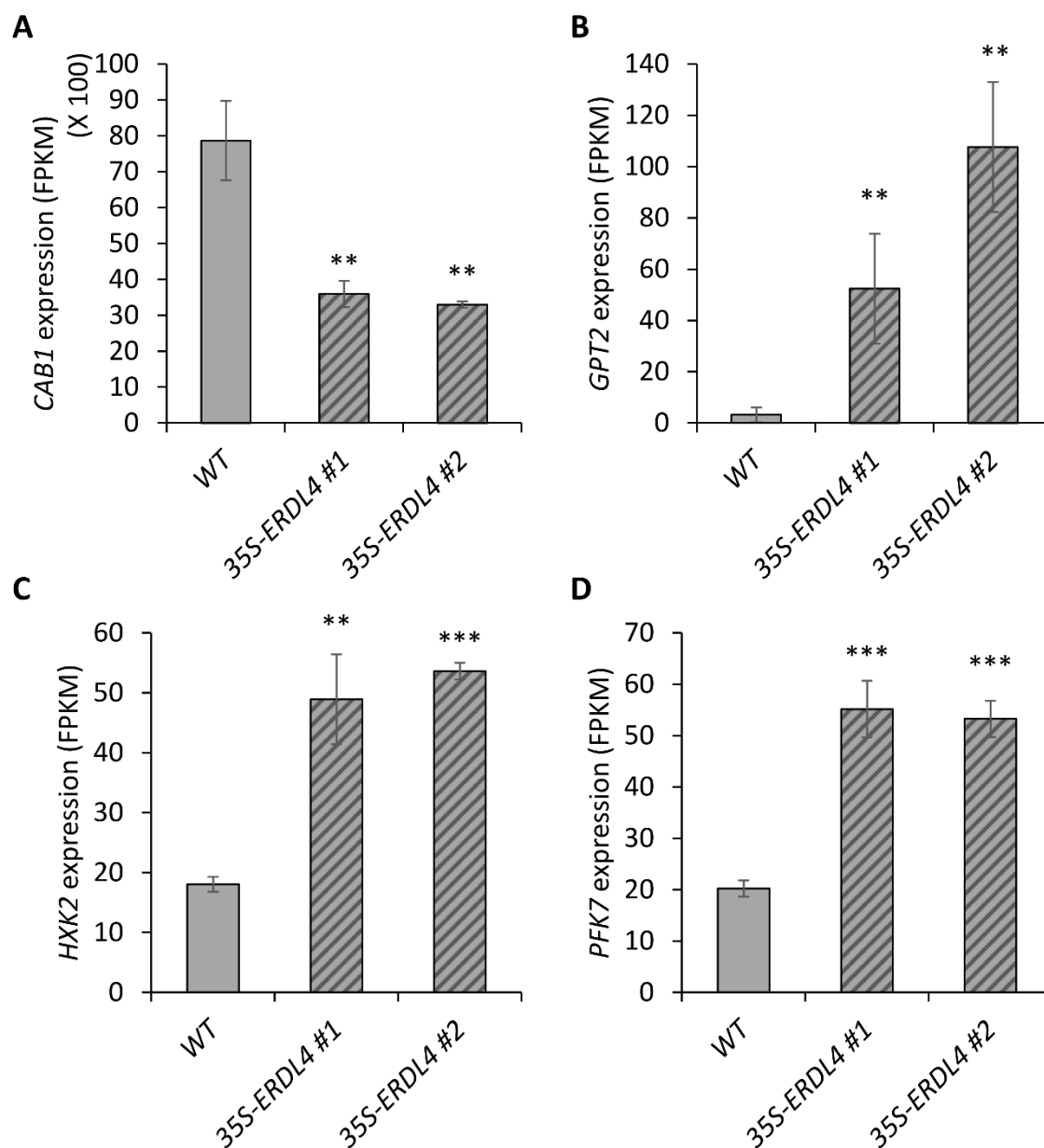


Figure 7.5. Expression of sugar responsive genes in *ERDL4* mutants. FPKM expression values of sugar responsive genes in *35S-ERDL4* lines and corresponding WT. **A-D.** Expression values of *CAB1*, *GPT2*, *HXK2* and *PFK7*. Plants grown for 6 weeks in standard condition ($120 \mu\text{mol Photons m}^{-2} \text{s}^{-1}$, 10h light/14h dark, 22°C) were harvested 4 hours after onset of light. Data represents mean \pm standard error from three biological replicates. Statistically significant differences were calculated using Student's one-tailed t-test (* $p \leq 0.05$; ** $p \leq 0.01$; *** $p \leq 0.001$).

| | | Man | Frc | Glc |
|-----------|---------|------------|------------|------------|
| AT2G34430 | LHB1B1 | 1719.67 | 94.21 | 13.03 |
| AT3G54890 | LHCA1 | 2753.72 | 512.89 | 59.65 |
| AT3G61470 | LHCA2 | 3298.07 | 746.20 | 86.44 |
| AT1G61520 | LHCA3 | 3262.35 | 716.52 | 89.21 |
| AT3G47470 | LHCA4 | 7617.28 | 1521.86 | 196.82 |
| AT1G45474 | LHCA5 | 86.85 | 44.80 | 27.01 |
| AT1G19150 | LHCA6 | 10.05 | 4.75 | 0.53 |
| AT1G29920 | LHCB1.1 | 7003.76 | 1744.36 | 142.57 |
| AT1G29910 | LHCB1.1 | 2412.05 | 802.09 | 69.74 |
| AT1G29930 | LHCB1.3 | 20708.35 | 4437.85 | 474.80 |
| AT2G05100 | LHCB2.1 | 4387.00 | 1175.65 | 147.88 |
| AT2G05070 | LHCB2.2 | 4049.19 | 935.83 | 106.25 |
| AT3G27690 | LHCB2.4 | 887.90 | 130.05 | 6.35 |
| AT5G54270 | LHCB3 | 4541.73 | 1151.89 | 113.72 |
| AT5G01530 | LHCB4.1 | 3799.87 | 943.23 | 153.74 |
| AT3G08940 | LHCB4.2 | 3871.77 | 757.07 | 75.29 |
| AT2G40100 | LHCB4.3 | 2.14 | 1.59 | 1.00 |
| AT4G10340 | LHCB5 | 3788.29 | 899.90 | 100.09 |
| AT1G15820 | LHCB6 | 2533.99 | 912.01 | 122.15 |

Figure 7.6. Similar regulation by glucose and fructose of LHCs genes. RNA-Seq analysis showed that most of the genes were regulated in the same manner by both glucose and fructose. Here genes related to light harvesting complexes (LHCs) of photosystem show similar regulation by both sugars making it difficult to dissect the specific sugar effect.

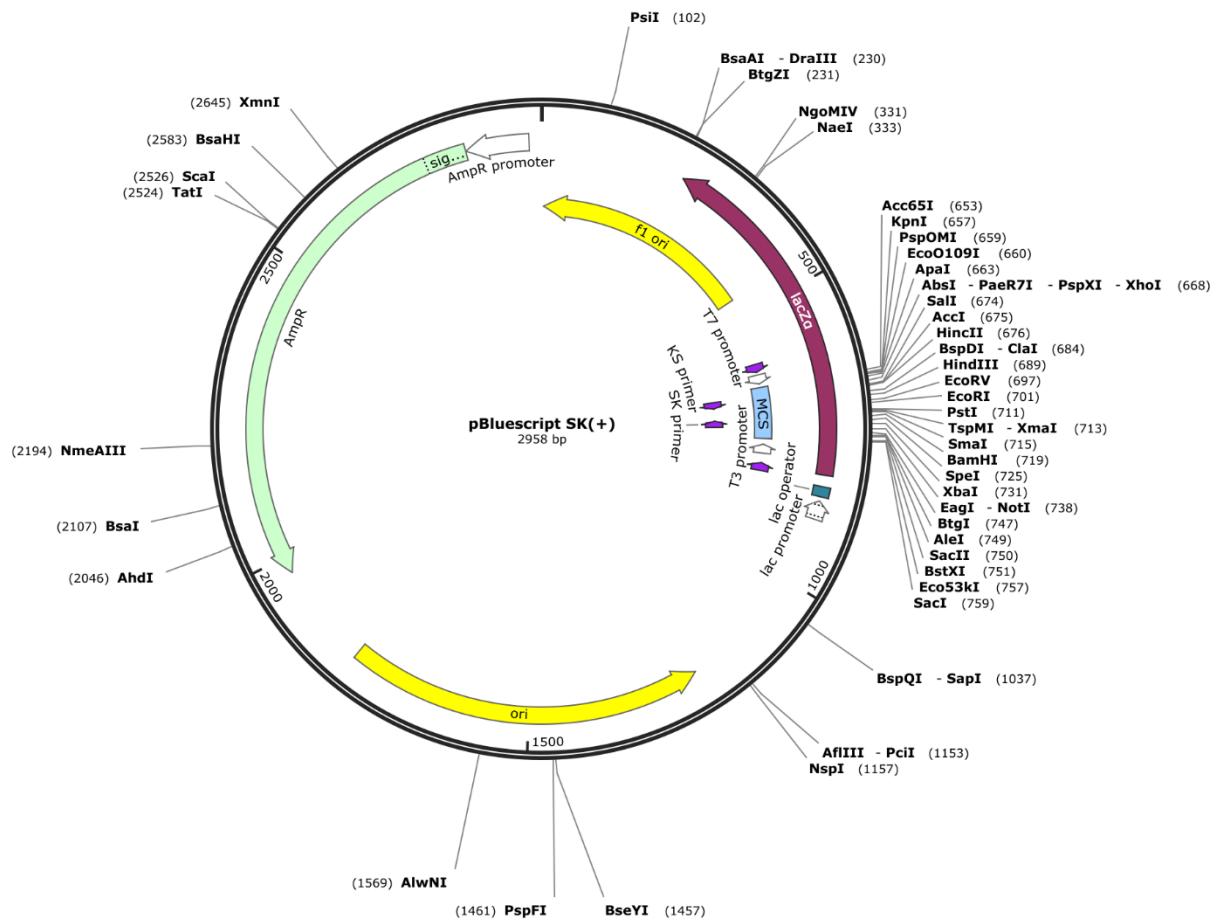


Figure 7.8. Vector map of plasmid pBSK.

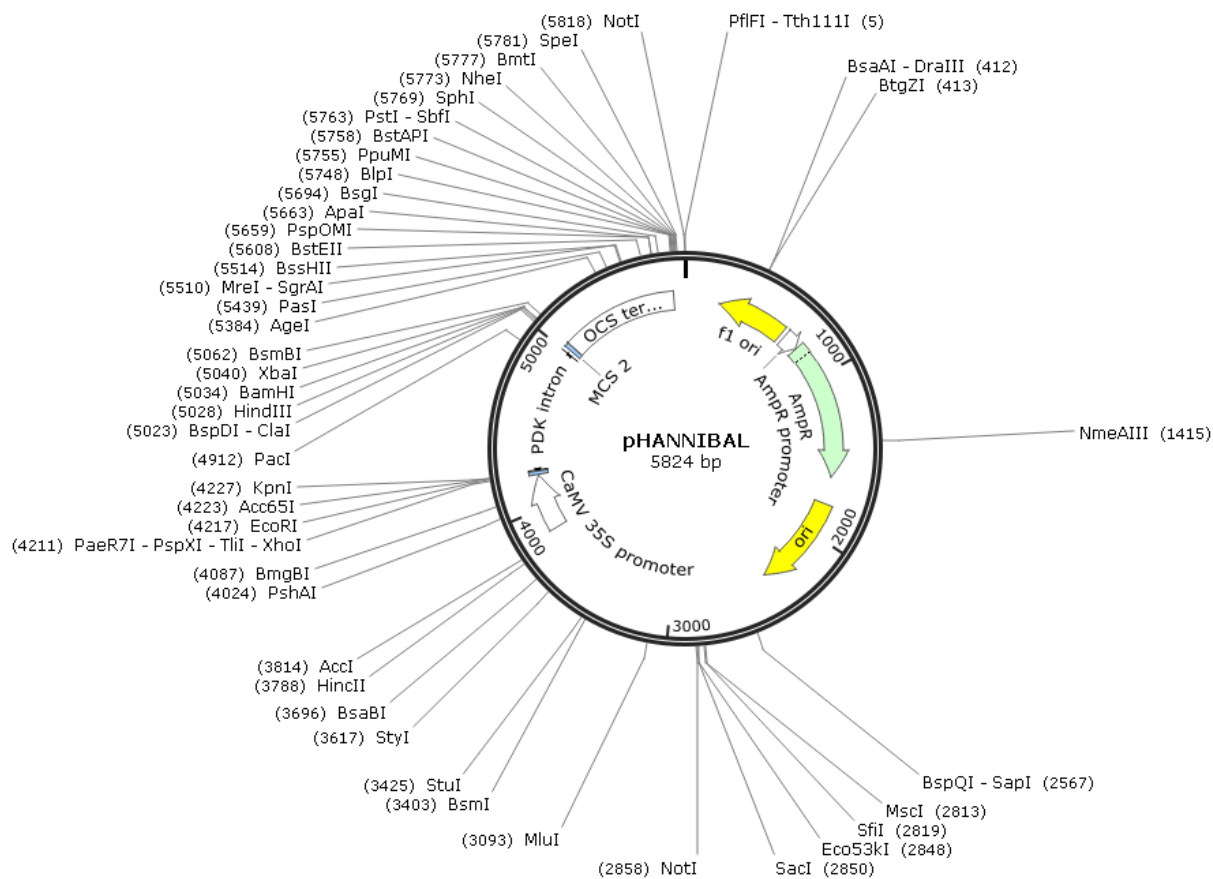


Figure 7.9. Vector map of plasmid pHannibal

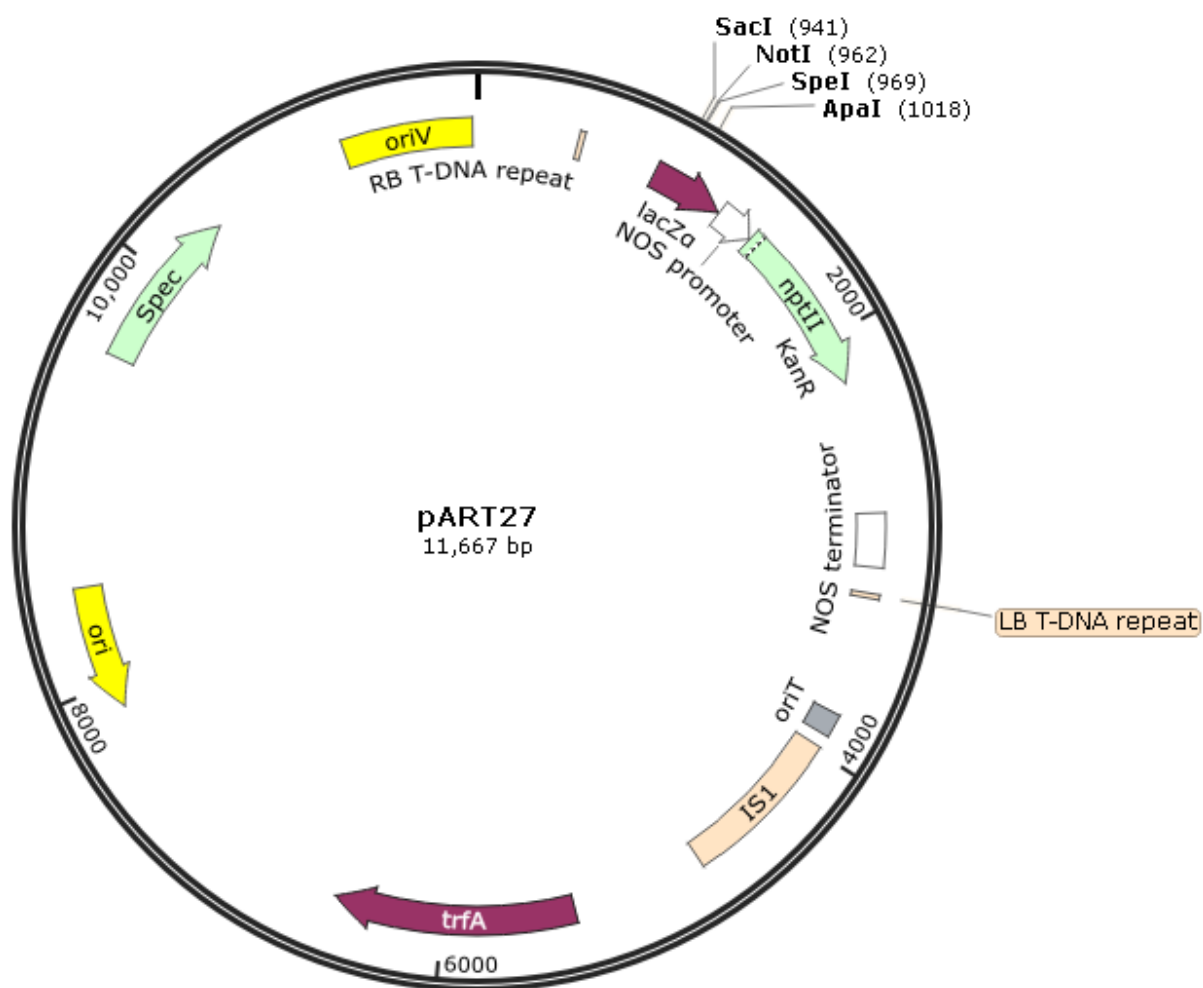


Figure 7.10. Vector map of plasmid pART27.

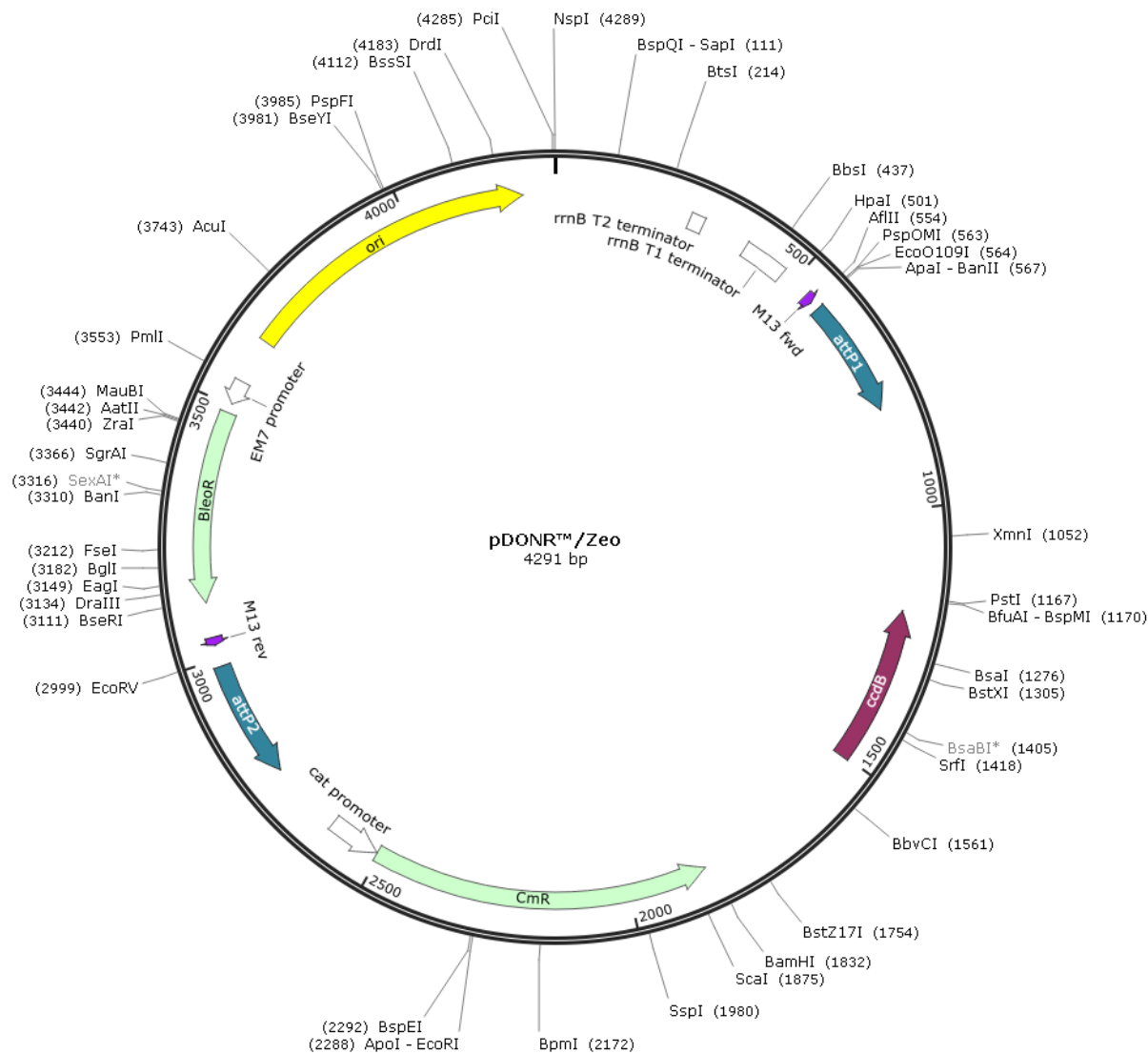


Figure 7.11. Vector map of plasmid, pDon/Zeo

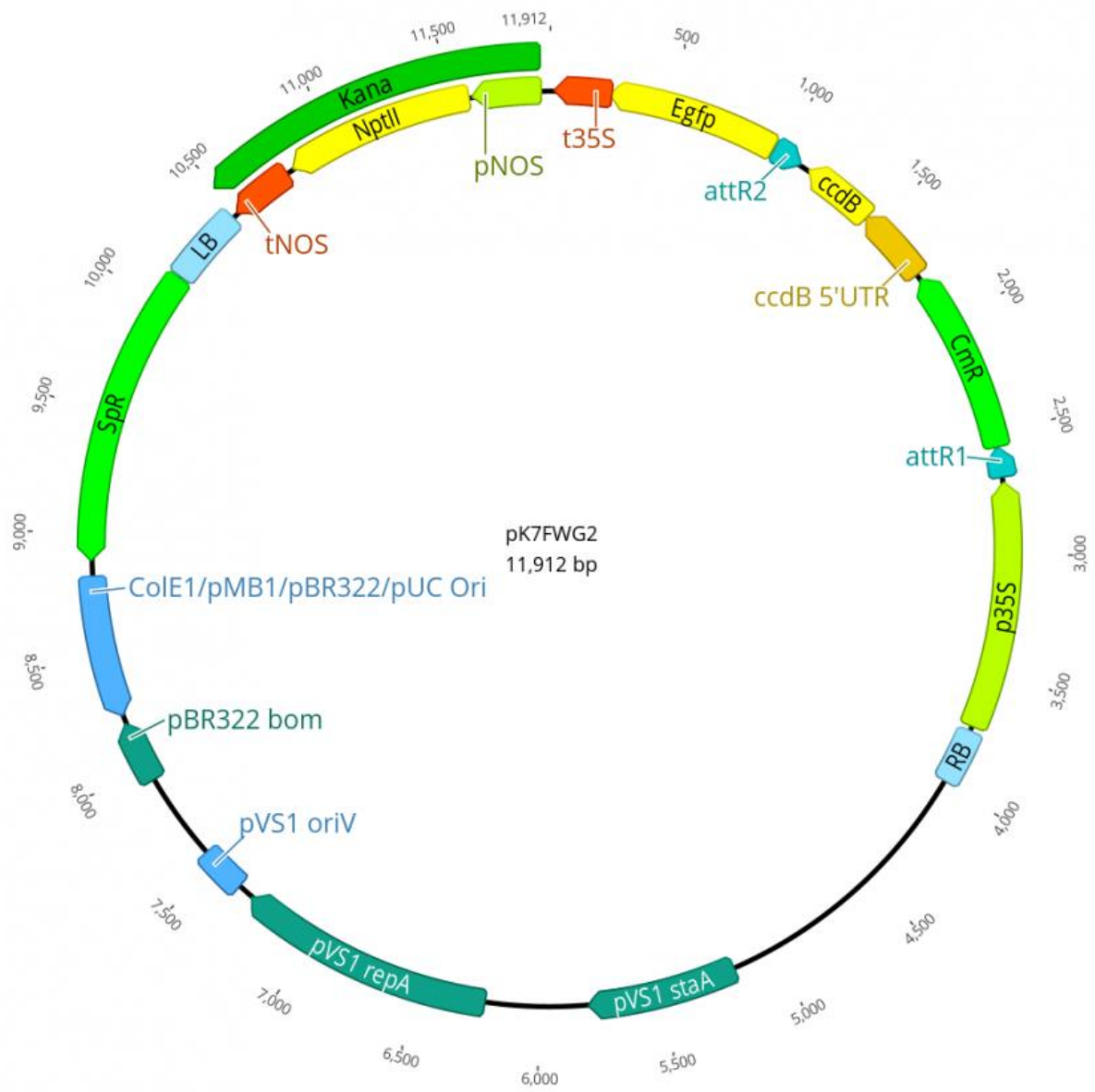


Figure 7.12. Vector map of plasmid pK7FWG2.

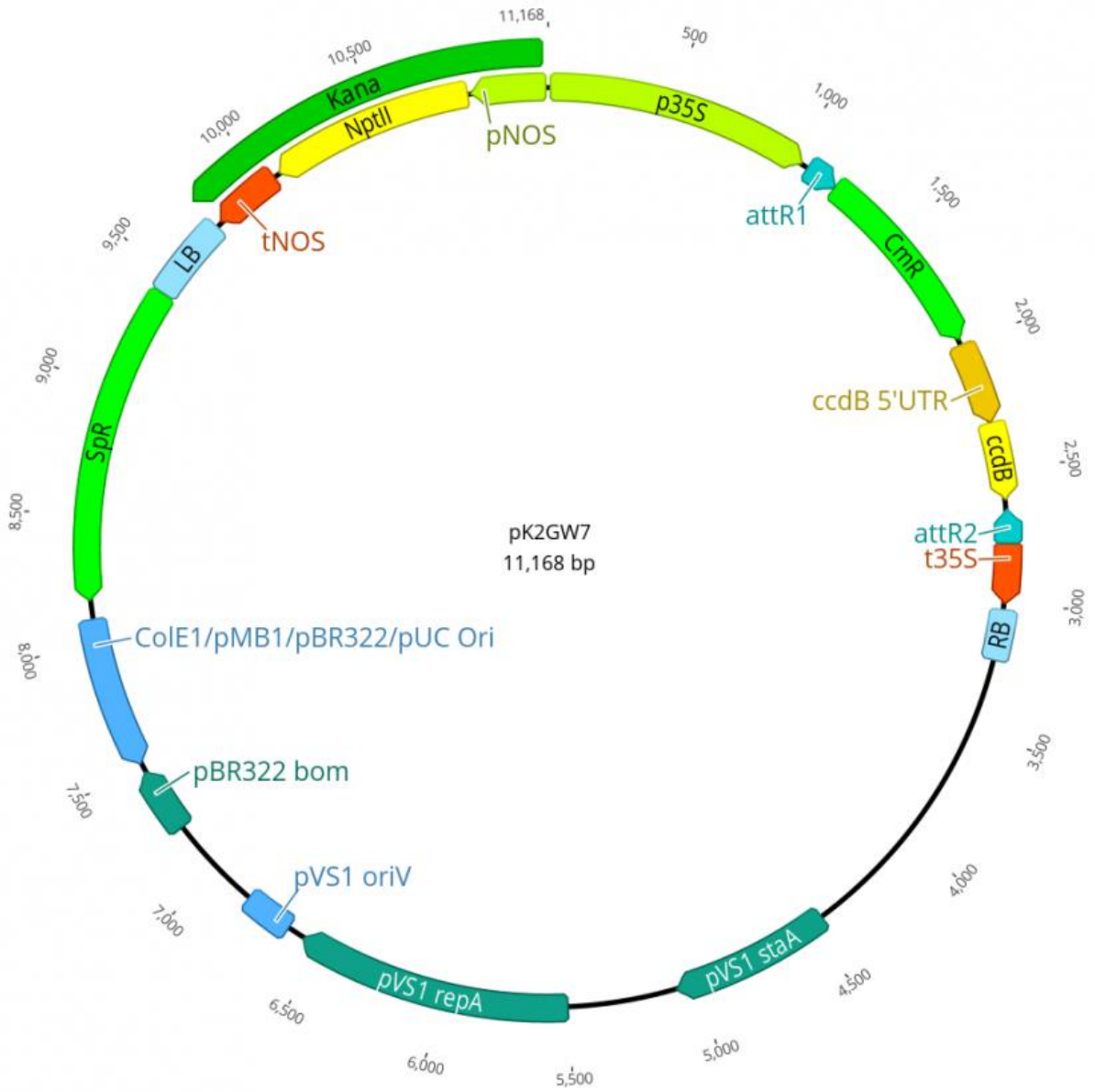


Figure 7.13. Vector map of plasmid pK2GW7.

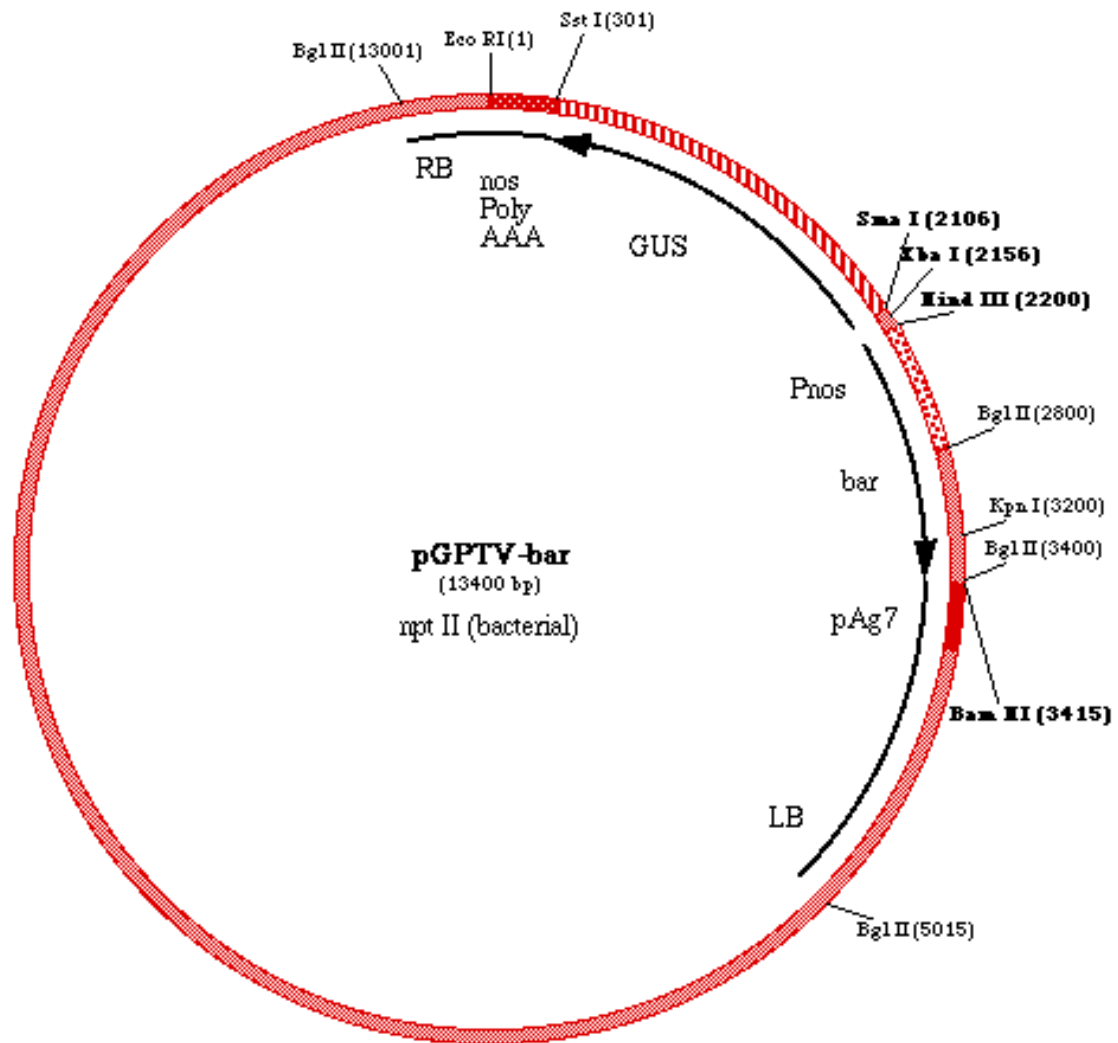


Figure 7.14. Vector map of plasmid pGPTV-bar.

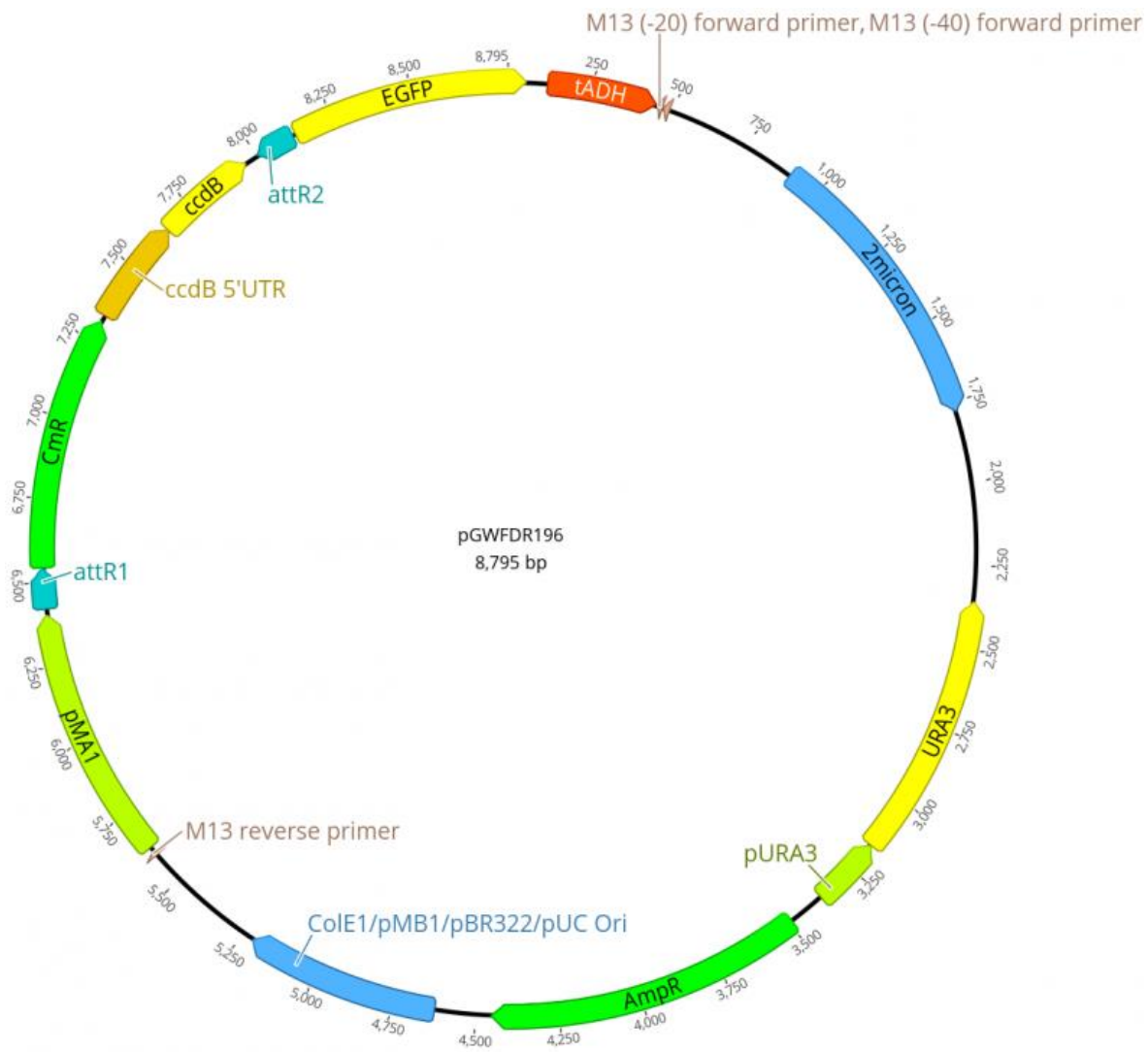


Figure 7.15. Vector map of plasmid pGWFD196.

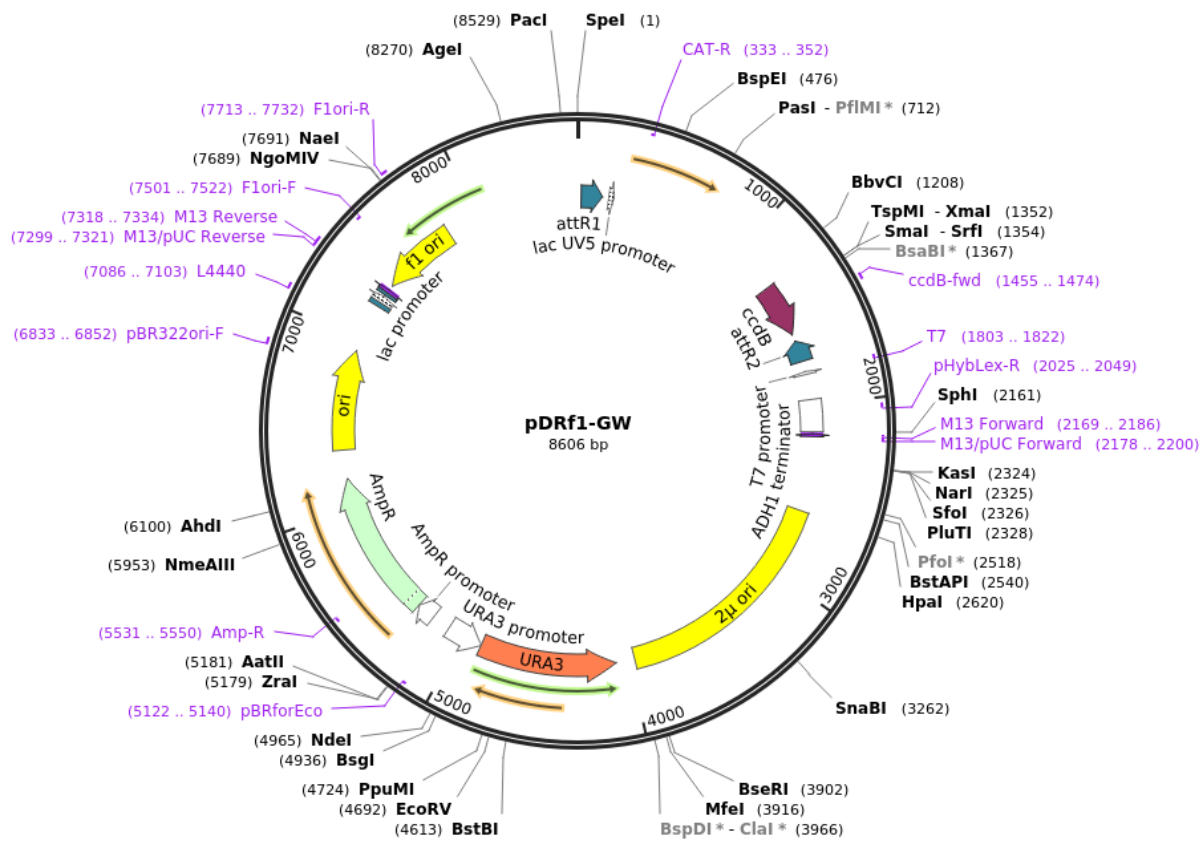


Figure 7.16. Vector map of plasmid pDRf1-GW.

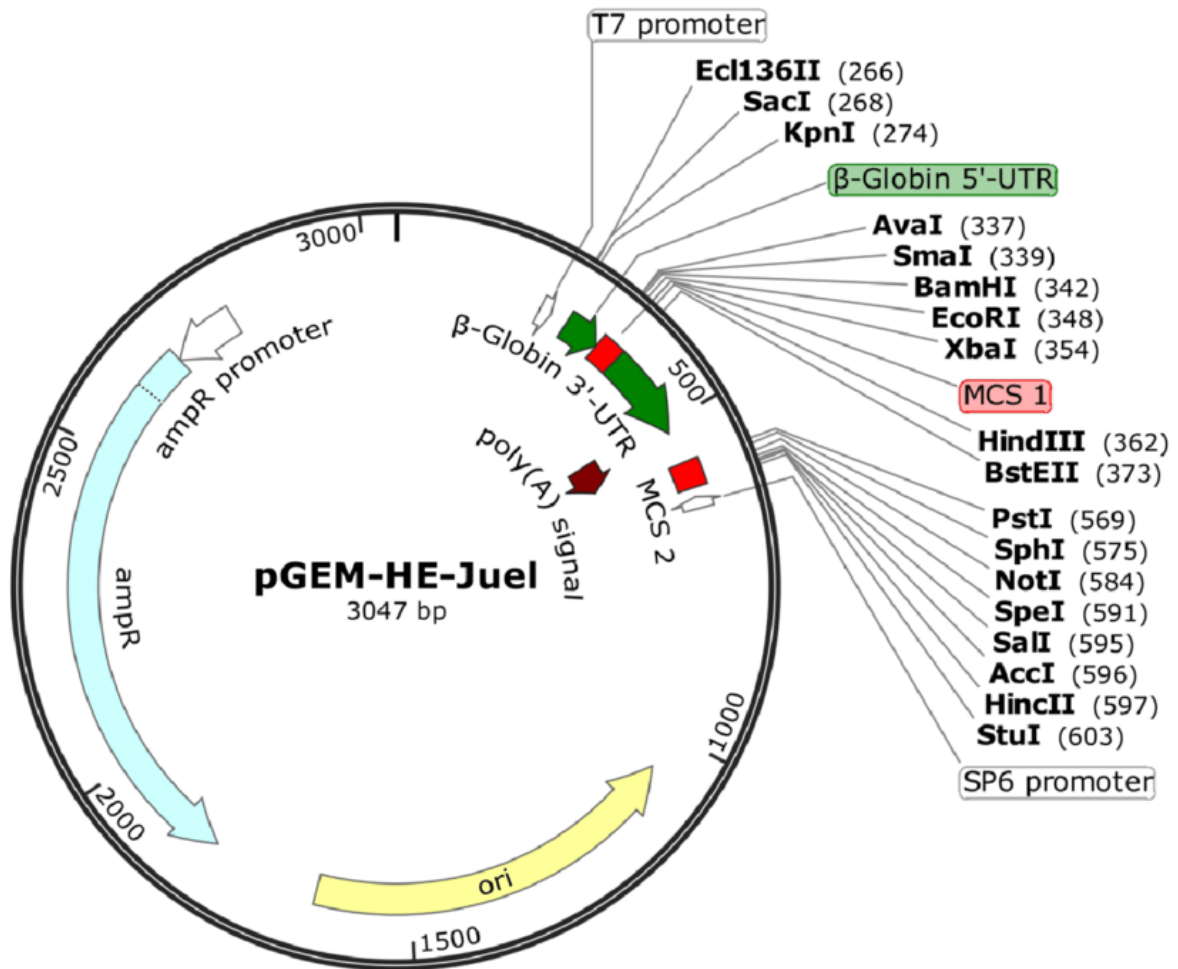


Figure 7.17. Vector map of plasmid pGEM-He-Juel.

7.2. Abbreviations

| Abbreviation | Meaning |
|---------------------|-----------------------------------|
| CW-INV | Cell wall invertase |
| C-INV | Cytosolic invertase |
| V-INV | Vacuolar invertase |
| HXK | Hexokinase |
| SPS | Sucrose phosphate synthase |
| SUS | Sucrose synthase |
| MST | Monosaccharide transporter family |
| MFS | Major facilitator superfamily |
| Glc | Glucose |
| Frc | Fructose |
| Suc | Sucrose |
| G6P | Glucose-6-phosphate |
| F6P | Fructose-6-phosphate |
| UDP-G | Uridine diphosphate glucose |
| FRK | Fructokinase |
| EON | End of night |
| EOD | End of day |
| PFK | Phosphofructokinase |
| CIPK | CBL-Interacting protein kinase |
| CBL | Calcineurin-B-Like protein |

7.3. List of Figures

Figure 1.1. Generation of starch and transport sugar sucrose. During the course of photosynthesis, triose phosphate is formed, which after export into the cytosol is converted into UDP-glucose in several reactions and with the participation of various enzymes. Then UDP-glucose and fructose-6-bisphosphate react to sucrose phosphate through sucrose phosphate synthase. Finally, sucrose phosphate phosphatase catalyzes the dephosphorylation of sucrose phosphate, which produces sucrose. As per the demand of the cell sucrose is then hydrolyzed into monosaccharides glucose, fructose or UDP-glucose via cytosolic invertases (cINV) or sucrose synthase (SUS) respectively. Different sugar transporters are present on the tonoplast to transport this sugar in and out of the vacuole. At night the stored starch is degraded, and the degradation products are transported to the cytosol via specialized transporters..... 3

Figure 1.2. Sugar transport and phloem loading. Sucrose synthesized via photosynthesis in the mesophyll cell is transported symplastically into parenchyma cells (PCs) and then to phloem parenchyma transfer cells (PPTCs) through plasmodesmata pores. Depending on endogenous sucrose concentration, part of this sucrose is deposited as cell wall ingrowths in PPTCs and the rest is transported via *SWEET11/12* transporters to the apoplast. *SUC2* transporters uptake this sugar from the apoplast into companion cells and subsequently to the sieve element for the long-distance transport via phloem. 5

Figure 1.3. Sugar transporters present on the vacuolar membrane. The import of monosaccharides glucose and fructose is mediated via *VGT* (vacuolar glucose transporter) or *TST* (tonoplast sugar transporter) proteins in counter-exchange of a proton H^+ . They both represent subclasses of MST (monosaccharide transporter) family proteins. *TSTs* can also mediate sucrose. Export of monosaccharides can be mediated by members of the *Early-Responsive to Dehydration 6-Like proteins ERDL6, ESL1 and ERDL4* and by the sugar facilitator proteins *SWEET16* or *SWEET17* belonging to SWEET family, or via sucrose/ H^+ symporter *SUC4*-type proteins. 7

Figure 3.1. A. Multiple sequence alignment of *AtERDL4* and *AtERDL6* protein sequence. *AtERDL4* protein consist of 488 a.a whereas, *AtERDL6* protein is 487 amino acid long. Both exhibiting 92% protein sequence identity (Clustal Omega;

<https://www.ebi.ac.uk/Tools/msa/clustalo/>). Shaded alignment is generated using BoxShade software (https://embnet.vital-it.ch/software/BOX_form.html). Black colour shows conserved regions, gray colour indicates a.a substituted with similar characteristics/properties and white colour shows the mutant regions. **B.** Phylogenetic tree is generated using protein sequences of all the 19 members of ERDLs subfamily via neighbor joining method with CLUSTAL alignment and viewed with online tool, interactive tree of life, available at (<https://itol.embl.de/>) (Lutenic and Bork, 2021). **C.** Schematic depiction of the *AtERDL4* (left) and *AtERDL6* (right) protein's secondary structure visualized via the webtool Protter (<http://wlab.ethz.ch/protter/start/>). Transmembrane domains, colored in dark blue, were identified using the tool TMHMM (<http://www.cbs.dtu.dk/services/TMHMM/>). Highly conserved motifs indicating a sugar transport activity of the respective protein are highlighted in red. Putative phosphorylation sites assigned with a score higher than 0.7 detected via the web tool NetPhos 3.1 Server (<http://www.cbs.dtu.dk/services/NetPhos/>) were colored in green and additional a.a in *AtERDL4* is in cyan. 37

Figure 3.2. Pie distribution of cis-acting elements. Upstream promoter region (1500 bp) of *AtERDL4* was analysed with PlantCare database (<http://bioinformatics.psb.ugent.be/webtools/plantcare>) for identification of cis-acting elements. Pie chart represents the percentage of elements present within the promoter. In red are the elements related to stresses examined in this study. 38

Figure 3.3. Subcellular localization of *AtERDL4-GFP* in Arabidopsis. Arabidopsis protoplasts (**A to F**) were transiently transformed with an *AtERDL4-GFP* fusion protein construct. After 20 hours of incubation, protoplasts were lysed by mild osmotic shock and analysed by confocal laser scanning microscopy. **A.** Bright-field image of a protoplast after lysis, leaving the intact vacuole with attached chloroplasts. **B to F.** Fluorescence image of a lysed protoplast showing *AtERDL4-GFP* localization to the tonoplast (green) and chlorophyll autofluorescence (magenta) of attached chloroplasts. Bars = 10 µm. 39

Figure 3.4. Genotyping of Arabidopsis *ERDL4* mutants. **A.** Schematic representation of *ERDL4* T-DNA insertions, and promoter GUS region (blue). Boxes represent exons and lines represent introns. **B.** Amplification of *ERDL4* gene from WT and T-DNA mutants gDNA using primers (*ERDL4_F+ERDL4_R*) **C.** Confirmation of T-DNA insertion in WT and knockout mutants with primers (LBb1.3+RP for salk line and GK_LBP+GK_Rev for gabi-kat line). **D.** Amplification of *ERDL4* full length transcript from WT and knockout mutants cDNA with primers (*ERDL4_F +*

ERDL4_R). **E.** Amplification of housekeeping gene (*ef1- α*) from WT and knockout plants cDNA with primers (*EF1-alpha_F+EF1-alpha_R*). **F.** Expression of *ERDL4* (FPKM values) in *ERDL4* overexpression lines expressed under a 35S-constitutive promoter in wild type. **G.** Expression of *ERDL4* (FPKM values) in *erdl4* knockout mutants..... 40

Figure 3.5. Total and subcellular sugar accumulation in WT, *ERDL4*-overexpressing and mutant plants. **A.** Contents of glucose (*glc*), fructose (*frc*), sucrose (*suc*) in shoots. **B-D.** subcellular contents of glucose. **B.** fructose **(C)**, sucrose **(D)** in vacuoles, chloroplast, and cytosolic fractions of shoots from WT, *ERDL4*-overexpressing and mutant plants as obtained by non-aqueous fractionation. Plants were grown in standard condition ($120 \mu\text{mol Photons m}^{-2} \text{s}^{-1}$, 10h light/14h dark, 22°C) in soil and harvested at the end of light phase. Bars represent means from $n=5$ plants \pm SE. Different letters above bars denote significant differences according to *One-Way* ANOVA with post-hoc Tukey test ($p < 0.05$). *nd* = no quantifiable amount detected..... 42

Figure 3.6. Phenotypic characterization of *ERDL4* mutants. Plants were grown in soil or in hydroponic medium for 5 weeks in standard conditions ($120 \mu\text{mol Photons m}^{-2} \text{s}^{-1}$, 10 h light/14 h dark, 22°C) **A.** Rosettes of 5 weeks old *ERDL4* mutants and corresponding WT. **B.** Rosettes and roots of *ERDL4* mutants and WT grown in hydroponic medium **C.** Rosette fresh weight of WT and *ERDL4* mutants. Data represents the mean \pm standard error from 6 biological replicates. **D.** Root dry weight of WT and *ERDL4* mutants grown in hydroponics. The mean \pm standard error is shown from six biological replicates. Statistically significant differences were calculated using the one-tailed Student's t-test ($*p \leq 0.05$; $**p \leq 0.01$; $***p \leq 0.001$)..... 43

Figure 3.7. Root growth analysis of *ERDL4* overexpressors. *ERDL4* overexpressors and corresponding WT were grown under standard conditions ($120 \mu\text{mol photons m}^{-2}\text{s}^{-1}$, 10 h day/14 h, 22°C) on $\frac{1}{2}$ MS agar plates with no additional sugars. **A.** Root length of Arabidopsis seedlings determined on the corresponding days after germination (DAG). The mean \pm standard error is shown in each case from ≥ 30 biological replicates. The mean \pm standard error is shown in each case from ≥ 30 biological replicates. 44

Figure 3.8. Phloem sugar export and *SWEET* proteins expression. Plants were grown in soil for 6 weeks in standard conditions ($120 \mu\text{mol Photons m}^{-2} \text{s}^{-1}$, 10h light/14h dark, 22°C). The leaves from well-watered plants were harvested 4h after the onset of light phase and phloem sap was collected in water for 6 hours in the dark. The sugar levels in the phloem sap were determined enzymatically. **A.** Sugar export quantified from phloem exudates Shown is the

mean \pm standard error of eight biological replicates. Statistically significant differences were calculated using Student's one-tailed t-test (* $p \leq 0.05$; ** $p \leq 0.01$; *** $p \leq 0.001$). FW = fresh weight. **B.** *SWEET11/12* expression analysis in *ERDL4* overexpressors and corresponding WT. FPKM values obtained from RNA-seq results. The mean \pm standard error is shown from 3 biological replicates. Statistically significant differences were calculated using Student's one-tailed t-test (* $p \leq 0.05$; ** $p \leq 0.01$; *** $p \leq 0.001$)..... 45

Figure 3.9. *ERDL4* overexpressors plants exhibit longer and more inflorescence stems than

WT. A. Representative image of inflorescence stems of WT and *ERDL4* overexpressor plants.

B. Inflorescence stem length of WT and *ERDL4* overexpressors. Plants were grown in control condition ($120 \mu\text{mol Photons m}^{-2} \text{s}^{-1}$, 10h light/14h dark, 22°C) in soil for 4 weeks and then transferred to long day conditions ($120 \mu\text{mol Photons m}^{-2} \text{s}^{-1}$, 14h light/10h dark, 22°C). Data collection started the first day plants started bolting and continued until the inflorescence stem length stopped to increase (~30 days after transfer to long day). Data represents the mean \pm standard error of ≥ 20 individual plants per line. **C.** Inflorescence stem fresh weight. Inflorescence stems from the corresponding plants were harvested before going to drying phase and weighed. Data represents the mean \pm standard error of ≥ 20 individual plants per line. Statistically significant differences were calculated using Student's one-tailed t-test (* $p \leq 0.05$; ** $p \leq 0.01$)..... 46

Figure 3.10. Analysis of siliques from WT and *ERDL4* mutants. A. Silique length of WT and

ERDL4 mutants. Mature siliques were harvested from the lower part of the inflorescence stem. For length determination 30 siliques from $n \geq 15$ plants were analyzed. **B.** Soluble sugars quantified in the siliques of *ERDL4* mutants and the WT. Siliques from inflorescence stem of the corresponding plants were harvested before the drying phase and sugars were determined enzymatically. The mean \pm standard error is shown from six biological replicates. Data represents the mean \pm standard error. Significant differences were calculated using one-tailed Student's t-test referred to WT (* $p \leq 0.05$; ** $p \leq 0.01$; *** $p \leq 0.001$). 47

Figure 3.11. *ERDL4* overexpressors have high seed yield. A. Seeds counted per silique. For

analysis 10 mature and dry siliques per plant from $n \geq 6$ plants were harvested and seeds were carefully extracted and counted from *ERDL4* mutants and corresponding WT plants. Data represents the mean \pm standard error. Significant differences were calculated using one-tailed Student's t-test referred to WT (* $p \leq 0.05$; ** $p \leq 0.01$; *** $p \leq 0.001$). **B.** Seed yield calculated per plant. Plants were grown for 4 weeks in short day ($120 \mu\text{mol Photons m}^{-2} \text{s}^{-1}$, 10h light/14h

dark, 22°C) in soil and then transferred to long day conditions (120 $\mu\text{mol Photons m}^{-2} \text{s}^{-1}$, 14h light/10h dark, 22°C). Inflorescence stems were carefully wrapped and harvested after drying. Seeds were harvested from the inflorescence stems of the corresponding plants. The mean \pm standard error is shown from $n \geq 12$ biological replicates. Statistically significant differences were calculated using Student's one-tailed t-test (* $p \leq 0.05$; ** $p \leq 0.01$; *** $p \leq 0.001$). 48

Figure 3.12. Seed quality and physiology from *ERDL4* mutants. After growing for 4 weeks in standard conditions plants were transferred to long day conditions (120 $\mu\text{mol Photons m}^{-2} \text{s}^{-1}$, 14h light/10h dark, 22°C). Fully mature and air-dried seeds were harvested from WT and *ERDL4* mutant plants. **A.** 1000 seeds weight. The mean \pm standard error is shown for three replicates (seed pool of 10 plants derived from the same harvest). **B.** Lipid quantification from 100mg of WT and *ERDL4* mutant seeds. Shown is the mean \pm standard error of 3 replicates (seed pool from 10 plants, from the same harvest). Statistically significant differences were determined using Student's one-tailed t-test calculated (* $p \leq 0.05$; ** $p \leq 0.01$; *** $p \leq 0.001$). **C.** Representative picture of seeds phenotype from WT and *ERDL4* mutants (derived from the same harvest). Bar = 200 μm 50

Figure 3.13. Venn-diagram and correlation analysis. Venn-diagram and correlation analysis between differentially expressed genes (DEGs) from *ERDL4*-overexpressing and WT plants and from fructose (Frc) or glucose (Glc) and mannitol (Man = control) incubated leaf discs. **A)** and **B)** show Venn-diagrams of DEGs. Numbers within circles represent the number of DEGs (significant at $p < 0.001$ according to the double-sided *t*-test of three replicates). There were 484 *35S-ERDL4*-dependent DEGs, 4340 Frc-dependent DEGs, and 5148 Glc-dependent DEGs. **A)** Diagram showing overlap of DEGs from *35S-ERDL4* and Frc-treatment. There were 130 DEGs regulated by both *ERDL4*-overexpression and Frc **B)** Diagram showing overlap of DEGs from *35S-ERDL4* and Glc-treatment. There were 155 DEGs regulated by both *ERDL4*-overexpression and Glc **C)** Correlation between relative expression (based on log₂-fold-change) of 130 DEGs between *35S-ERDL4* (against WT) and Frc (against Man). r = Pearson coefficient calculated from *ERDL4*/WT and Frc/Man matrices **D)** Correlation between relative expression (based on log₂-fold-change) of 155 DEGs between *35S-ERDL4* (against WT) and Glc (against Man). r = Pearson coefficient calculated from *ERDL4*/WT and Glc/Man matrices. (Data is kindly provided by Dr. Benjamin Pommerrenig, TU KL). 52

Figure 3.14. List of DEGs oppositely regulated by frc or glc ranked after their Log₂FCs. The upper part of the table lists the 10 most strongly frc-induced genes that were at the same time

repressed by *glc* and the lower part the 10 most strongly *glc*-induced genes that were at the same time repressed by *frc* (Log₂FCs cutoff ≤ 0.25). (Data is kindly provided by Dr. Benjamin Pommerrenig, TU KL). 53

Figure 3.15. Diurnal expression of transporters. **A.** Diurnal expression profile of *ERDL4*. 6 weeks old WT plants were harvested at given time points grown under standard condition (120 $\mu\text{mol Photons m}^{-2} \text{s}^{-1}$, 10h light/14h dark, 22°C). **B.** Diurnal expression profile of *ERDL6*. **C.** Diurnal expression profile of *TST1*. **D.** Diurnal expression profile of *TST2*. Expression is normalized to *Actin*. Grey-shaded areas indicate values recorded at night-time (without illumination). Data represents mean \pm standard error from three biological replicates. Statistically significant differences were calculated using Student's one-tailed t-test (* $p \leq 0.05$; ** $p \leq 0.01$; *** $p \leq 0.001$). **E.** Fructose to glucose ratio determined from sugar levels quantified at end of night (EON) and end of day (EOD). Data represents mean \pm standard error from five biological replicates. Statistically significant differences were calculated using Student's one-tailed t-test (* $p \leq 0.05$; ** $p \leq 0.01$; *** $p \leq 0.001$)..... 55

Figure 3.16. Expression of vacuolar sugar transporters in *ERDL4* mutants. Expression of vacuolar sugar importers in 35S-*ERDL4* lines and corresponding WT. **A-D.** Expression values of *TST1*, *TST2*, *VGT1* and *VGT2*. Expression of vacuolar and plastidic sugar exporters in 35S-*ERDL4* lines and corresponding WT. **E-H.** Expression values of *SWEET16*, *SWEET17*, *ERDL6* and *pSUT*. Expression of vacuolar sugar importers and exporters in *erd14* knockout lines and corresponding WT. **I-L.** Expression values of *TST1*, *TST2*, *ERDL6* and *SWEET16*. Plants grown for 6 weeks in standard condition (120 $\mu\text{mol Photons m}^{-2} \text{s}^{-1}$, 10h light/14h dark, 22°C) were harvested 4 hours after onset of light. Data represents mean \pm standard error from three biological replicates. Statistically significant differences were calculated using Student's one-tailed t-test (* $p \leq 0.05$; ** $p \leq 0.01$; *** $p \leq 0.001$)..... 57

Figure 3.17. Soluble sugar content in *tst-ERDL4* overexpressors. **A.** Expression of *ERDL4* in 4 weeks old *tst-ERDL4* overexpressor plants. Expression levels are normalized to *Actin*. The mean \pm standard error is shown from five biological replicates. Statistically significant differences were calculated using Student's one-tailed t-test (* $p \leq 0.05$; ** $p \leq 0.01$; *** $p \leq 0.001$). **B-D.** Soluble sugar quantification from WT, *tst1/2* and *tst-ERDL4* overexpressor. Plants were grown for 4 weeks in standard condition (120 $\mu\text{mol Photons m}^{-2} \text{s}^{-1}$, 10h light/14h dark, 22°C) and harvested 4 hours after onset of light. Data represents mean \pm standard error from

six biological replicates. Statistically significant differences were calculated using Student's one-tailed t-test (* $p \leq 0.05$; ** $p \leq 0.01$; *** $p \leq 0.001$). 58

Figure 3.18. Sequence alignment and evolutionary relationship between CIPKs. Protein sequences of both *AtCIPK6* and *GhCIPK6* were used to check sequence homology between the two **A.** Protein sequence alignment of *AtCIPK6* and *GhCIPK6*. **B.** Unrooted tree showing evolutionary relationship between *GhCIPK6* and the 26 *AtCIPKs*. Arrowhead points towards the CIPK6 from both species. In red are the branch support values (reliability factor) and branch length corresponds to 0.2. (Data for the tree is kindly provided by Dr. Benjamin Pommerrenig, TU KL)..... 60

Figure 3.19. Sugar and *ERDL4* dependent expression of CIPKs. **A.** The heat map representation on the left side indicates log₂ fold-changes of the expression of different CIPKs in fructose/mannitol treatment, glucose/mannitol and in *35S-ERDL4* lines. On the right side is the heatmap representation of the corresponding significance values (*p*-values) for each corresponding log₂ fold change. Pearson coefficient *r* indicates the correlation between CIPKs expression in glucose treatment/*35S-ERDL4* lines and CIPKs expression in fructose/*35S-ERDL4* lines. **B.** *CIPK5* and *CIPK6* fpkm values indicating their expression abundance in plants. **C.** Relative expression levels of *CIPK6* checked via qRT-PCR in WT and *35S-ERDL4* lines. (Heat map data is kindly provided Dr. Benjamin Pommerrenig, TU KL)..... 61

Figure 3.20. Cold induced changes in expression of *ERDL4* and *ERDL6*. **A-B.** Expression of *ERDL4* and *ERDL6* in response to cold (4°C). WT plants were placed in cold at 4°C for 1 day. Expression is normalized to *PP2A* and *SAND*. Data represents mean ± standard error from three biological replicates. Statistically significant differences were calculated using Student's one-tailed t-test (* $p \leq 0.05$; ** $p \leq 0.01$; *** $p \leq 0.001$). **C,** Representative picture of 2 weeks old leaf and root from control and cold conditions used for GUS staining. **D.** Root cross-sections from control condition (20°C) and cold (4°C). Plants were grown for 2 weeks in ½ MS agar plates supplemented with 0.5% sucrose. For cold treatment plates were transferred to cold (4°C) for 3 days and then used for GUS staining. R represents rhizodermis, C represents cortex and E represents endodermis. Stained tissues were fixed with 2% glutaraldehyde and embedded in Technovit® 7100 resin before making the 5 µm thin cross-sections with microtome. 63

Figure 3.21. Soluble sugars in cold acclimated plants and freezing tolerance. Sugars were quantified from rosettes harvested after 3 days 12of cold exposure. **A-C.** Glucose, fructose and

sucrose content in WT and *ERDL4* mutants. Plants were grown in soil for four weeks in control conditions (120 $\mu\text{mol Photons m}^{-2} \text{s}^{-1}$, 10h light/14h dark, 22°C) and then transferred to cold conditions (120 $\mu\text{mol Photons m}^{-2} \text{s}^{-1}$, 10h light/14h dark, 4°C) for another four weeks. Plants were harvested at mid-day and sugars were quantified enzymatically. Data represents mean \pm standard error from 5-6 biological replicates. Statistically significant differences were calculated using Student's one-tailed t-test (* $p \leq 0.05$; ** $p \leq 0.01$; *** $p \leq 0.001$). 65

Figure 3.22. Long-term cold adaptation. Analysis of WT and *ERDL4* mutant plants after four weeks of cold exposure. Plants were grown in control conditions (120 $\mu\text{mol Photons m}^{-2} \text{s}^{-1}$, 10h light/14h dark, 22°C) for 4 weeks and then transferred to cold conditions (120 $\mu\text{mol Photons m}^{-2} \text{s}^{-1}$, 10h light/14h dark, 4°C) for another four weeks. **A.** Phenotype of WT and *ERDL4* mutant plants after 4 weeks in cold (4°C). **B.** Rosette fresh weight of WT and *ERDL4* mutants after 4 weeks in cold. **C.** Anthocyanin content in rosettes harvested at mid-day. **D.** Heat map of log2 fold changes of anthocyanin biosynthesis related genes differentially expressed in *ERDL4* overexpressors in comparison with WT. Data represents mean \pm standard error from 5-6 biological replicates. Statistically significant differences were calculated using Student's one-tailed t-test (* $p \leq 0.05$; ** $p \leq 0.01$; *** $p \leq 0.001$). 67

Figure 3.23. Soluble sugars in cold adapted plants. Sugars were quantified from rosettes harvested after 4 weeks of cold exposure. **A-C.** Glucose, fructose and sucrose content in WT and *ERDL4* mutants. Plants were grown in soil for four weeks in control conditions (120 $\mu\text{mol Photons m}^{-2} \text{s}^{-1}$, 10h light/14h dark, 22°C) and then transferred to cold conditions (120 $\mu\text{mol Photons m}^{-2} \text{s}^{-1}$, 10h light/14h dark, 4°C) for another four weeks. Plants were harvested at mid-day and sugars were quantified enzymatically. Data represents mean \pm standard error from 5-6 biological replicates. Statistically significant differences were calculated using Student's one-tailed t-test (* $p \leq 0.05$; ** $p \leq 0.01$; *** $p \leq 0.001$). 68

Figure 3.24. Analysis of WT and *ERDL4* mutants after dark treatment. Plants were grown for 5 weeks in standard conditions (120 $\mu\text{mol Photons m}^{-2} \text{s}^{-1}$, 10h light/14h dark, 22°C) in soil and then transferred to complete dark for five days. After dark treatment plants were again placed in standard conditions for recovery (7 days). **A.** Phenotype of WT and *ERDL4* mutants after 5 days in dark. **B.** Phenotype of WT and *ERDL4* mutants after 7 days of dark recovery. **C.** Expression of *ERDL4* in dark over the course of 5 days. Expression is normalized to *Actin*. Data represents mean \pm standard error from 4 biological replicates. **D.** Survival rate of WT and *ERDL4* mutants determined after 7 days of dark recovery in light. Data represents mean \pm

standard error from 15 biological replicates. **E.** Level of soluble sugars analysed from WT and *ERDL4* mutants. Data represents mean \pm standard error from 5 biological replicates. **F.** Expression analysis of *AtSAG13* and *AtDIN2* (senescence markers) dark treated WT and *ERDL4* mutants. Samples were collected after five days in dark. Data represents mean \pm standard error from 3 biological replicates. Statistically significant differences were calculated using Student's one-tailed t-test (* $p \leq 0.05$; ** $p \leq 0.01$; *** $p \leq 0.001$). 69

Figure 4.1. Schematic overview of *ERDL4* mediated processes. *ERDL4* mediates glc/frc release from the vacuole. Increased cytosolic fructose levels causes induction of CIPK6 which is recruited by an unknown CBL protein to the tonoplast phosphorylating TST2 which mediates glucose import back into the vacuole. High cytosolic sugars cause upregulation of GPT2 and downregulation of CAB1 and STP1, serving as cytosolic sugar sensors. Sugars are being exported and loaded into apoplast via SWEET11 and SWEET12 transporters suggesting increased provision of sugars to the sink. 78

Figure 4.2. Overview of *ERDL4* in dark induced senescence. **A.** Export of monosaccharides via *ERDL4* elevates cytosolic sugar levels. The free sugars can be phosphorylated by HXK and FRK to form G6P and F6P respectively. F6P can be successively converted to G6P which is the precursor for growth related processes and inhibits senescence. **B.** In *erdl4* knockout plants the sugars are trapped inside the vacuole resulting in less cytosolic sugars available for growth promoting senescence. 82

Figure 7.1. Expression pattern of *ERDL4* (At1g19450) in Arabidopsis during different developmental stages in the eFP browser (Arabidopsis electronic fluorescent pictographer; Winter et al. 2007). 103

Figure 7.2. Tissue specific expression of *ERDL4*. *ERDL4_{Pro}::GUS* fusion protein was transformed into WT Col-0 plants and subjected to histochemical GUS staining. **A, B.** In two weeks old plants *ERDL4* expression was mainly found in the vasculature of leaf and roots. **C, D.** GUS staining in root tip and inflorescence. **E, F.** GUS staining was observed in anthers and strongly in pollens. **G.** GUS staining in shoot apical meristem region and hypocotyl **H.** GUS staining in silique pedicel. 104

Figure 7.3. Native and mutated *ERDL4* localization in different yeast strains. Native and mutated *ERDL4* fused with C-terminal GFP constructs were expressed in W303 and EBY.VW-4000 yeast strains. **A.** Native *ERDL4* expression in W303 yeast. **B.** Mutated AA-*ERDL4* fused with GFP and expressed in W303. **C.** Truncated ΔN -*ERDL4* fused with GFP and expressed in

| | |
|--|-----|
| W303. D. Native <i>ERDL4</i> expressed in the vacuole and in cytosol in EBY.VW-4000. E. Mutated <i>AA-ERDL4</i> fused with GFP and expressed in EBY.VW-4000. F. Truncated ΔN - <i>ERDL4</i> fused with GFP and expressed in EBY.VW-4000. Bar=10 μ m. | 105 |
| Figure 7.4. ^3H fructose uptake via <i>Xenopus</i> oocytes expressing <i>ERDL4</i> . Fructose uptake activity of water or <i>ERDL4</i> expressing oocytes was determined using 2.5 μ Ci ^3H -labelled Frc as described in material and methods section. Values are means of \pm sd (n=6) | 106 |
| Figure 7.5. Expression of sugar responsive genes in <i>ERDL4</i> mutants. FPKM expression values of sugar responsive genes in <i>35S-ERDL4</i> lines and corresponding WT. A-D. Expression values of <i>CAB1</i> , <i>GPT2</i> , <i>HXK2</i> and <i>PFK7</i> . Plants grown for 6 weeks in standard condition (120 μ mol Photons $\text{m}^{-2} \text{s}^{-1}$, 10h light/14h dark, 22 $^{\circ}$ C) were harvested 4 hours after onset of light. Data represents mean \pm standard error from three biological replicates. Statistically significant differences were calculated using Student's one-tailed t-test (* $p \leq 0.05$; ** $p \leq 0.01$; *** $p \leq 0.001$)..... | 107 |
| Figure 7.6. Similar regulation by glucose and fructose of LHCs genes. RNA-Seq analysis showed that most of the genes were regulated in the same manner by both glucose and fructose. Here genes related to light harvesting complexes (LHCs) of photosystem show similar regulation by both sugars making it difficult to dissect the specific sugar effect. | 108 |
| Figure 7.7. TST2 Ser ⁴⁴⁸ conservation across plant species. Alignment is created using Arabidopsis TST2 sequence and is viewed via NCBI multiple sequence alignment viewer. Blue highlighted Serine (S) denotes Ser ⁴⁴⁸ in 4 th column. Blue highlighted rows denote Arabidopsis and <i>Gossypium hirsutum</i> (cotton) TST2 sequence alignment. | 109 |
| Figure 7.8. Vector map of plasmid pBSK. | 110 |
| Figure 7.9. Vector map of plasmid pHannibal | 111 |
| Figure 7.10. Vector map of plasmid pART27. | 112 |
| Figure 7.11. Vector map of plasmid, pDon/Zeo..... | 113 |
| Figure 7.12. Vector map of plasmid pK7FWG2..... | 114 |
| Figure 7.13. Vector map of plasmid pK2GW7..... | 115 |
| Figure 7.14. Vector map of plasmid pGPTV-bar. | 116 |
| Figure 7.15. Vector map of plasmid pGWFDR196. | 117 |
| Figure 7.16. Vector map of plasmid pDRF1-GW. | 118 |
| Figure 7.17. Vector map of plasmid pGEM-He-Juel..... | 119 |

7.4. List of Tables

| | |
|--|----|
| Table 2.1. Arabidopsis plants used in this study..... | 13 |
| Table 2.2. Composition of ½ MS medium..... | 15 |
| Table 2.3. Bacterial and yeast strains used..... | 15 |
| Table 2.4. Composition of LB medium..... | 16 |
| Table 2.5. Composition of YEB medium..... | 16 |
| Table 2.6. Antibiotics and their respective concentration | 17 |
| Table 2.7. Plasmids used..... | 17 |
| Table 2.8. Primers used for genotyping of knock out mutants | 18 |
| Table 2.9. Primers used for cloning | 18 |
| Table 2.10. Primers used for qRT-PCR expression analysis | 19 |
| Table 2.11. Primers used for sequencing..... | 19 |
| Table 2.12. Composition of shorty extraction buffer | 20 |
| Table 2.13. Composition of Pfu reaction buffer | 20 |
| Table 2.14. Pfu PCR reaction setup..... | 21 |
| Table 2.15. PCR program used for Pfu polymerase..... | 21 |
| Table 2.16. Composition of 1X TAE buffer..... | 21 |
| Table 2.17. Composition of ψB medium..... | 22 |
| Table 2.18. Composition of TFBI medium..... | 23 |
| Table 2.19. Composition of TFBII medium..... | 23 |
| Table 2.20. Composition of TE buffer | 24 |
| Table 2.21. Composition of YPD medium | 24 |
| Table 2.22. Composition of SC medium..... | 24 |
| Table 2.23. Setting up of yeast transformation reaction..... | 25 |
| Table 2.24. Composition of oocyte Ringer buffer medium | 26 |
| Table 2.25. Reaction setup for qRT-PCR | 28 |
| Table 2.26. Program used for qRT-PCR..... | 29 |
| Table 2.27. Composition of GUS staining buffer and solution | 29 |
| Table 2.28. Composition of enzyme master mix for starch digestion | 31 |

| | |
|--|----|
| Table 2.29. Composition of premix for sugar quantification..... | 31 |
| Table 2.30. Enzymes used for NADP-coupled enzymatic test | 32 |

Azkiya Khan

Resume

Contact: akhan@rhrk.uni-kl.de

Education

- 2016 – 2022 **Ph.D.** Rheinland-Pfälzischen Technischen Universität Kaiserslautern-Landau, Germany
- Department of Plant Physiology
 - Supervisor: **Prof. Dr. Ekkehard Neuhaus**
- 2012 – 2014 **Master of Science (Plant Biotechnology)**, National University of Science and Technology (NUST), Islamabad, Pakistan
- ASAB, Department of Plant Biotechnology
 - Master's thesis: Detection and Cloning of Begomovirus(es) from Different Plant Samples
 - Supervisor: **Prof. Dr. Muhammad Tahir**
- 2005 – 2009 **Bachelor of Science (Bioinformatics)**, COMSATS University Islamabad, Pakistan
- Bachelor thesis: In-Silico Analysis of Hepatitis C Virus (HCV) NS3 Protease Cleavage Sites and Development of HCV Cleavage Sites Prediction Tool
 - Supervisor: **Prof. Dr. Farah Mustafa**

Acknowledgment

All glory to Allah, the Almighty, for bringing me from the darkness of ignorance to the light of understanding and for all the blessings and infallible grace He bestowed upon me.

I would like to extend my deepest gratitude to **Herr Prof. Dr. H Ekkehard Neuhaus**. It has been a privilege to have him as my Ph.D supervisor. He provided the best supervision, guidance and motivation (which I needed quite often) a young researcher could think of.

In addition, I would like to thank **Herr. Prof. Dr. Matthias Hahn**, for assessing my dissertation as well as the friendly and proactive support of **Jun. Prof. Dr. Timo Mühlhaus** as chairman of my doctoral committee.

My very special thanks go to **Benjamin**, who gave me an incredible support and a new start to my old project. This complete dissertation is a bundle of his suggestions, ideas and analysis. Hats off to him for the multiple collaborations he developed to solve this riddle and for lending me his sincere ear whenever I needed.

I would like to thank **Prof. Dr. Thomas Nägele** for mediating the NAF studies and to **Dr. Joachim Scholz-Starke** who has put a lot of effort in transport studies and still trying different approaches. Your patience and commitment are much appreciable.

I would like to thank **DAAD** for providing the funds for the first 4.5 years of my stay and **IRTG 1830** for the numerous workshops and courses they offered from time to time.

I would also like to thank the entire lab: My thanks go to **Gabi** and **Christa** for all the support they extended from day one when I arrived here. I am grateful to **Torsten** and **Ilka** for their valuable suggestions. In addition, I would like to thank **Marzieh** for her valuable time, motivation and advice. I learnt a lot from her experience and discussions. I will always be appreciative to **Ruth and Ute** for being so humble and helpful. How can I not mention **Verena, Maike**, and **Regina**. Other than the lab stuff they helped me to know the new culture, introduced me to german cakes and baking. Our discussions will always be a happy part of my memory.

I would also like to thank **Leo** for being a good listener, for all the motivation and advice he gave from time to time. I am thankful to **Crissi, Isabel, Sherry, Annalisa, Vanessa** and **Kathy** for the support they offered through these years.

I'd like to express my gratitude for **Kuni**, my former office mate and a dear friend who made a tough start at a new place easier with her always calm and supportive personality. I learnt the value of planning from her. I also would like to thank **Gloria**, my current office mate, for always listening and answering my so many questions with patience. I would like to thank **Pratiwi** and **Jelena** for their support in the lab as well.

A big and special thanks to **Zayef**, my son, whose cute and sincere love enlightened my life whenever I felt stressful through these years. He deserves a special thanks for his patience and always being a motivation for me to move forward. I express special appreciations for **Umer**, my husband, whose faithful support, thoughtful patience and critical thinking have frolicked an essential role to accomplish this task. I am indebted to my parents **Sabeeh Ahmad Khan (L)**, my father, and **Shahnaz Sabeeh**, my mother, who gave me a matchless brought up, never made any compromise on education, gave confidence that everything is possible and for countless love and prayers. I want to thank my brothers **Arsalan Ahmad Khan** and **Shayan Sabeeh Khan** for all the love, care, efforts, time and support they offered. Last but not least, I want to express my gratitude to my parents-in-law **K.K. Zai** and **Shabana Bibi** for their countless prayers and unwavering support in every way.

Statutory Declaration

I hereby declare that I have written this dissertation independently and without unauthorized help from other parties and that I have not used any sources nor resources other than those specified.

I confirm that I have neither submitted a dissertation nor have taken a doctoral examination at the Technical University of Kaiserslautern beforehand or in any other way.

Kaiserslautern, 11. May 2022

(Azkia Khan)

